In presenting this thesis in partial fulfillment of the requirements for an advanced degree at Idaho State University, I agree that the Library shall make it freely available for inspection. I further state that permission for extensive copying of my thesis for scholarly purposes may be granted by the Dean of the Graduate School, Dean of my academic division, or by the University Librarian. It is understood that any copying or publication of this thesis for financial gain shall not be allowed without my written permission.

Signature   _____

Date   _____

Procedure for utilizing a special geometry container

for rapid processing of gamma-emitting

radionuclides in food

By

Jessica Graeber

A thesis

submitted in partial fulfillment

of the requirements for the degree of

Master of Science in the Department of Physics, Electrical, and Nuclear Engineering

Idaho State University

Fall 2018

To the Graduate Faculty:

The members of the committee appointed to examine the thesis of Jessica Graeber find it satisfactory and recommend that it be accepted.

_____

Dr. Richard Brey

Major Advisor

_____

Dr. DeWayne Derryberry

Graduate Faculty Representative

_____

Dr. Chad Pope

Committee Member

TABLE OF CONTENTS

LIST OF FIGURES

LIST OF TABLES

Procedure for utilizing a special geometry container

for rapid processing of gamma-emitting

radionuclides in food

Thesis Abstract -- Idaho State University (2018)

This study aims to modify a Food and Drug Administration (FDA) procedure used in the Food Emergency Response Network (FERN) for the rapid gamma-spectrometry screening of food samples in the event of a radiological incident. Using a container in which samples can be both homogenized and counted, by utilizing a closure thread which can mate to common blenders, for this procedure could aid in reducing time-consuming preparation and decontamination steps. This will enable laboratories to more rapidly process and evaluate food samples for potential contamination, as well as diminish the risk of cross-contamination among samples. The emission of radiation from this container and the efficiency of detection relative to an externally located high purity germanium (HP(Ge)) detector will be modelled by software and validated by empirical measurements. These results will determine whether FDA data quality objectives (DQOs) can be met using the proposed container.

Key Words: gamma-spectroscopy, food-screening, FDA, FERN

Chapter 1: Introduction

The terrorist attacks of September 11, 2001 caused many changes in the fabric of the United States' government and society. One result was a growing concern regarding the preparedness of the government to respond to an act of bioterrorism or agroterrorism. The legislation which followed called for cohesive and effective coordination between government agencies in the event of an accidental or intentional compromise of the United States' food supply system. In response, the coordinated efforts of many departments resulted in the development of the Integrated Consortium of Laboratory Networks (ICLN). A subset of the ICLN is the Food Emergency Response Network (FERN), run by the United States Department of Agriculture (USDA) and the Food and Drug Administration (FDA).

FERN is an integrated network of laboratories operating at the federal, state, and local levels (fernlab.org 2018). The guiding principle behind FERN is to provide a uniform platform and standard procedures for these labs to cooperate effectively should a food contamination event, such as a nuclear incident, occur. Rapid, standardized, and accurate processing of samples is a necessity in the event of any disaster, natural or otherwise, which may compromise the United States' food supply (fernlab.org 2018).

Procedures currently exists for FERN labs with the capability to analyze food samples potentially contaminated with radionuclides. The procedure of interest for this research involves the processing of the edible portions of food samples for analysis regarding specific gamma-emitting radionuclides which have been deemed to be of concern by the FDA. The procedure of interest is Laboratory Procedure WEAC-RN-Method.3.0 Version 9.1 "Determination of Gamma-Ray Emitting Radionuclides in Foods by High-Purity Germanium Spectroscopy." The radionuclides of concern are Cs-137, Cs-134, Ru-103, Ru-106, and I-131, though the detection of

other gamma-ray emitting radionuclides is also possible with this method (WEAC-RN-Method.3.0 Ver. 9.1 2014).

The unhomogenized, edible portions of a food sample are obtained as a part of this procedure and blended using a food processor or other adequate blender to ensure the homogeneity of the sample. The homogenized sample is then transferred from the blender pitcher into a standardized container before being analyzed using a high-purity germanium (HP(Ge)) detector. The blender pitcher and blade must then be decontaminated and the residual, potentially contaminated, sample material collected before the pitcher or blade can be used to prepare another sample. The collected sample residue must be stored until analysis can confirm it is safe to dispose. This process is not only time intensive, but inadequate decontamination could result in sample cross-contamination and less accurate results.

This research examines the possibility of using a proposed container, the Thermo Scientific Nalgene PPCO Mason Jars with Closure[1], in place of the current container. The proposed container was chosen because it has a closure thread pitch, also known as a neck finish, which is compatible with most common blender blade finishes. Oster blender blades and blade replacements, specifically, are compatible with the 70-450G neck finish common to regular mouth mason jars, as well as the proposed container (SKS Bottle & Packaging 2018). Using a container which is compatible with a common blender blade would allow the edible portions of a food sample to be homogenized and analyzed in a single container. The use of a single container would reduce both the amount of equipment decontamination needed and the potential for

---

[1] Fisher Scientific
275 Aiken Road
Asheville, North Carolina 28804 U.S.A

sample cross-contamination. Limiting the time spent on equipment decontamination would allow for increased sample through-put, which becomes increasingly important during an emergency.

The current FERN procedure used for gamma analysis of food samples, WEAC-RN-Method.3.0 Ver. 9.1, is designed to be repeatable and accurate across the variable laboratories which will use the procedure in the event of a nuclear incident. The procedure itself has specific data quality objectives (DQOs) which align with DQOs held by FERN in general. FERN has established network action levels based off an Environmental Protection Agency (EPA) established, and FDA adopted, level known as a derived intervention level (DIL). A DIL is an activity concentration in Becquerel per kg (Bq/kg) which is used to determine whether the amount of radioactive contamination present is a safety concern (CPG Sec.560.750 2005). DILs are calculated for various radionuclide groups. FERN's DQOs include the ability of a lab to detect, at a minimum, one third of the appropriate DIL for each radionuclide of concern. This is known as the minimum detectable concentration (MDC), which is inversely proportional to the efficiency of the detector, the volume of the sample, and the amount of time a sample is analyzed. Additional DQOs for this procedure are the ability of a lab to report activity results with less than 10% inaccuracy and a 1-sigma imprecision of less than 5%.

The efficiency of the detector when using the proposed container must be known to determine the MDC. The proposed container has a different geometry than the current container, so the efficiency is also different. HP(Ge) detector efficiency is highly dependent on the geometry in which a sample is to be counted. Additionally, the efficiency of the detector can change dramatically depending on the type of sample and amount of said sample which will fill the container being used. Thus, this research seeks to establish a relationship between the

efficiency of the detector using the proposed container and both the density of the expected

samples as well as the typical volumes of samples which may be used for this procedure.

Efficiency can be determined in a variety of ways. The most common is to use National

Institute of Standards and Technology (NIST) traceable gamma-emitting standards in a

geometry, and having a density and volume, similar to those of the samples to be analyzed. An

alternate method of increasing popularity makes use of computer modelling programs. Both

methods were used to complete this research. The computer modelling program LabSOCS[2], in

conjunction with the Genie2000 software suite, was used to model the efficiencies of the detector

in various sample analysis scenarios. A liquid mixed gamma source provided by Eckert and

Ziegler[3], a company which maintains traceability to NIST, was used to create calibration

standards in sample analysis scenarios matching the modelled scenarios, to provide

corresponding empirical data sets. The results were used to establish efficiency curves for six

different sample volumes within the proposed container. Density correction factors (DCFs),

based on the corresponding density dependent efficiencies for dried, crushed tea leaves and

honey, and baseline efficiencies for water, were also determined. The efficiency curves and

DCFs were used to determine MDC across a range of expected sample analysis scenarios, as

well as a variety of analysis times. An appropriate analysis time sufficient to obtain MDC was

then determined. The efficiency curves were also applied to an actual sample analysis data set,

called a MAPEP, analyzed using the proposed container to determine how accurately the results

were corrected compared to the true sample activity.

---

[2] Canberra Industries, Inc.
800 Research Parkway
Meriden, Connecticut 06450 U.S.A

[3] Eckert & Ziegler Isotope Products
24937 Ave Tibbitts
Valencia, California 91355 U.S.A

Chapter 2: Background and Literature Review

2.1 Food Emergency Response Network

The Food Emergency Response Network (FERN) was established by the FDA and USDA in response to the increased government responsibilities laid out in the "Public Health Security and Bioterrorism Preparedness and Response Act of 2002" (fernlab.org 2018). FERN brings together the capabilities of local, state, and federal laboratories and works to create a cohesive and efficient network. FERN focuses on four distinct areas: prevention, preparedness, response, and recovery. Prevention focuses on early detection, which involves diligent screening and maintaining sensitive, accurate equipment. Preparedness involves the proficiency testing of FERN laboratories' competence and accuracy on a regular basis to identify areas of improvement and provide pertinent training. Response emphasizes the immense surge capabilities of the FERN program, ensuring a large volume of emergency samples can be processed rapidly and accurately. Recovery is the restoration of the faith the public holds in the safety of the US food system through acts such as removing, safely disposing, and decontaminating the source and spread of the problem (fernlab.org 2018). FERN takes responsibility for both food defense (protecting against intentional adulteration) and food safety (protecting against unintentional contamination) when implementing these four goals (Brooks 2016).

The actions and success of FERN has been seen in several scenarios, both real and simulated, since FERN was established. These include chemical and biological responses during the Deepwater Horizon oil spill in 2010, where polyaromatic hydrocarbon contamination of seafood was a concern, and Salmonella Typhimurium peanut butter outbreak in 2009 (Brooks 2016). FERN also responded following the Fukushima Daiichi nuclear disaster in 2011, when

large quantities of radioactive materials where released into the environment. This response involved five out of the available 34 FERN radiological laboratories working together to process 1,332 samples in the eight months following the incident (Brooks 2016). This event demonstrated both the available surge capacity left to process a larger event, but also the length of time it can take to screen and confirm samples satisfactorily.

TOPOFF 4 – 9385, was an exercise conducted in October of 2007 as part of the Top Officials National Domestic Counterterrorism Exercise Series which attempted to quantify the nation's ability to respond to a Radiological Dispersal Device (RDD) (Day 2009). Officials determined following this study that 100,000 individuals would need to be screened following such an event, which would take approximately four years to complete with the nation's 2007 radiological laboratory capabilities. The EPA determined that 350,000 radiological environmental samples would need to be collected during the 12 months following a single RDD event involving one city, which could take up to six years to complete with the capabilities in place in 2007 (Committee on Science and Technology 2007). These numbers indicate the real need to process samples both quickly and accurately, further supporting FERN's mission.

Another part of FERN's mission and methodology is to establish standardized procedures and reporting practices that rely heavily on a participating laboratory's ability to meet the listed DQOs for a given procedure. These DQOs include items such as standard levels of accuracy and precision for confirmatory procedures as well as *a priori* levels for minimum detection limits, turnaround times, and uncertainty estimates for both screening and confirmatory procedures (Healey 2016). The end goal of using the proposed container in this research is to decrease turnaround times, and potentially increase accuracy and precision, by using a single container for sample preparation and analysis. Other ancillary benefits include the reduced possibility of

sample cross contamination. However, the proposed container must be capable of meeting the minimum detectable concentration (MDC) DQO prior to use. This measured value is compared to the derived intervention levels to evaluate sufficiency. Specifically, the procedure WEAC-RN-Method.3.0 Version 9.1 requires that MDC be one third of a DIL for the applicable radionuclides (Cs-137, Cs-134, Ru-103, Ru-106, and I-131).

The DILs followed by FERN labs are laid out in CPG Section.560.750. and are displayed in Table 1. Table 1 includes the DILs for the alpha-emitting radionuclides Pu-238, Pu-239, and Am-241 and for the beta-emitting Sr-90; these radionuclides are not included in this study as this study focuses on the procedure for gamma-emitting radionuclides only. These DILs are used as guidance to determine whether the radioactivity concentration in contaminated food represents a safety concern. DILs are based on protective action guides (PAGs) which recommend evaluation and potential intervention to reduce exposures if an activity concentration in food could result in a committed effective dose equivalent of 5 mSv or a committed dose equivalent to an individual tissue or organ of 50 mSv, whichever is more limiting (Accidental Radioactive Contamination of Human Food and Animal Feeds 1998).

Table 1. A table of the Derived Intervention Levels as listed in CPG Section.560.750.

Derived Intervention Levels (DILs) for Each Radionuclide Group for Food in Domestic Commerce and Food Offered for Import[a,b]

Radionuclide Group	DIL (Bq/kg)
Strontium-90	160
Iodine-131	170
Cesium-134 + Cesium-137	1200
Plutonium-238 + Plutonium-239 + Americium-241	2
Ruthenium-103 + Ruthenium-106[c]	(C3/6800) + (C6/450) < 1

[a] The DIL for each radionuclide group is applied independently. Each DIL applies to the sum of the concentrations of the radionuclides in the group at the time of measurement.

[b] Applicable to foods as prepared for consumption. For dried or concentrated products, such as powdered milk or concentrated juices, adjust by a factor appropriate to reconstitution, and assume the reconstitution water is not contaminated. For spices, which are consumed in very small quantities, use a dilution factor of 10.

[c] Due to the large differences in DILs for Ruthenium-103 and Ruthenium-106, the individual concentrations of Ruthenium-103 and Ruthenium-106 are divided by their respective DILs and then summed. The DIL for the Ruthenium group is set at less than one. C3 and C6 are the concentrations, at the time of measurement, for Ruthenium-103 and Ruthenium-106, respectively.

DILs set a limit for how much radioactivity is permissible in a set mass of human food distributed in commerce and are thus given units of Becquerel per kilogram (Accidental Radioactive Contamination of Human Food and Animal Feeds 1998). DILs are intended to be applicable only for the first year after a given incident; should exposure levels continue or be projected past one year, the DILs should be reevaluated to determine if they are appropriate for a longer-term exposure. Part of this can be understood by looking at the assumptions and variables used to compute a basic DIL, illustrated on the following page.

$$\text{DIL}\left(\frac{\text{Bq}}{\text{kg}}\right) = \frac{\text{PAG(mSv)}}{\text{f} \times \text{Food Intake (kg)} \times \text{DC}\left(\frac{\text{mSv}}{\text{Bq}}\right)} \qquad \text{Equation 1}$$

Where: DC = the dose coefficient (the radiation dose received per unit of activity ingested in mSv/Bq)
f = the fraction of the food intake assumed to be contaminated (usually set to 0.3, except in the case of I-131 in infant diets, then 1.0 is used)
food intake = the quantity of food consumed in kg for an appropriate period of time (usually one year)
PAG = the protective action guide

These values can be found in the "Accidental Radioactive Contamination of Human Food and Animal Feeds: Recommendations for State and Local Agencies published in 1998. Food intake values and fractions are based off prior FDA knowledge garnered from years of conducting the Total Diet Study.

It should be noted that DILs are calculated very conservatively and are based off the highest projected exposure for the most vulnerable cohort if said cohort were exposed to that DIL sustained over the course of a year. The impact of this approach is that food containing activity concentrations below a DIL can be released for public use or consumption without restriction, though officials have flexibility when making that decision. Several international organizations have also developed DILs with similar but slightly different parameters; DILs used for international trade can be found in the Codex Alimentarius. The FDA has not developed DILs for every radionuclide, just the majorly released radionuclides for different types of nuclear incidents (Accidental Radioactive Contamination of Human Food and Animal Feeds 1998).

2.2 High Purity Germanium Detectors

2.2.1 Semiconductors

The ability of a material to conduct electricity varies widely, from excellent to poor, and depends greatly upon the inherent physical properties of the material. The electrical conductivity of a material allows said material to be characterized as a conductor, a semiconductor, or an insulator. The distinction between an insulator and a semiconductor is determined by the width of the energy gap or band gap, for solids. A larger energy gap (E_g) is associated with insulator materials, while a narrower E_g is associated with semiconductors (Knoll 2010).
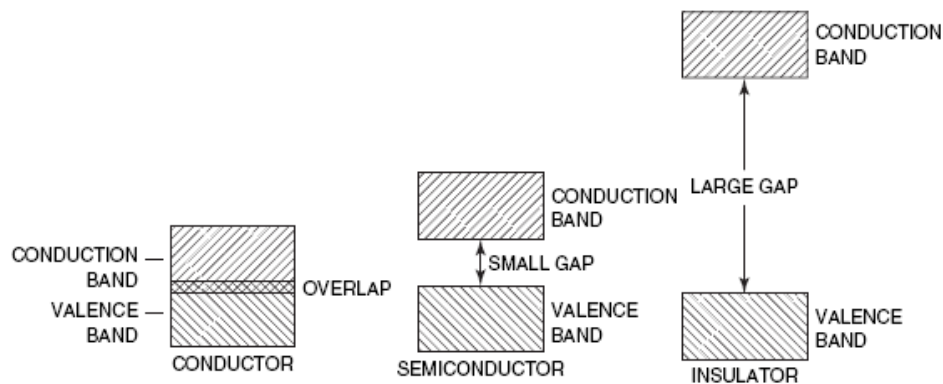
Figure 1. A diagram of the different energy gaps for conductors, semiconductors, and insulators (Hecht 2008).

Solids composed of a crystalline or polycrystalline structure have different energy levels which are a function of a specific crystal's lattice. These energy bands are discrete and consist of three levels: the valence band, the forbidden gap, and the conduction band. The valence band consists of electrons at a low enough energy state as to be essentially bound at specific crystal lattice sites. The forbidden gap is an intermediate energy band at which electrons of a pure crystal cannot exist. The conduction band consists of electrons at an energy state high enough to allow the electrons to move throughout the crystal lattice. The distance between the valence band and the conduction band is known as the energy or band gap and has a defined band or gap width (Tsoulfanidis, Landsberger 2011). The energy required to raise an electron across the E_g of an

insulator is usually greater than or equal to five electron volts (eV), while the energy required for a semiconductor is closer to one eV (Knoll 2010).

An electron which receives enough energy to cross the E_g from the valence band to the conduction band leaves behind a "hole" in the valence band; a space previously occupied by an electron which now has a net positive charge. This pair, known as an electron-hole pair, consists of two charge carriers, a negative electron and a positive hole, both of which will move in opposite directions should an electric potential be applied to the semiconductor material. This is the principle behind a semiconductor's conductivity. A noteworthy characteristic of some semiconductor materials is the ability of sufficient temperatures, or thermal energy, to elevate electrons across the E_g. Consequently, at very low temperatures close to zero Kelvin, semiconductors have essentially zero conductivity (Knoll 2010).

Semiconductors may be "doped," or have intentionally added impurities. These dopants will affect the semiconductor in one of two ways: making the semiconductor either an n-type or a p-type semiconductor. Either dopant will have added atoms of an element which has a different number of valence electrons than the atoms of the semiconductor material. These atoms will energetically reside in the E_g, thus effectively changing the E_g width and the energy required for its transition. A donor impurity is one which has one more valence electron than the semiconductor material, thus increasing the number of potential migrating electrons in proportion to holes. This creates an n-type semiconductor. An acceptor impurity is one which has one fewer valence electrons than the semiconductor material, thus increasing the number of potential migrating holes in proportion to electrons. This creates a p-type semiconductor. A doped semiconductor, whether the impurity is added or naturally occurring as a function of the

crystal growth and purification process, will always have increased conductivity compared to a completely pure or intrinsic semiconductor (Knoll 2010).

2.2.2 Semiconductor Radiation Detectors

The theory behind using a semiconductor material as the interaction medium for ionizing radiation (IR) in a radiation detector relies on the principles of the electron-hole pairs previously discussed. IR incident on a semiconductor will create an equal number of electrons and holes within a very short time-period, a few picoseconds, by depositing sufficient energy to elevate the electrons from the valence band to the conduction band. The electric potential which has been applied in a reverse bias condition across the semiconductor material, causes the created charge carriers to migrate in opposite directions, according to polarity, until each is collected on the appropriate electrode, generating a pulse. The number of charge carriers generated is proportional to the energy deposited in the semiconductor material, which is a discrete magnitude intrinsic to a specific radionuclide's decay (Knoll 2010).

2.2.3 HP(Ge) Detectors

The electrical field applied to a semiconductor usually needs to be hundreds or thousands of volts in magnitude to ensure efficient charge carrier collection. This large of an electric potential is inherently associated with some amount of leakage current, which can be large enough to obscure any additional pulse collected from incident charge carriers at the electrodes. This problem is solved by placing an n-type material and a p-type material next to each other, forming a p-n semiconductor junction with a depletion depth which dampens the current. This can also be accomplished by adding an area of intrinsic semiconductor material between the p and n-type materials, known as a p-i-n junction, which can further increase the depletion depth. The depletion depth is an area where mobilized charge carriers cannot remain; if created in this

area, the charge carriers will rapidly diffuse away. The depletion depth correlates to the active

volume of the detector and has an inverse relationship with the purity of the semiconductor.

More penetrating types of radiation require a larger depletion depth, which can be formed by

decreasing the impurities present in a semiconductor to approximately 10^{10} atoms/cm^3. Creating

an ultra-pure semiconductor material essentially allows the entire semiconductor to become a

depletion region. This is a difficult process, but is possible for germanium. The use of ultrapure

germanium for HP(Ge) detectors has thus gained popularity, especially for use in gamma

spectroscopy (Knoll 2010). A box diagram of the operating components of a typical HP(Ge) is

shown in Figure 2.
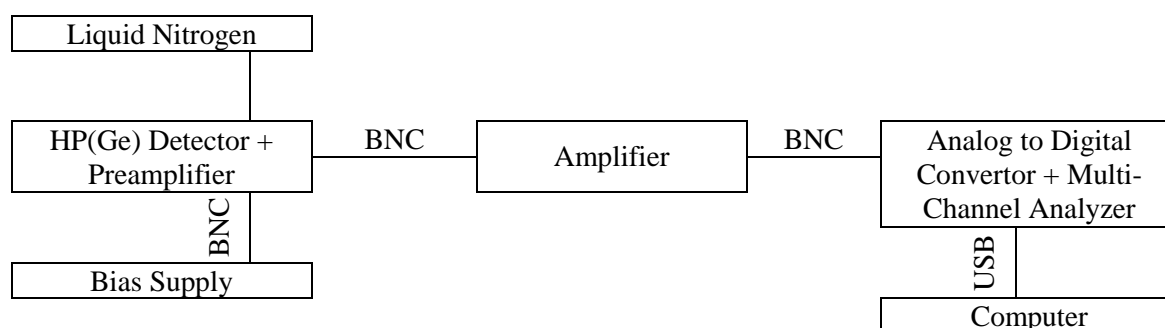
Figure 2. A box diagram of the operating components of a typical HP(Ge).

HP(Ge)s are usually used in conjunction with a multi-channel analyzer (MCA), making

use of the MCA's discriminatory ability to sort multiple energy levels at one time to create

spectra of radionuclides detected and the respective activity present. However, the MCA is only

an accurate tool if calibrated correctly. This may involve up to three calibrations: energy,

efficiency, and full width half max (FWHM). The energy calibration allows the known energy of

a full energy peak to be assigned to an appropriate channel based off the desired range needed to

cover the spectra of energies to be measured. This is done using the following equations:

$$\text{Energy per channel } = \frac{\text{Energy range}}{\text{\# of channels being used}} \qquad \text{Equation 2}$$

Channel of representative full energy peak = (energy of full energy peak) x (energy per channel)

Equation 3

where the representative full energy peak is a function of the chosen calibration source. Each full energy peak in a known spectrum of sources is assigned a channel; this data is plotted in a graph of energies versus channel numbers. A linear fit of this graph gives energy calibration by establishing a mathematical relationship between the two values (Knoll 2010).

The efficiency calibration is a measure of the net integrated area under a photopeak, which correlates to net counts[4]. This is associated with photon energy and divided by the known disintegrations per second of the source in question. This data is plotted in a graph of the efficiencies versus energy; a polynomial fit of this data gives efficiency calibration. The FWHM calibration is used to fit a Gaussian curve to each peak and can be used to determine peak area. This is usually performed when setting up a detector, initially or after a major system change, and too large of a FWHM can be a sign of problems with electric noise often experienced with loss of vacuum in the cold finger of the detector. A FWHM calibration will not be performed for this thesis (Tsoulfanidis, Landsberger 2011).

The equation found for energy calibration allows a qualitative determination to be made regarding the energy level of an unknown full energy peak observed at a known channel. This energy level can be correlated to a certain radionuclide because the energy level of an emitted photon during a radionuclide's decay process is discrete and known. The equation found for efficiency calibration allows a quantitative determination to be made regarding the activity of the

---

[4] A "count" is used here to mean a pulse generated and "counted" by the detector, associated with a photon depositing in the active volume of the detector.

radionuclides present. This is done by observing the net integrated area under the full energy

peak and dividing this number by count time, yielding net count rate (NCR). The efficiency of

the detector at the observed energy level is known, and the yield of the associated radionuclide

regarding the type of radiation particles being counted is also known. Activity is then found

using the equation

$$A \ = \frac{NCR}{(E \times f)} \qquad \text{Equation 4}$$

 Where: E = the efficiency
    NCR = the net count rate in seconds
    A = the decay corrected activity of the source in disintegrations per second f = the
    yield of the source for type of particle in question (i.e. yield for γ) (Knoll 2010)

 The procedure used by the FDA to determine the activity concentration, WEAC-RN-

Method.3.0 Version 9.1 uses an expansion of this equation, displayed below.

$$A_d = \frac{P}{q \times \epsilon_d \times b \times E_1} \times e^{\lambda T_s} \qquad \text{Equation 5}$$

 Where: A_d = the activity concentration in Bq/kg
    P = the net peak area after subtraction of background
    q = the sample quantity in kg
    ε_d = the density corrected efficiency
    b = the gamma ray abundance
    E_1 = the elapsed live time in seconds
    λ = the decay coefficient of the radionuclide in question
    T_s = the time between the sample date and acquisition date in seconds
    (WEAC-RN-Method.3.0 Ver. 9.1 2014)

2.3 Detector Efficiency, Variables Which Affect Efficiency, and Counting

Statistics

2.3.1 Detector Efficiency

 Proper operation of an HP(Ge) semiconductor detector includes keeping the detector

cooled using liquid nitrogen during operation to minimize electrical noise. However, proper

operation does not equate to perfect operation. A detector efficiency must be calculated to

account for possible detector and analyses deficits. Specifically, not every interaction occurring in the detector will be detected, indicating the detector is not 100% efficient. Multiple types of efficiencies can be considered, with the main two being *absolute* versus *intrinsic* efficiency. Absolute efficiency is the ratio of pulses recorded to radiation emitted from the source and is heavily dependent upon the geometry, specifically distance, of the source within the detector system. Intrinsic efficiency is the ratio of pulses recorded to radiation incident on the detector and does not depend as heavily upon geometry (Knoll 2010).

Efficiencies can be further categorized by the type of pulse assumed to be detected and included in the efficiency calculated. The first type is a *total* efficiency and assumes every pulse regardless of magnitude is detected. The second is a *peak* efficiency and assumes only pulses resulting from a full deposition of IR energy upon reaction are counted. The efficiencies calculated for this research will utilize an absolute total detector efficiency and will be calculated using the following equation:

$$E = \frac{NCR}{A \times f} \qquad \text{Equation 6}$$

Where: E = the efficiency
   NCR = the net count rate in seconds
   A = the decay corrected activity of the source in disintegrations per second
   f = the yield of the source for the type of radiation in question (e.g. what percent of disintegrations result in the emission of a certain energy gamma ray)

NCR can be found by subtracting the background number of counts from the observed number of counts for the sample, then dividing this quantity by the count time (Tsoulfanidis, Landsberger 2011). The FDA procedure also identifies an uncorrected counting efficiency (ε_u), which is the efficiency at a reference density of water (taken to be 1g/cc), as well as a density corrected counting efficiency (ε_d). This is found by dividing ε_u by a density correction factor (WEAC-RN-Method.3.0 Ver. 9.1 2014).

2.3.2 Variables Which Affect Efficiency

The variables which affect efficiency are largely based off the different ways photons interact with matter. The three primary ways are photoelectric absorption, Compton scattering, and pair production. Photoelectric absorption dominates for low energy photons and results in the gamma ray, or photon, being completely absorbed and an electron ejected from the impacted atom. The probability of this occurring is represented by the equation displayed below (Martin 2013).

$$\tau \propto \frac{Z^n}{E_\gamma^3} \qquad \text{Equation 7}$$

Where: τ = the probability of interaction
Z = the atomic number of the interaction medium
n = 4 or 5, depending on the incident photon's energy
E_γ = the energy of the incident photon

Compton scattering dominates photon interaction with matter at mid-range energies and results in the incident photon being absorbed and a scattered photon and Compton electron being emitted from the impacted atom. The probability of this occurring is represented by the equation below (Martin 2013).

$$\sigma \propto \frac{Z}{E_\gamma} \qquad \text{Equation 8}$$

Where: σ = the probability of interaction
Z = the atomic number of the interaction medium
E_γ = the energy of the incident photon

Pair production is only possible at energies greater than or equal to 1.022 MeV and does become the primary form of interaction until higher photon energies are reached. Pair production results in the incident photon being absorbed and a negatron and positron being emitted from the impacted atom, 180° from each other. The probability of this occurring is represented by the equation displayed on the following page (Martin 2013).

$$\text{K} \propto Z^2(E_\gamma - 1.022 Mev) \qquad \text{Equation 9}$$

Where: κ = the probability of interaction
Z = the atomic number of the interaction medium
E_γ = the energy of the incident photon

Equation 6 is a deceptively simple equation for determining efficiency, utilizing only three variables. However, there are other variables which are well known to affect a detector's ability to collect the by-products of radiation interacting with said detector (commonly called counts), thus affecting the net count rate detected. Among these are geometry, self-absorption, backscatter, resolving time, and statistical variations, all of which can affect the number of counts collected by the detector (DOE 2.01 Radiological Documentation Study Guide). Geometry and self-absorption will be the focus of this section.

Geometry primarily refers to the size and shape of both the sample source and the detector, and the composition and thickness of the material in the space distance the two (Tsoulfanidis, Landsberger 2011). The size, shape, and distance between the sample and the detector affect the fraction of particles or photons which will be emitted in such a way as to be capable of depositing energy in the detector and creating a measurable pulse. This is often illustrated with the concept of a solid angle, usually applicable to point isotropic sources, but which can be applied to homogenous volume sources as an integration of many point sources (Cember, Johnson 2009). This concept illustrates how a particle or photon emitted from a source has a chance to be emitted in any direction, but only a fraction of those emitted will be in a direction and at an angle subtended by the detector. This fraction is dependent on the size, shape, and distance of the source and detector (Tsoulfanidis, Landsberger 2011). Thus, a detector's efficiency at collecting radiation will change depending on the size and shape of the source, and will be different for different sample containers.

Self-absorption refers to the absorption of emitted particles or photons by the sample medium, prior to interaction with the detector. This is highly dependent on sample chemical composition, namely density, and sample thickness. The effects of self-absorption also vary with photon energy; lower energy photons are much more susceptible to self-absorption, requiring as much as a factor of two correction to detector efficiency. This is because, at lower energies, the photoelectric effect is the dominant form of interaction for photons and the probability of interaction is directly proportional to the atomic number (Z) raised to the fourth or fifth power (Oresegun, Decker, and Sanderson 1993). Thus, a denser sample material will interact with a greater probability (especially with lower energy photons) than will a less dense material. Additionally, the greater the amount of an absorber a photon must travel through, the higher the probability of interaction, leaving fewer photons available to interact with the detector (Knoll 2010). Therefore, sample thickness or volume can greatly change detector efficiency.

2.3.3 Counting Statistics

Reporting an incorrect decision regarding the presence of radioactivity could have far reaching negative effects. There is inherent fluctuation in measurements of radioactive decay, indicating these measurements have an intrinsic uncertainty. This necessitates having a set of decision rules to aid in rejecting likely erroneous results as well as for establishing a confidence interval and set of decisions regarding reporting protocol. A standardized method for calculating a set of decision rules is the Currie Method. Developed by L.A. Currie, this method includes three decision parameters known as the critical level (L_C), the detection limit (L_D), and the minimal detectable activity (MDA) which is sometimes converted to a measure of concentration (MDC) by dividing the MDA by volume (Currie 1968).

The critical level is a statistical decision rule used to establish a limit which a sample must exceed to confidently be declared above background level. Usually calculated to a confidence level of 95%, this value can be used to limit the probability of making a Type I (α-error), otherwise referred to as a false-positive. The decision can be made such that there is a 95% chance the radioactivity measured truly exceeds background and is not due to mere fluctuations in background, if the sample exceeds this level. This value should be calculated *a priori*, or before the sample measurement, to maintain the integrity of the experiment. The parameter L_c can be calculated at the 95% confidence level using the equation

$$LC = 2.33\sqrt{BKG} \qquad \text{Equation 10}$$

Where: BKG = the number of background counts observed using the specific detector and pertinent geometry in regards to the experiment expected to take place (Currie 1968)

The detection limit is a statement of capability used to establish a limit which a sample must exceed to confidently be declared free of radioactivity. L_D is calculated as a function of L_C and is used to understand Type II (β-error), otherwise referred to as false-negative result. L_D is a number of net counts. L_D is conventionally calculated to accommodate a 5% error. If there is activity in the sample at the L_D value, there is 95% confidence that it will be detected using the protocol established. The parameter L_D should also be calculated *a priori* and at the 5% level can be calculated using the equation

$$LD = 2.71 + 4.65\sqrt{BKG} \quad \text{Equation 11}$$

Where: BKG = the background counts observed in an experiment-specific fashion (Currie 1968).

The minimum detectable activity is also a statement of capability and is a conversion of L_D which relates the detection limit to a specific source having a specific yield for the particle of interest. MDA also accounts for the efficiency of the detector being used as well as the amount

of time the sample is being counted. Thus, MDA relates to activity, as the name indicates, rather

than counts and is a measure of the minimum activity a detector can confidently characterize.

MDA can be calculated using the equation

$$\text{MDA} = \frac{LD}{f \times E \times t} \qquad \text{Equation 12}$$

Where: f = the yield of the source in relation to the emission of the particle of
interest
E = the efficiency of the detector
t = the time the same was counted for (Knoll 2010).

The derivations for these equations in relation to standard propagation of error can be found in

Appendix A. The procedure used by the FDA, WEAC-RN-Method.3.0 Version 9.1 uses an

expansion of this equation to determine minimum detectable activity concentration (MDC),

displayed below.

$$\text{MDC}_u = \frac{(2.71 + 4.65 \times \sqrt{B})}{q \times \epsilon_u \times b \times E_1} \times e^{-\lambda T_s} \qquad \text{Equation 13}$$

Where: B = the background counts in the region of the radionuclide key-line
energy
q = the sample quantity in kg
ε_u = the uncorrected efficiency
b = the gamma ray abundance
E_1 = the elapsed live time in seconds
λ = the decay coefficient of the radionuclide in question
T_s = the time between the sample date and acquisition date in seconds
(WEAC-RN-Method.3.0 Ver. 9.1 2014)

This equation calculates an uncorrected MDC (MDC_u). Multiplying MDC_u by the density

correction factor will yield a density corrected MDC (MDC_d).

The density correction factor can be calculated using the equation displayed below.

$$DCF = \frac{\epsilon_u}{\epsilon_d} \qquad \text{Equation 14}$$

Where: ε_u = the uncorrected efficiency
ε_d = the density corrected efficiency

2.4 Laboratory Sourceless Object Calibration Software (LabSOCS)

LabSOCS, which stands for Laboratory Sourceless Calibration Software, is a software suite and detector characterization package sold by Canberra Industries, now a subsidiary of Mirion Technologies[5]. LabSOCS, originally developed in 1999, is a low-cost alternative to traditional efficiency calibration techniques, which require the costly and time-consuming acquisition of reliable sources in every sample geometry a lab may wish to use for sample analysis (Gilmore 2008). LabSOCS is a Monte Carlo N-Particle (MCNP) based software which utilizes specific detector characterization processes. These, along with MCNP code, are used to create a program capable of predicting a detector's efficiency when using a new geometry. This is done by modelling a new geometry and is meant to be an accurate replacement to empirically generated efficiency curves (Gilmore 2008).

The detector characterization process involves sending the specific detector to Canberra where accurate detector dimensions are determined. Empirical efficiencies are determined for the detector at a variety of points in a three-dimensional space around the detector. These empirical efficiencies, along with the specific detector dimensions, are input into a MCNP code and used to generate a look up table, called a par file, which is essentially a map of the detector's spatial efficiency response. This file contains a grid of 10,000 coordinate vacuum point efficiencies which cover an energy range from 10 keV to seven MeV. These points are generated for distances from zero to 500 meters away from the endcap of the detector (Canberra 2017). This par file is released to the user and, when combined with a geometry modelling software called Geometry Composer, allows the user to input a unique sample container shape and sample

---

[5] Mirion Technologies (MGPI) Inc
5000 Highlands Parkway Suite 150
Smyrna, GA 30081 U.S.A

matrix and find the efficiencies for such a geometry without having the in-depth knowledge required to model the situation from the ground up.

LabSOCS is considered accurate enough to replace empirical data. Canberra's own "Validation and Internal Consistency" document states that LabSOCS has a 7.1% SD accuracy for energies less than 150 keV. Energies between 150 and 400 keV have an accuracy of 6.0% SD and energies between 400 and 7,000 keV have an accuracy of 4.3% SD (Bronson 2002). Other external validations of LabSOCS have shown a trend for LabSOCS to underestimate low energy efficiencies and overestimate high energy efficiencies by an average of 10% (Gilmore 2008). This is consistent with a study conducted by Tian Zi-Ning et al. in 2014 which found that using LabSOCS to generate self-attenuation correction factors, called density correction factors in this research, yielded results that are consistent with experimental values within 7.9% (Zi-Ning, et al. 2014). A study conducted by the FDA, comparing LabSOCS with two other modelling software systems, along with empirical data, found that LabSOCS was the closest at predicting efficiencies across the typical range of food densities. The most deviation occurred at low energies, below 100 keV, but the conclusion was that LabSOCS is suitable to use for computer modelling of efficiencies in unusual geometry situations (Rolle, Healey, Lin 2016).

Chapter 3: Materials and Methods

3.1 Facility and Instrumentation

Data was collected in the Environmental Monitoring Lab (EML) at Idaho State University in Pocatello, Idaho. The HP(Ge) semiconductor detectors used for the empirical efficiency curves, validation data, and background data were the Canberra Model GC2520 closed ended coaxial type HP(Ge) detector and the ORTEC[6] Model GEM-25185-P coaxial type HP(Ge) detector. Only the Canberra Model GC2520 was used for the LabSOCS generated efficiency curves because only the Canberra Model GC2520 has been LabSOCS characterized by Canberra. The multichannel analyzer computer software used was the Genie 2000 Gamma Acquisition and Analysis, Version 3.4, software suite, distributed by Canberra. The LabSOCS and Geometry Composer software used were also included in the Genie 2000 software suite, owned by the EML.

3.2 LabSOCS Container Model and Initial Efficiency Curves

The proposed container, the Thermo Scientific Nalgene PPCO Mason Jars with Closure, was obtained from Fisher Scientific in two sizes, a 1-L bottle and a 500-mL bottle. A single bottle of each size was cut in half, as close to the vertical midline as possible, using a bandsaw. Measurements were then taken of the resulting center bottle cross sections using a CenTech[7] 6" Digital Caliper. These measurements included the height of each size bottle, the variable width and thickness along the walls of each bottle, and careful measurements to adequately model the

---

[6] ORTEC Int. USA, Inc.
3630 Peachtree Road NE
Suite 800
Atlanta, GA 30326
[7] CenTech Sp. Dz o.o
8 Narwicka Street
80-557 Gdansk, Poland

curve along the bottom of each bottle. Measurements were taken in triplicate and then averaged before use to account for differences in the amount of flex the plastic container experienced when the micrometer jaws were tightened around the point of measurement.

These measurements were formatted as (x, y) coordinate points with the diameter being the x-axis and the height being the y-axis. This allowed inner and outer contour lines to be modelled, which could be input into the software, Geometry Composer. This format allows for extremely customizable wall thickness and shape. The resulting measurements for each bottle are displayed in Tables 2 and 3. An Excel mockup of the inner and outer contours as coordinate point outlines are displayed in Figures 3 and 4. The threads around the neck of the bottle were ignored; instead the bottle was modelled as having a bottle neck continuous with the container lid. This was considered justifiable as this area of the bottle should have minimal impact on the geometry of the sample due to the lid and neck of the bottle not being between the sample and the detector.

Table 2. The average measurements used as coordinate points to build the 1-Liter bottle model.

1-Liter Bottle					
Outer Contour			Inner Contour		
Point #	Diameter (mm)	Height (mm)	Point #	Diameter (mm)	Height (mm)
1	0.00	3.61	1	0.00	6.97
2	26.20	3.33	2	26.20	6.30
3	52.40	2.58	3	52.40	5.83
4	79.06	0.00	4	68.00	4.91
5	88.80	2.44	5	78.76	4.66
6	92.30	4.83	6	84.00	11.16
7	94.36	8.77	7	87.76	16.82
8	91.46	165.00	8	88.44	32.00
9	89.44	170.00	9	87.60	75.00
10	83.20	175.00	10	86.20	110.00
11	75.00	177.00	11	87.66	141.00
12	75.14	181.00	12	87.06	165.00
13	76.60	182.00	13	85.74	169.00
14	82.04	182.00	14	79.30	173.00
15	82.04	185.00	15	70.42	176.00
16	70.64	185.00	16	70.42	181.00
17	70.64	187.42	17	63.10	185.00
18	79.46	187.42	18	63.04	205.72
19	76.46	214.05	19	0.00	205.72
20	73.28	214.05			
21	73.10	207.48			
22	0.00	207.48			
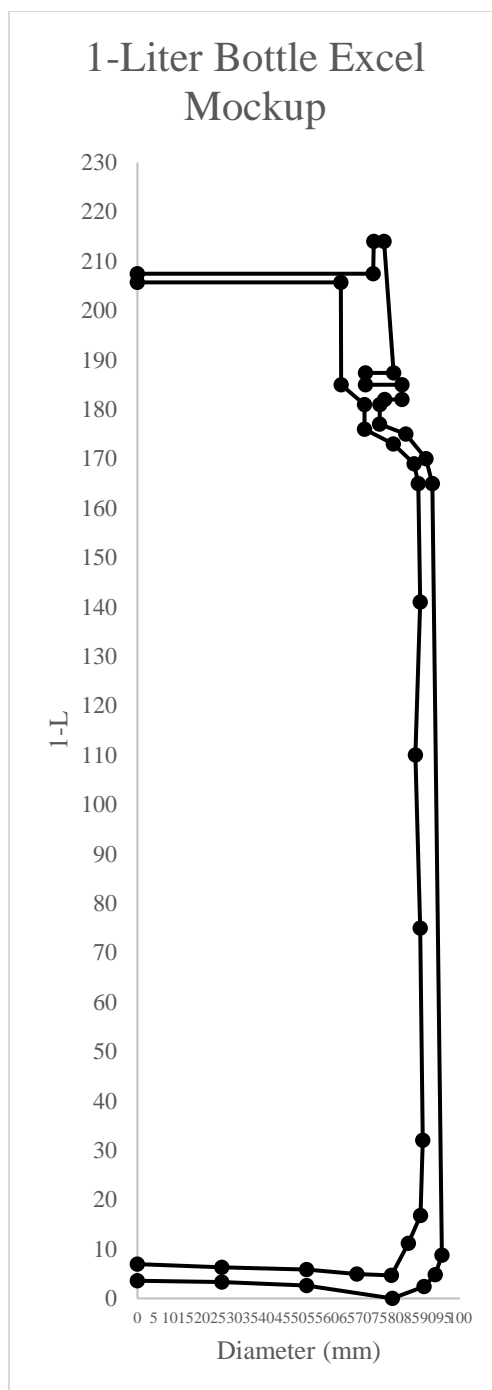
Figure 3. Excel mockup of 1-Liter bottle's inner and outer contour lines.

Table 3. The average measurements used as coordinate points to build the 500-mL liter bottle model.

	500-mL Bottle					
	Outer Contour				Inner Contour	
Point #	Diameter (mm)	Height (mm)	Point #		Diameter (mm)	Height (mm)
1	0.00	3.46	1		0.00	6.64
2	47.82	3.46	2		47.82	6.64
3	61.66	0.00	3		58.08	4.85
4	66.92	2.48	4		63.20	4.98
5	69.12	4.97	5		64.42	7.78
6	70.64	8.77	6		64.06	15.81
7	68.06	72.68	7		64.62	22.12
8	68.62	113.50	8		63.48	72.68
9	69.52	135.41	9		64.60	113.50
10	68.20	142.50	10		64.68	135.41
11	75.60	142.50	11		63.58	142.50
12	75.60	145.65	12		60.74	145.65
13	66.54	145.65	13		59.78	167.58
14	66.54	150.11	14		0.00	167.58
15	72.78	150.11				
16	71.22	175.59				
17	68.06	175.59				
18	66.86	169.53				
19	0.00	169.53				
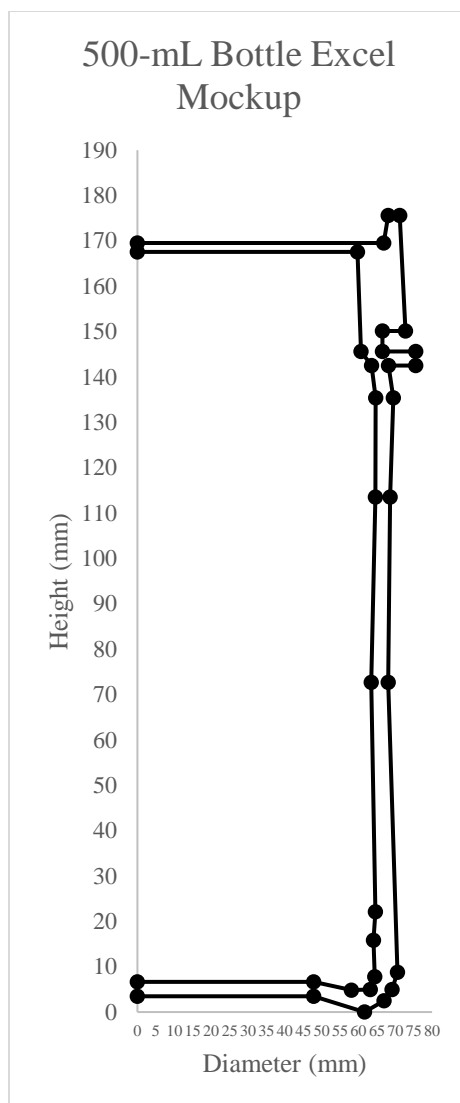
Figure 4. Excel mockup of 500mL bottle's inner and outer contour lines.

These measured values were input into the Geometry Composer software and a 3D model

was generated by spinning the initial points 360° about the axis of symmetry. The 3D model for

each bottle size was then assigned to the Canberra Model GC2520 detector characterization file.

An image of the 3D 1-L bottle oriented on the Canberra Model GC2520 detector in the

appropriate geometry is shown in Figure 5.
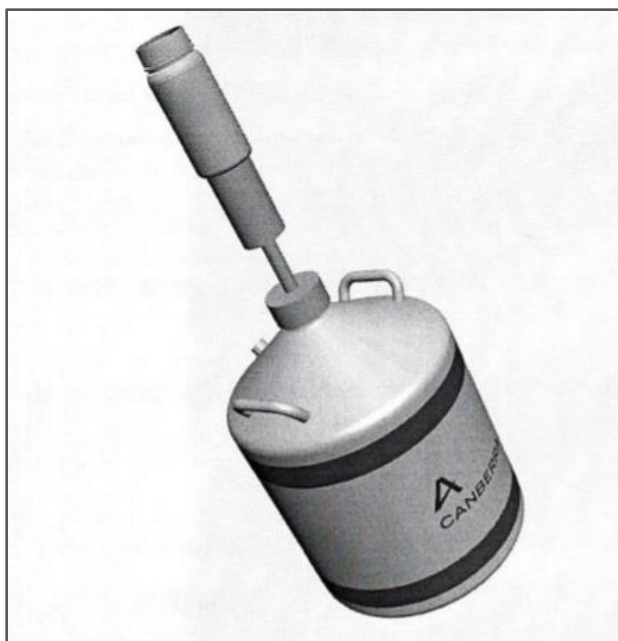
Figure 5. An image of the 3D bottle generated in Geometry Composer and assigned to the LabSOCS Canberra Model GC2520 characterization file. The bottle was aligned with the vertical axis of the detector, with no vertical offset used.

The sample matrices of tea, water, and honey were chosen because these encompass the typical range of density found in most foods. Typical foods usually fall within approximately 0.31 g/mL to 1.40 g/mL (Healey 2015). The initial bulk densities used for tea, water, and honey were 0.453 g/mL, 1.000 g/mL, and 1.363 g/mL. These densities, along with the elemental composition of each sample type shown in Table 4, were input into the Geometry Composer software to build specific sample matrices. Each matrix was then input into the 3D modelled geometry for each bottle three times, each at a different fill volume. The volumes used were 300-mL, 400-mL, and 500-mL in the 500-mL bottle, and 500-mL, 750-mL, and 1000-mL in the 1-L bottle, resulting in six total volumes.

Table 4. The food products used, listed with the corresponding density and elemental analysis per Rolle, Healey, Lin 2016.

Food Matrices		
Food Product	Density (g/mL)	Elemental Analysis
Tea	0.453	55.59% Carbon, 6.10% Hydrogen, 35.16% Oxygen, 3.02% Nitrogen, 0.07% Sulfur, 0.07% Phosphorous
Water	1.000	11.19% Hydrogen, 88.81% Oxygen
Honey	1.363	40.00% Carbon, 7.00% Hydrogen, 53.00% Oxygen

The manufacturer's activity certificate for the specific liquid mixed-gamma radiation source that would be used to create the empirical efficiency samples was also input into LabSOCS. This would allow LabSOCS, using a combination of MCNP modeling and the measured detector efficiency look up table, to generate efficiency points for the specific energy lines that would be seen in the empirical samples. A copy of the certificate can be found in Appendix B. This resulted in a complete geometry built in LabSOCS, encompassing the type of container, specific detector characteristics, orientation of the container relative to the detector, and sample matrix used for each of the 18 (6 volumes each for 3 densities) desired efficiency curves. The efficiency curves for each geometry were then generated in LabSOCS.

The initial curves generated in LabSOCS were used to determine how long the empirical samples would likely need to be counted to achieve the desired uncertainty. A widely accepted standard for good efficiency curve statistics is to count the sample for the length of time which would yield at least 10,000 counts under each full energy peak (Gilmore 2008). The reasoning behind this is that the error in counts is simply the standardized square root of the counts, meaning the error associated with 10,000 counts would be only 1% (see Appendix A for the

derivation of count error). Determining the count time was a matter of manipulating Equation 5 to solve for E_1, using the appropriate variables provided by the source certificate, the associated LabSOCS efficiency, and a desired 10,000 net counts in each full energy peak. This was repeated for all the energy lines across all 18 efficiency curves. The most limiting time was chosen and rounded up to be conservative and ensure 10,000 counts were reached under even the least efficient full energy peak. This was determined to be 75-minutes.

3.3 Empirical Efficiency Curves and Validation

A set of empirical standards where then made to mirror the geometries modelled in LabSOCS; namely, a set of standards using the sample matrices of honey, tea, and water which would be analyzed at the six volumes. To make the empirical efficiency standards, the original 5-mL liquid mixed gamma source was first diluted into a more workable volume of 100-mL. The radioactive material of the source was suspended in a 2M Hydrochloric Acid and deionized lab water solution, per manufacture recommendations. The amount of the source used was determined gravimetrically. A Class A 100-mL volumetric flask was used to contain the diluted source. The volumetric flask was partially filled with the 2M Hydrochloric Acid solution. Of the 5.30982 ± 0.00001 g of source available, 5.2678 ± 0.0001 g of source was added to the volumetric. The 2M Hydrochloric Acid solution was added to achieve a total volume of 100 ± 0.080-mL. The solution was agitated using a Thermolyne Maxi Mix II Model 37600 vortex shaker, such as those used for blood draw samples in the medical field.

The dilution was then added to the first volume of each sample matrix (300-mL of water[8], honey[9], or tea contained within a 500-mL bottle). Each bottle was first filled with 250-mL of

---

[8] The water used was also a 2M Hydrochloric Acid and deionized water solution in an effort to keep the source suspended in the water for the duration of the count time.

[9] The honey, for the initial volume and all subsequent volumes, was heated using a temperature controlled water bath to approximately 90° F to aid in viscosity and homogeneity issues (Gómez-Díaz, et al. 2009)

either water, honey, or tea prior to being spiked with the diluted source. The volume was based off the bulk density of the respective food matrix and the corresponding expected weight. Each bottle was then spiked with 25-mL of the diluted source using a Class A pipet. The bottle was then filled with the remaining 25-mL of sample matrix needed to reach a 300-mL fill volume. The total weight of the bottle was appropriate for a volume of 275-mL of the sample matrix and 25-mL of diluted source, based off sample matrix bulk density and the calculated dilute source density. A corresponding deionized (DI) lab water blank was also made at the 300-mL fill volume.

The honey and tea were both mixed using an Oster[10] blender and individual blade for approximately 2 to 3 minutes, until visually homogenized. The water was shaken by hand for approximately 2 to 3 minutes, as was the DI blank. The blender was not used for the water or the blank because adequate homogenization could be reached via hand mixing and the increased amount of Hydrochloric Acid contained in the spiked water was deemed a potential hazard to the metal blender blades. Each spike was counted for 75 minutes on the Canberra detector, then 75 minutes on the ORTEC, as well the DI blank. The honey and tea were counted with the blender blade top installed in the container, due to a desire to avoid any potential loss of radioactive material. The water and blank were counted with the normal top on because a blender blade was not used to mix the water solutions.

This process was repeated for each sample matrix until all volumes had been counted for all sample matrices, including the DI blank. It should be noted that the original spiked mixture was transferred from the 500-mL bottle to the 1-L bottle due to a limited quantity of sample

---

[10] Newell Brands
221 River Street
Hoboken, NJ 07030

matrix available. The transfer was done gravimetrically so mass balance data would be available to understand possible sample loss during the process. The manufacturer's activity certificate for the specific liquid mixed-gamma radiation source was modified to account for the amount of source actually present in each efficiency sample. This was then applied to the raw data to obtain an empirically generated efficiency curve.

Due to limitations inherent to the LabSOCS modelling software and the size of the Canberra detector's shielding, the samples were counted on the Canberra with the shield open. A study was therefore undertaken to count multiple backgrounds of a given volume over the course of a morning. This allowed a determination to be made on how much background counts likely fluctuate over a sample analysis count time. Corresponding backgrounds were also counted on the ORTEC so a comparison of background fluctuations with an open shield and a closed shield in the same lab at the same time of day could be made.

Both the Environmental Assessment Lab (EAL) and the EML at ISU participate in the Mixed Analyte Performance Evaluation Program (MAPEP) conducted by the Radiological and Environmental Sciences Laboratory (RESL) as part of an external quality assurance program. To verify the accuracy of the sets of efficiency curves, MAPEP samples with known activity levels were used for independent sample counts. An old water MAPEP sample and an old vegetation MAPEP sample was obtained from the EAL and transferred to a 1-L new container and a 500-mL new container, respectively. These MAPEP samples were then counted on both the Canberra and the ORTEC detectors for a time of 20 hours, the standard time for counting MAPEPs used by the EML. A corresponding 20-hour background was also counted on each detector. The true activities contained in both MAPEP samples were obtained from documentation provided by RESL. The empirical efficiency curves and the modelled efficiency curves were then applied to

the obtained sample data from each MAPEP sample analyzed and on each detector to obtain an estimate of activity. These estimates were then compared to known activity to determine which set of efficiencies more accurately corrected the obtained data.

3.4 Adjusted LabSOCS Efficiency Curves

The bulk densities used for the water and tea LabSOCS generated efficiency curves were very close to the measured densities for the materials used for these sample matrices (0.453g/mL bulk tea versus 0.4±0.06 g/mL measured tea). However, the bulk density used for honey deviated to a greater degree from the measured density for the material used (1.363g/mL bulk versus 1.448±0.002g/mL measured). The LabSOCS generated efficiency curves for honey were rerun using the measured density rather than the bulk density. The new modelled honey efficiency curves and the original modelled water and tea efficiency curves were all compared to the respective empirically generated efficiency curves to determine how well the models both fit and predict the empirical data, for both the Canberra empirical data and the ORTEC empirical data.

3.5 Hypotheses

H0 (1): The modelled efficiency data will adequately model the empirical data.

H0 (2): Using the proposed container, the empirical and modelled efficiency data will yield an MDC value capable of meeting the FDA DQO of a minimum MDC of one-third of a DIL.

H0 (3): The known activity for the MAPEP verification samples and the measured activity calculated using the efficiency curves determined in this study have the same mean value.

HA (1): The modelled efficiency data will not adequately model the empirical data.

HA (2): Using the proposed container, the empirical and modelled efficiency data will yield an MDC value not capable of meeting the FDA DQO of a minimum MDC of one-third of a DIL.

HA (3): The known activity for the MAPEP verification samples and the measured activity

calculated using the efficiency curves determined in this study differ in mean value.

Null hypothesis 1 will be rejected if the R^2 predicted is less than or equal to 0.75 or the

standard deviation (SD) for the regression is greater than or equal to 0.10, indicating a poor fit

(Peck 2015). Null hypothesis 2 will be rejected if any of the empirically generated or modelled

MDCs are greater than or equal to one-third of the associated DIL when the associated sample

count time is 30 minutes or less.

$$R^2 \text{ Predicted} = 1 - \frac{SSR\left(\frac{n}{n-p}\right)^2}{SST} \qquad \text{Equation 15}$$

Where: SSR = the sum of the squared residuals
SST = the total sum of the squares
n = the total number of observations
p = 2
(Peck 2015)

$$\text{Regression SD} = \sqrt{\frac{SSR}{n-2}} \qquad \text{Equation 16}$$

Where: SSR = the sum of the squared residuals
n = the total number of observations
(Peck 2015)

Null hypothesis 3 will be rejected if the calculated t values are greater than or equal to the

corresponding one-tailed critical t value at an alpha level of 0.05, using the following one sample

t test formula:

$$t = \frac{\bar{x} - \mu}{\frac{s}{\sqrt{n}}}$$

Where: t = calculated t value
$\bar{x}$ = the sample mean
μ = the population mean
s = the sample standard deviation
n = the number of observations

Chapter 4: Data Analysis and Results

4.1 Empirical versus Modelled Efficiency Curves Comparison

The modelled and empirically collected efficiency curves and the percent efficiency of each radionuclide by energy line contained within the source can be found in Appendix C for every sample geometry studied. The tables and curves for the 500-mL in the 500-mL bottle for each Canberra sample matrix is shown in Tables 5 through 7 and Figures 6 through 8, respectively, as an example of the results. These tables also include the R^2 predicted and regression standard deviation calculated for each detector when compared to the LabSOCS generated model. It should be noted that the LabSOCS model was never intended to accurately model the ORTEC HP(Ge) detector but was still compared here for interest. The reader is reminded that a complete description of the ORTEC detector, providing the details of geometry required for accurate LabSOCS estimates, was not available.

The efficiencies seen here are on an order that is typical of the efficiencies seen in the Environmental Monitoring Lab. Each empirical curve generated for the ORTEC and the Canberra detectors was evaluated to see if the corresponding LabSOCS curve would have given a conservative higher estimate of activity. Specifically, an empirical data point for efficiency which is larger than the corresponding modelled data point would result in a higher activity estimate due to the inverses relationship between activity and efficiency demonstrated in equation 6. A simplified version of this statement is shown on the next page.

$$IF \ \epsilon_{model} < \epsilon_{empirical}$$

$$THEN \ \frac{counts}{\epsilon_{modelled}} \rightarrow Conservative \ Higher \ Activity$$

Each empirical data set was compared to the LabSOCS modelled data set using equations 14 and 15 to determine a goodness of fit for the model to the data. The larger the R^2 predicted value, maximum being 1, the better a model can be said to fit the predicted data. The smaller the regression SD, minimum being 0, the more accurate the predictions can be said to be (Peck 2015). An arbitrary decision rule was chosen *a priori* to indicate a poor fit by the model if the R^2 predicted values were less than or equal to 0.75 or standard deviation (SD) for the regression values were greater than or equal to 0.10.

The LabSOCS model was determined to be conservative for every fill volume of water empirically counted on the Canberra detector. Conservative in this circumstance indicates that the LabSOCS estimated values were smaller than the measured empirical values. All the generated data points resulted in a larger empirical efficiency when compared with the corresponding modelled efficiency. The predicted versus the measured efficiency values were also conservative for the ORTEC water data set, except for the two lowest energy lines. This lower energy lack of a conservative estimate was consistently observed for all the fill volumes. This is potentially due to the geometry used by the model be less accurate for the ORTEC detector. Specifically, the true location of the ORTEC detector crystal is likely farther away from the source than the distance that was used by the model. This would result in pronounced higher modelled efficiency estimates at lower energies compared to the corresponding measured, empirical efficiencies.

The honey and tea data sets, for both detectors, had less patterned variability in whether the modelled efficiency was lower than the empirical efficiency. We think this is due to variability in the degree of homogeneity obtained and sustained when mixing and analyzing each volume of sample, respectively. The tea was difficult to attain adequate homogeneity due to

clumping of the dry, ground tea leaves when mixed with the liquid, dilute source. The honey was capable of being visually homogenized prior to analysis, but tended to settle and become heterogenous over the course of the 75-min analysis time. These were significant issues that likely contributed to additional variability in the generated, empirical efficiency curves.

Overall, the LabSOCS model fit and predicted the data for both the ORTEC and the Canberra well, according to the *a priori* regression decision rules of an R^2 predicted less than or equal to 0.75 or a standard deviation (SD) for the regression greater than or equal to 0.10. Consistently, the LabSOCS model did a better job of fitting and predicting the Canberra data than it did the ORTEC, as indicated by higher R^2 predicted values and lower regression SD values, which is to be expected. The LabSOCS calibration file used was built specifically for use with the characterized Canberra detector. All the Canberra data sets had R^2 predicted values greater than 0.98 and very low regression SDs, with the best fit being for the water sample matrix data set which had R^2 predicted values greater than 0.99. When compared with the decision rules, the decision was made that this indicated a good fit. The data set having the largest regression SDs for the Canberra detector was the tea data set; the regression SD values were on the order of $3x10^{-4}$ to $5x10^{-4}$, compared to the water values of $1x10^{-4}$ to $2x10^{-4}$. However, these were still considered very low regression SD values and still met the decision rule criteria of having an R^2 predicted value greater than 0.75 and a regression SD value less than 0.10. Difficulties with the liquid dilute source mixing inadequately with the dry, ground tea leaves and creating localized, unhomogenized hot spots likely contributed to this increased variability.

The ORTEC data sets also had very high R^2 predicted values, many were greater than 0.90, with low regression SDs, with the best fit being for the water sample matrix data set. The lowest R^2 predicted value was 0.7766 and the largest regression SD value was 0.0017, indicating that all the data sets for the ORTEC still met the decision rule criteria for good fit. Again, the largest regression SDs were seen for the tea sample matrix data set, supporting the theory that the increased variability is related to the sample matrix not attaining adequate homogeneity, not the detector used for analysis. These SD values were on the order 1×10^{-3} to 2×10^{-3}, compared to the water values of 7×10^{-4} to 1×10^{-3}. These were still considered very low regression SD values and still met the decision rule criteria for a good fit.

Table 5. The efficiencies and associated error by energy line contained within the liquid mixed-gamma source, for the honey 500-mL fill volume in the 500-mL bottle on the Canberra detector. The density correction factors and an analysis of whether the LabSOCS model would have given a conservative estimate of activity is also included.

Canberra Honey 500-mL in 500-mL Bottle				
R^2 Predicted:	0.9954	Regression SD	0.0002	
Energy (keV)	Efficiency (%)	Error (%)	DCF	Model Conservative
88	0.0092	0.0003	1.2676	Y
122.1	0.0100	0.0002	1.2800	Y
165.9	0.0093	0.0002	1.2969	Y
279.2	0.0063	0.0001	1.2528	N
391.7	0.0051	0.0001	1.2559	Y
661.7	0.0035	0.0001	1.1977	Y
898	0.0027	0.0001	1.1896	Y
1173.2	0.0022	0.0001	1.1892	Y
1332.5	0.0020	0.0001	1.2030	N
1836.1	0.0016	0.0000	1.2194	N
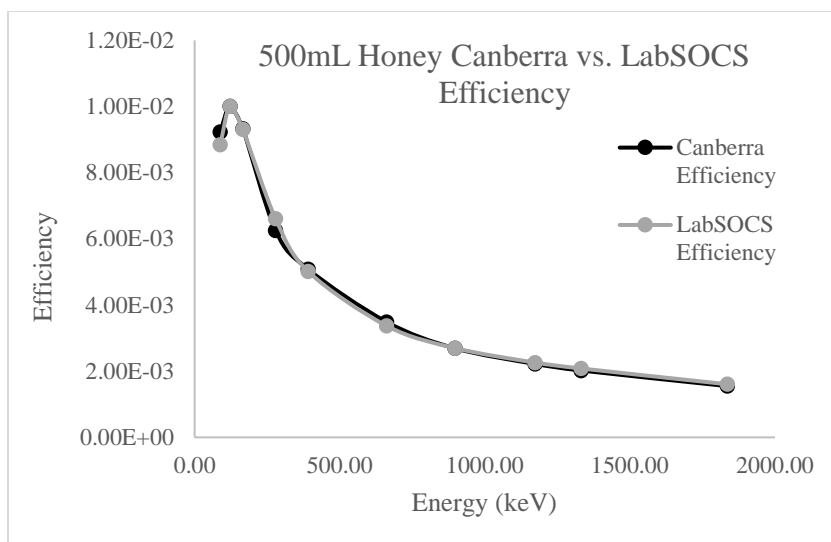
Figure 6. A graph of the Canberra empirical efficiency points versus the LabSOCS modelled efficiency point for the honey 500-mL fill volume in the 500-mL bottle on the Canberra detector.

Table 6. The efficiencies and associated error by energy line contained within the liquid mixed-gamma source, for the water 500-mL fill volume in the 500-mL bottle on the Canberra detector. The density correction factors and an analysis of whether the LabSOCS model would have given a conservative estimate of activity is also included.

Canberra Water 500 mL in 500-mL Bottle			
R^2 Predicted:	0.9965	Regression SD	0.0002
Energy	Efficiency	Error	Model Conservative
88	0.0117	0.0003	Y
122.1	0.0128	0.0002	Y
165.9	0.0121	0.0003	Y
279.2	0.0078	0.0001	Y
391.7	0.0064	0.0002	Y
661.7	0.0042	0.0001	Y
898	0.0032	0.0001	Y
1173.2	0.0026	0.0001	Y
1332.5	0.0024	0.0001	Y
1836.1	0.0019	0.0000	Y
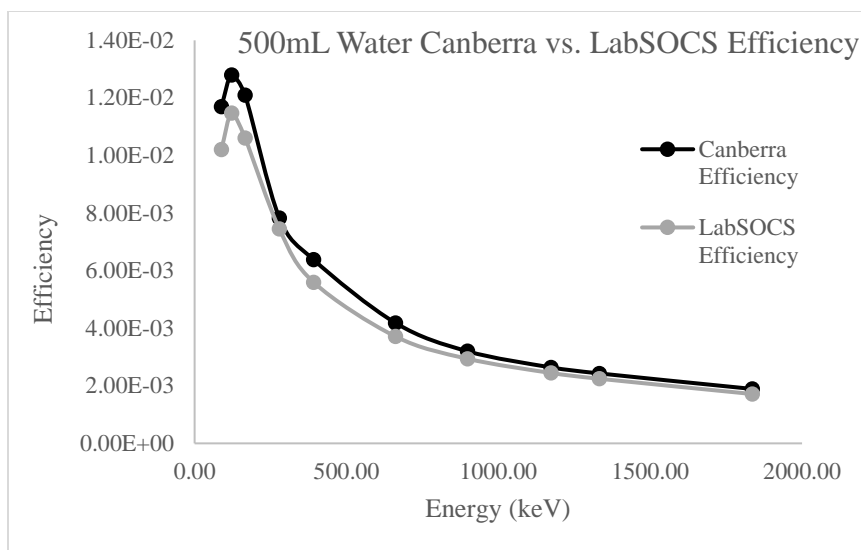
Figure 7. A graph of the Canberra empirical efficiency points versus the LabSOCS modelled efficiency point for the water 500-mL fill volume in the 500-mL bottle on the Canberra detector.

Table 7.The efficiencies and associated error by energy line contained within the liquid mixed-gamma source, for the tea 500-mL fill volume in the 500-mL bottle on the Canberra detector. The density correction factors and an analysis of whether the LabSOCS model would have given a conservative estimate of activity is also included.

Canberra Tea 500 mL in 500-mL Bottle				
R^2 Predicted:	0.9950	Regression SD	0.0003	
Energy	Efficiency	Error	DCF	Model Conservative
88	0.0132	0.0004	0.8864	N
122.1	0.0140	0.0002	0.9143	N
165.9	0.0127	0.0003	0.9528	N
279.2	0.0094	0.0002	0.8294	Y
391.7	0.0070	0.0001	0.9180	Y
661.7	0.0043	0.0001	0.9654	Y
898	0.0033	0.0001	0.9786	N
1173.2	0.0026	0.0001	1.0038	N
1332.5	0.0024	0.0001	1.0167	N
1836.1	0.0018	0.0000	1.0272	Y
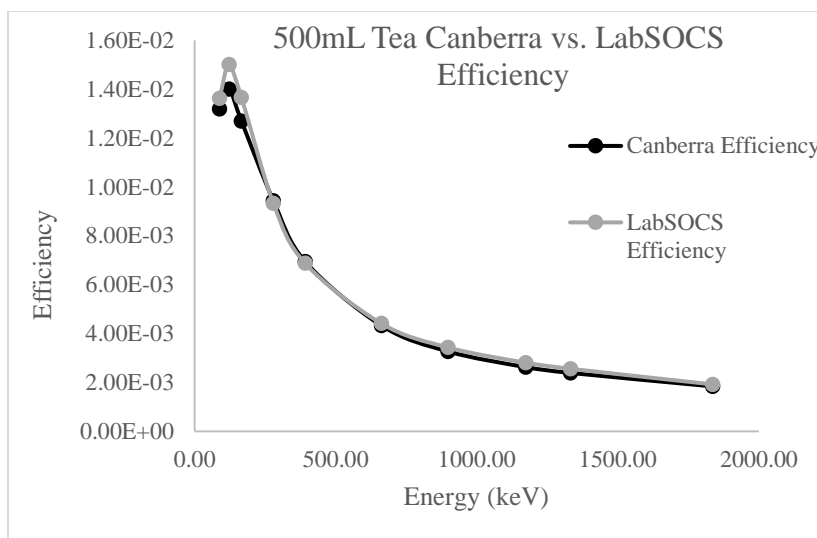
Figure 8. A graph of the Canberra empirical efficiency points versus the LabSOCS modelled efficiency point for the tea 500-mL fill volume in the 500-mL bottle on the Canberra detector.

4.2 DCF and MDC

The reference FDA procedure, WEAC-RN-Method.3.0 Ver. 9.1, uses an indirect method to calculate MDC for sample matrices having a density other than water. This method involves multiplying the appropriate water MDC, which is calculated from first principles, by the corresponding DCF. This method was used for this research. The MDC was therefore calculated directly only for the water sample matrices. The MDCs for the honey and tea sample matrices were calculated indirectly using the water sample MDCs multiplied by the calculated DCFs. Furthermore, MDA and MDC are quantities which are calculated to encompass a predetermined level of uncertainty, in this case, 5% (refer to Section 2.3.3 "Counting Statistics" and Appendix A). Therefore, there is no uncertainty reported with the MDCs calculated for the water sample matrices. The uncertainty introduced by the mathematical manipulation of multiplying the water MDCs by the DCFs was accounted for as the upper bound for the honey and tea sample matrix data set MDCs as a conservative value.

Appendix D contains all the DCFs used to calculate MDC for each radionuclide of concern in the honey and tea sample geometries studied, as well as the MDC values for each circumstance. Appendix D also contains the MDCs for the water sample geometries. The tables of MDCs and DCFs for the 500-mL in the 500-mL bottle for each Canberra sample matrix is shown in Tables 8 through 10, as an example of the results.

Table 8. The FDA DQO for MDC by radionuclide of concern, the corresponding calculated MDC, and the density correction factors for the honey 500-mL fill volume in the 500-mL bottle on the Canberra detector.

Canberra Honey 500-mL in 500-mL Bottle			
Radionuclide	1/3 DIL (Bq/kg)	Calculated MDC (Bq/kg)	DCF
I-131	57	4.19	1.2457
Cs-134+Cs-137	400	8.32	1.2082, 1.2017
Ru-103	2267	3.75	1.2190
Ru-106	150	15.63	1.1981

Table 9. The FDA DQO for MDC by radionuclide of concern, as well as the corresponding measured MDC for the water 500-mL fill volume in the 500-mL bottle on the Canberra detector.

Canberra Water 500-mL in 500-mL Bottle		
Radionuclide	1/3 DIL (Bq/kg)	Calculated MDC (Bq/kg)
I-131	57	4.30
Cs-134+Cs-137	400	8.84
Ru-103	2267	3.91
Ru-106	150	16.60

Table 10. The FDA DQO for MDC by radionuclide of concern, the corresponding calculated MDC, and the density correction factors for the tea 500-mL fill volume in the 500-mL bottle on the Canberra detector.

Canberra Tea 500-mL in 500-mL Bottle			
Radionuclide	1/3 DIL (Bq/kg)	Calculated MDC (Bq/kg)	DCF
I-131	57	8.03	0.8755
Cs-134+Cs-137	400	17.87	0.9423, 0.9535
Ru-103	2267	7.64	0.9110
Ru-106	150	34.43	0.9675

The DCFs were expected to be greater than one for the honey sample matrix data sets and less than one for the tea sample matrix sets. This is because the reference efficiency of water should have been greater than the corresponding efficiency for honey because the less dense water should have experienced less sample self-attenuation. For tea, this reference efficiency of water should have been less than the corresponding efficiency for tea because the less dense tea should have experience less sample self-attenuation. As we observed, 95% of the DCFs calculated for honey were greater than one. However, only 90% of the tea DCFs were less than one. This deviation from the expected density corrections is thought to be due to inadequate homogenization of the tea. If the activity was concentrated in a hot spot of clustered, spiked tea leaves, then the tea sample matrices may have experienced greater geometry-related attenuation (i.e. increased height between the source and the detector), lowering the efficiency to be closer to or below the corresponding water efficiency. This speculation is supported by the observation that the LabSOCS DCFs were all lower than one, and to a consistently greater degree than either the ORTEC or the Canberra DCFs. The LabSOCS DCFs were based on using an ideal, perfectly homogenized modelled sample matrix and were not affected by inadequate homogenization, that was apparently experience by the empirical data sets were.

The calculated MDCs for all radionuclides of concern for all sample geometries studied were found to be less than one third of the corresponding derived intervention limits. This is the DQO the FDA uses to determine whether the method of detection used can meet the desired sensitivity for the reference procedure, WEAC-RN-Method.3.0 Ver. 9.1. The MDCs were calculated based off the 75-minute count time used to collect the DI water blank background information. The largest calculated MDC for each radionuclide were all associated with the Canberra tea 400-mL in the 500-mL bottle sample scenario that are displayed in Table 11. These most conservative MDCs were then recalculated for various count time increments and plotted to illustrate how they would increase with decreasing count times, as shown in Figures 9 through 12. The minimum count that could then be used to analyze a sample, based off these most conservative MDCs, would need to be around 20-minutes. At 20-minutes, the detectors can detect less than the goal of one third of a DIL. This is a reasonable sample analysis time for the type of rapid, qualitative screening this procedure is associated with and is less than the decision rule for maximum count time associated with hypothesis 2.

Table 11. The most conservative MDCs for both a 75-min count time and a 20-min count time for each radionuclide of concern.

Most Conservative MDCs			
Radionuclide	1/3 DIL (Bq/kg)	75-min Calculated MDC (Bq/kg)	20-min Calculated MDC (Bq/kg)
I-131	57	11.50	43.13
Cs-134+Cs-137	400	20.18	75.68
Ru-103	2267	8.03	30.10
Ru-106	150	36.35	136.30
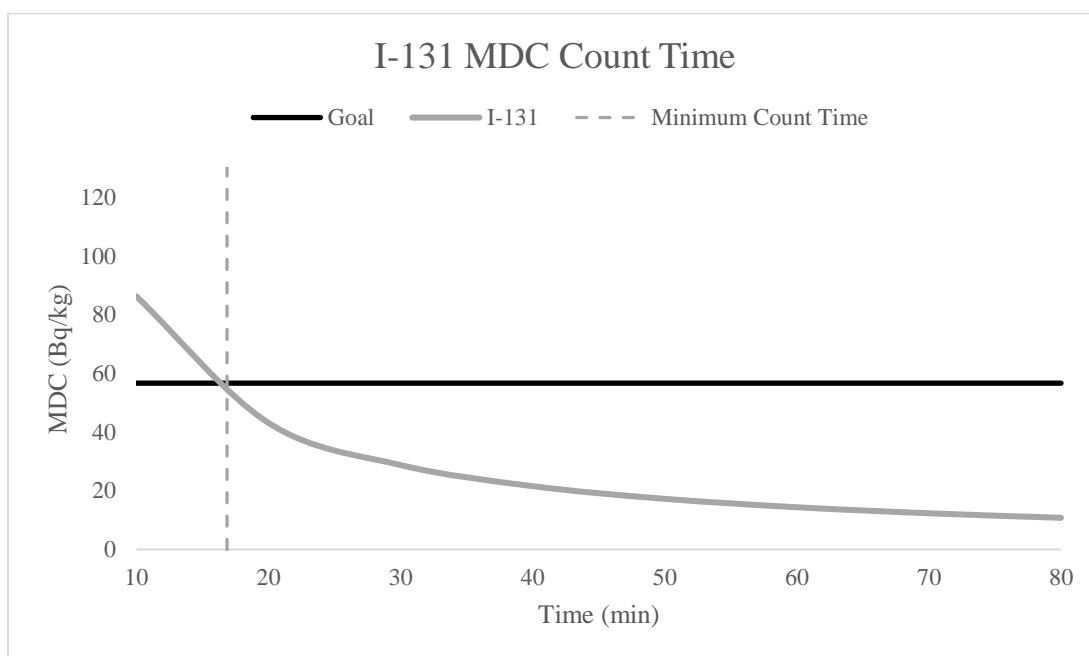
Figure 9. A graph of how the MDC for I-131 would change over various count times.
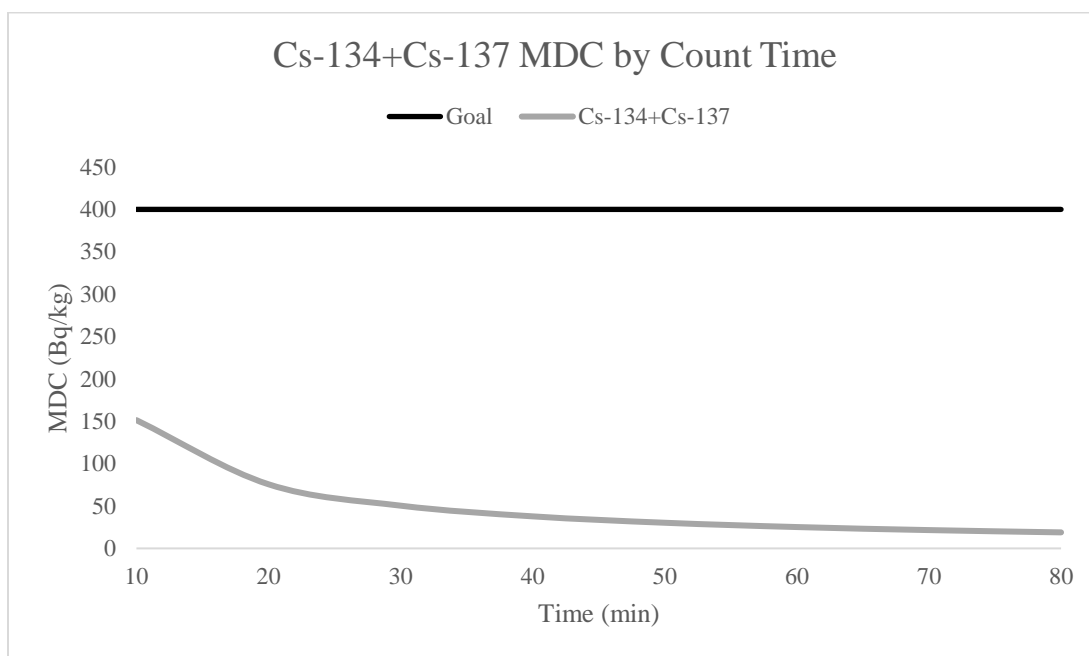
Figure 10. A graph of how the MDC for Cs-134+Cs-137 would change over various count times.

Ru-103 MDC by Count Time
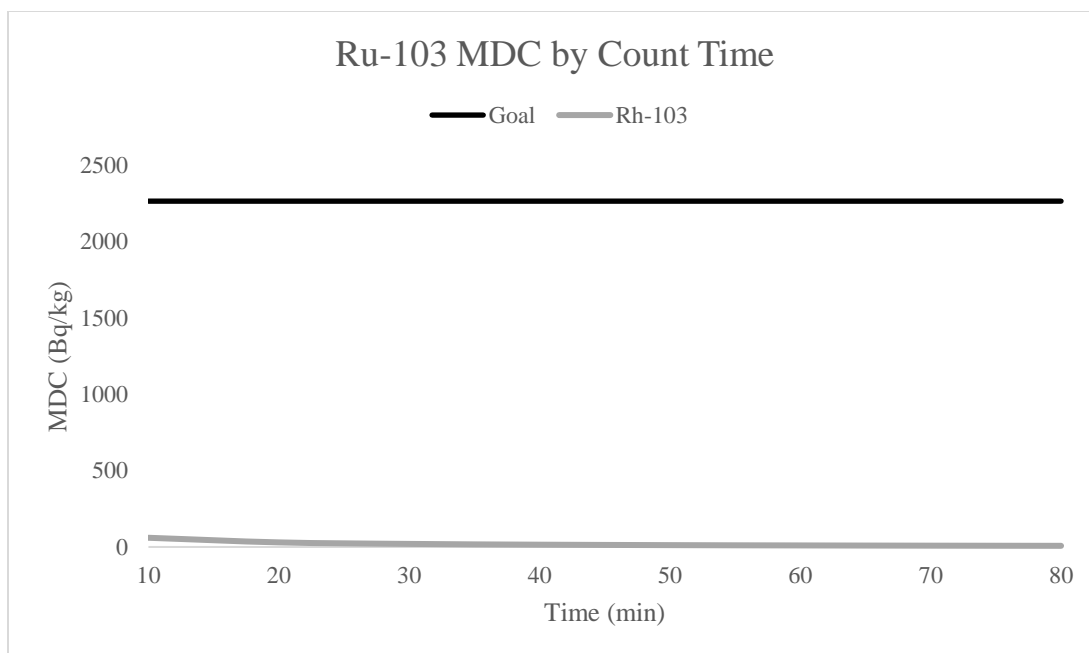
Figure 11. A graph of how the MDC for Rh-103 would change over various count times.

Ru-106 MDC by Count Time
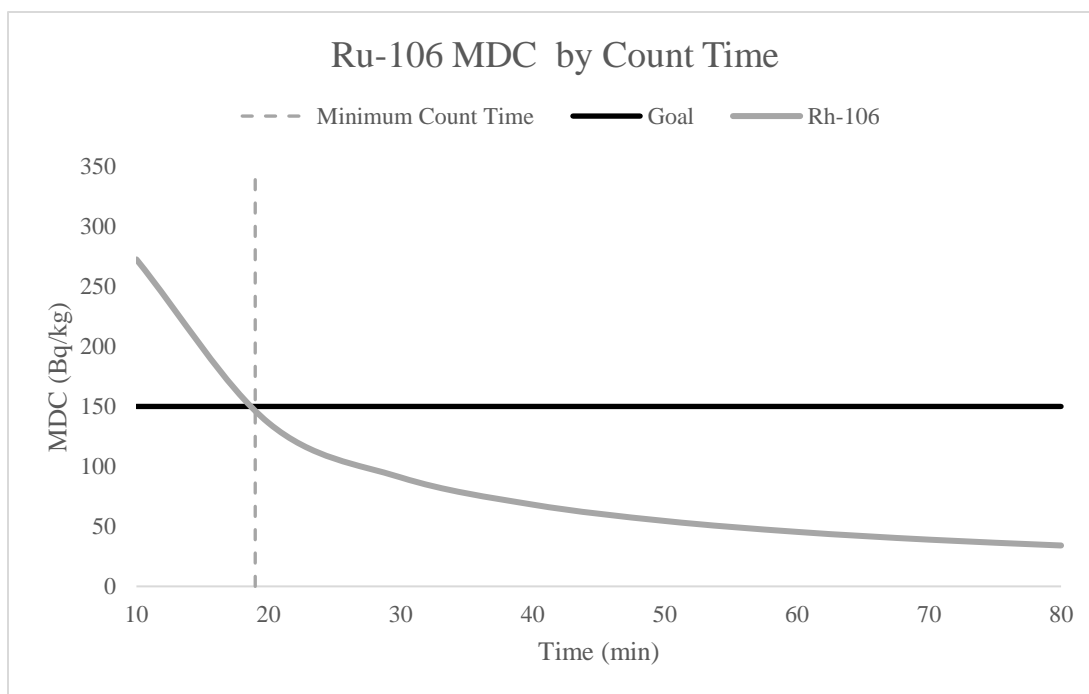
Figure 12. A graph of how the MDC for Rh-106 would change over various count times.

4.3 MAPEP Verification

The results of the MAPEP sample counts are displayed in Tables 12 through 19. Each

sample was counted twice on the Canberra detector and twice on the ORTEC detector. The net

counts for each were then associated with the either the LabSOCS or ORTEC tea 500-mL in the

500-mL bottle efficiency curves, or the LabSOCS or ORTEC water 1-L in the 1-L bottle

efficiency curves, according to the sample matrix and appropriate detector, to determine activity.

The Canberra efficiency curves were not used here because the LabSOCS efficiency curves were

considered representative of the Canberra efficiencies if adequate homogenization for the tea

samples had been attained. MAPEPs are considered to have uniform and constant suspension,

without settling, of the spiked radioactive material used, therefore the LabSOCs values were

considered more appropriate.

Table 12. The known activity and associated uncertainty and the measured activity and associated uncertainty for the vegetation MAPEP, first count, on the Canberra detector.

Canberra Veg MAPEP Count #1				
Radionuclide	Known Activity (Bq/sample)	Uncertainty (Bq/sample)	Measured Activity (Bq/sample)	Uncertainty (Bq/Sample)
Cs-134	3.2	0.1	5.3	0.8
Cs-137	3.7	0.1	2.9	0.6
Co-57	4.4	0.1	5.6	1.3
Co-60	2.3	0.1	2.4	0.7
Mn-54	2.7	0.1	2.7	0.8

Table 13. The known activity and associated uncertainty and the measured activity and associated uncertainty for the vegetation MAPEP, second count, on the Canberra detector.

Canberra Veg MAPEP Count #2				
Radionuclide	Known Activity (Bq/sample)	Uncertainty (Bq/sample)	Measured Activity (Bq/sample)	Uncertainty (Bq/Sample)
Cs-134	3.2	0.1	5.2	0.8
Cs-137	3.7	0.1	3.2	0.6
Co-57	4.4	0.1	4.4	5.9
Co-60	2.3	0.1	2.8	0.8
Mn-54	2.7	0.1	2.6	0.6

Table 14. The known activity and associated uncertainty and the measured activity and associated uncertainty for the water MAPEP, first count, on the Canberra detector.

Canberra Water MAPEP Count #1				
Radionuclide	Known Activity (Bq/L)	Uncertainty (Bq/L)	Measured Activity (Bq/L)	Uncertainty (Bq/L)
Cs-134	11.5	0.2	10.8	2.1
Cs-137	16.3	0.3	15.1	2.0
Co-57	12.1	0.3	11.8	0.3
Co-60	10.7	0.3	11.8	3.3
Mn-54	14.9	0.3	14.0	2.3

Table 15. The known activity and associated uncertainty and the measured activity and associated uncertainty for the water MAPEP, second count, on the Canberra detector.

Canberra Water MAPEP Count #2				
Radionuclide	Known Activity (Bq/L)	Uncertainty (Bq/L)	Measured Activity (Bq/L)	Uncertainty (Bq/L)
Cs-134	11.5	0.2	10.8	2.1
Cs-137	16.3	0.3	14.8	2.0
Co-57	12.1	0.3	13.5	3.5
Co-60	10.7	0.3	11.2	1.4
Mn-54	14.9	0.3	14.5	2.4

Table 16. The known activity and associated uncertainty and the measured activity and associated uncertainty for the vegetation MAPEP, first count, on the ORTEC detector.

ORTEC Veg MAPEP Count #1				
Radionuclide	Known Activity (Bq/sample)	Uncertainty (Bq/sample)	Measured Activity (Bq/sample)	Uncertainty (Bq/Sample)
Cs-134	3.2	0.1	3.3	0.3
Cs-137	3.7	0.1	4.1	0.4
Co-57	4.4	0.1	4.5	1.6
Co-60	2.3	0.1	2.5	0.3
Mn-54	2.7	0.1	3.1	0.4

Table 17. The known activity and associated uncertainty and the measured activity and associated uncertainty for the vegetation MAPEP, second count, on the ORTEC detector.

ORTEC Veg MAPEP Count #2				
Radionuclide	Known Activity (Bq/sample)	Uncertainty (Bq/sample)	Measured Activity (Bq/sample)	Uncertainty (Bq/Sample)
Cs-134	3.2	0.1	3.2	0.3
Cs-137	3.7	0.1	4.2	0.4
Co-57	4.4	0.1	4.7	1.4
Co-60	2.3	0.1	2.3	0.4
Mn-54	2.7	0.1	2.9	0.4

Table 18. The known activity and associated uncertainty and the measured activity and associated uncertainty for the water MAPEP, first count, on the ORTEC detector.

ORTEC Water MAPEP Count #1				
Radionuclide	Known Activity (Bq/sample)	Uncertainty (Bq/sample)	Measured Activity (Bq/sample)	Uncertainty (Bq/Sample)
Cs-134	11.5	0.2	11.1	0.7
Cs-137	16.3	0.3	16.4	0.9
Co-57	12.1	0.3	12.1	0.9
Co-60	10.7	0.3	10.3	0.8
Mn-54	14.9	0.3	14.7	1.2

Table 19. The known activity and associated uncertainty and the measured activity and associated uncertainty for the water MAPEP, second count, on the ORTEC detector.

ORTEC Water MAPEP Count #2				
Radionuclide	Known Activity (Bq/sample)	Uncertainty (Bq/sample)	Measured Activity (Bq/sample)	Uncertainty (Bq/Sample)
Cs-134	11.5	0.2	10.3	0.7
Cs-137	16.3	0.3	16.7	0.9
Co-57	12.1	0.3	11.1	0.8
Co-60	10.7	0.3	11.0	0.8
Mn-54	14.9	0.3	14.9	1.2

A one-sample T-test using a significance level of 5% was used to compare the measured activity to the known activity as reported by RESL. The calculated t values were less than the critical t values in all instances, indicating the differences between the measured activities and the known activities are not statistically significant. Therefore, the data is consistent with H0 (3) and HA (3) is rejected. The use of the efficiency curves determined in this study to calculate an activity for these MAPEP samples results in an activity that does not differ in a statistically significant manner at a significance level of 0.05, to the known activities.

4.4 Background Fluctuation

An increase in the number of background counts would result in an increase in the MDA or MDC. However, this is only true if the background counts detected were caused by the presence of the radionuclide of interest for which the MDC is being calculated, or by a radionuclide with a characteristic energy line very close to the characteristic energy line of the radionuclide of interest. The background study was conducted to obtain a visual of the fluctuation of the background counts for the FDA radionuclides of interest if the detector shield was left open. Under normal operations, a detector shield would not be left open; however, due

to the small size of the Canberra detector's shielding and limitations in the LabSOCS software, the detector shield was left open during analysis for this research.

The radionuclides of interest for the reference FDA procedure are all fission products, and thus are not expected to be a part of a typical background spectrum. Thus, the peak area value for the region of interest for these radionuclides of interest was "forced" by the Genie 2000 analysis software, regardless of whether a peak could be observed in this energy region or not, for the purpose of this study. Subsequently, the values reported often had very large uncertainties associated with them. This data is displayed graphically in Figures 13 through 16.

The data gathered using the Canberra detector with the shield open yielded larger values of detected counts than those observed using the ORTEC detector with the shield closed, as displayed in Figures 13 through 16. The error associated with those larger values was also considerably larger.
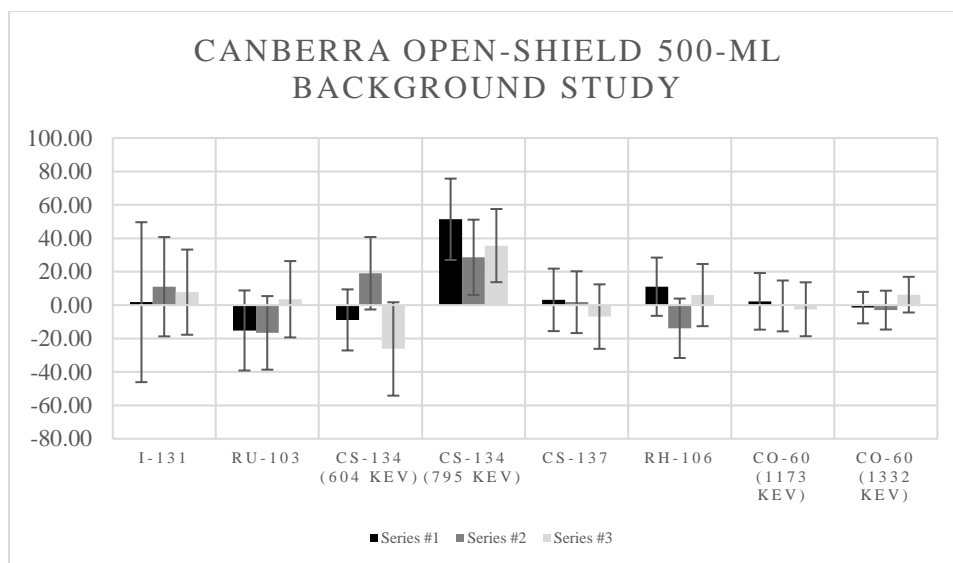
Figure 13. The net peak area counts detected by the Canberra detector, open-shield, for the three 500-mL background water studies.
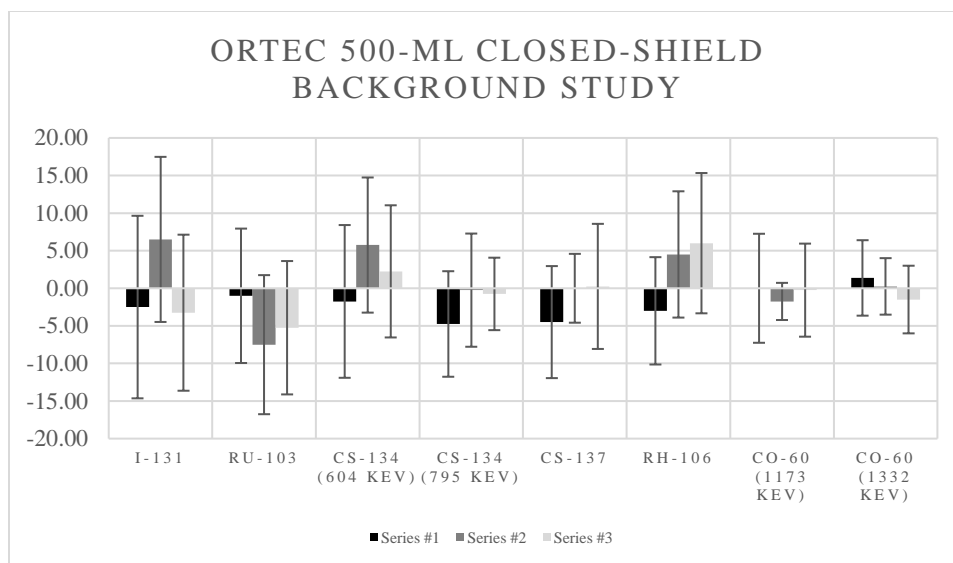
Figure 14. The net peak area counts detected by the ORTEC detector, closed-shield, for the three 500-mL background water studies.
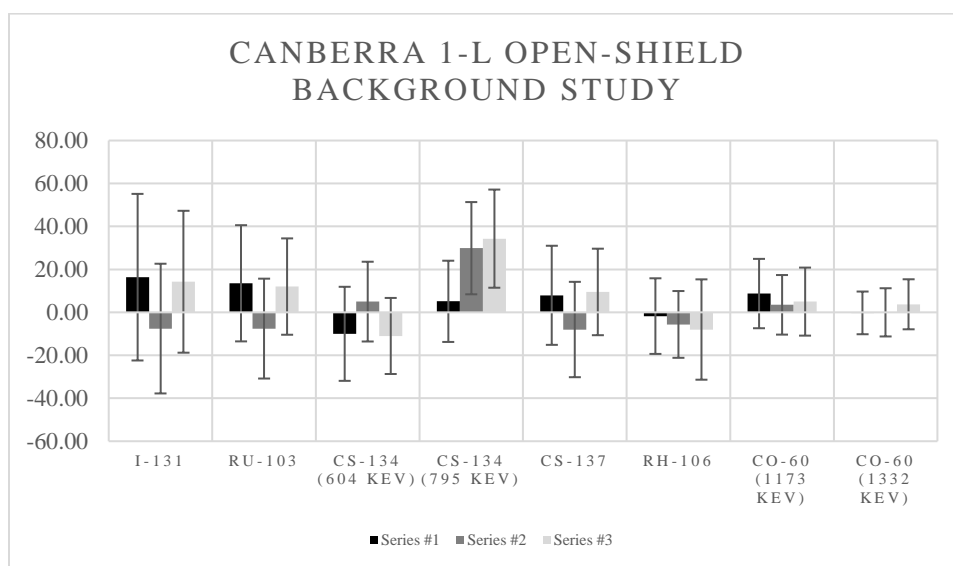
Figure 15. The net peak area counts detected by the Canberra detector, open-shield, for the three 1-L background water studies.
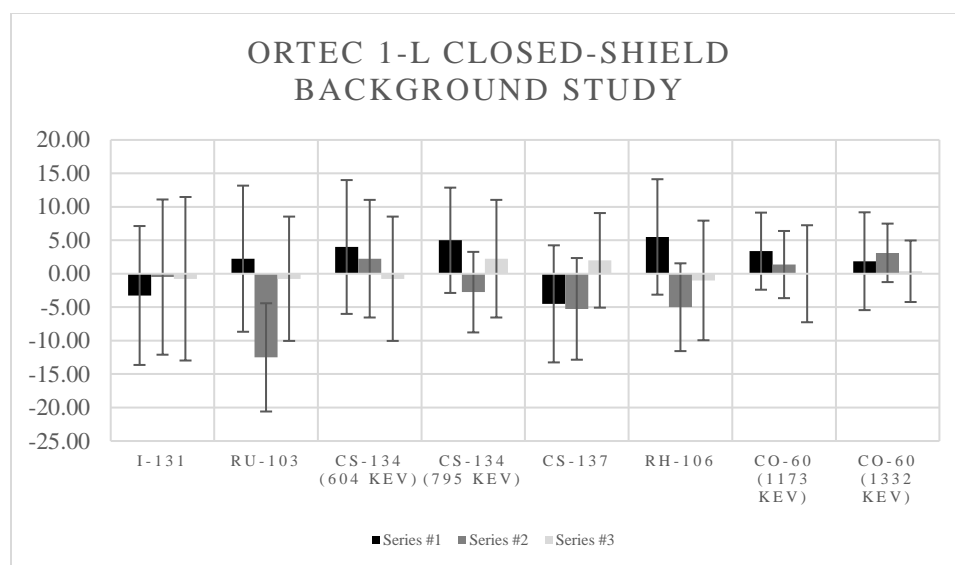
Figure 16. The net peak area counts detected by the ORTEC detector, closed-shield, for the three 1-L background water studies.

The largest peak areas reported for the open-shield Canberra study was for Cs-134. This

is possibly due to the characteristic energy line of Cs-134, at 795.8 keV, being very close to that

of the naturally occurring radionuclide Pa-234, at 796.1 keV, causing some instances of Pa-234

detection to be incorrectly summed in to the Cs-134 region of interest (Chu, Ekström, Firestone

1999). An analysis of these results led to the conclusion that counting with the shield open may

increase the error in the background values used to calculate MDC if a forced analysis is used to

determine region of interest peak areas. However, if an unforced analysis is used, it is unlikely

that this would affect the MDCs for this procedure because all the radionuclides of interest are

fission products and should not be naturally present in the background spectrum. Therefore, an

unforced analysis would not be expected to detect a peak in the region of interest for the

radionuclides of interest, and no background peak value would be reported.

Chapter 5: Conclusion

The LabSOCS model met the decision criteria established for the first null hypothesis, therefore the data is consistent with H0 (1) and HA (1) is rejected. Consistent with the result of this hypothesis test, using an appropriately characterized LabSOCS system to model the proposed container yields efficiency data that adequately represents the corresponding empirical efficiency data for these sample matrices. The calculated MDCs all met the decision criteria established for the second null hypothesis, therefore the data is consistent with H0 (2) and HA (2) is rejected. Consistent with the results of the hypothesis tests, using the proposed container for these sample matrices resulted in an MDC for the used detectors that was adequate per FDA DQOs. Additionally, these MDCs are attainable in a count time that is considered reasonable (i.e. less than 30 minutes) for this type of analysis screening process. This was acceptably verified using a set of standard, external quality assurance samples. The proposed container is therefore considered to have geometrical properties sufficient to meet the data quality objectives of the FDA and could viably be used to complete Laboratory Procedure WEAC-RN-Method.3.0 Version 9.1 "Determination of Gamma-Ray Emitting Radionuclides in Foods by High-Purity Germanium Spectroscopy." The potential for this container to be used for both time saving and cross contamination mitigation purposes is considered viable and worthy of further evaluation.

Chapter 6: Future Works

For the proposed container to be adopted by FERN as an approved method, the modification to procedure WEAC-RN-Method.3.0 Version 9.1 would need to be submitted to the FERN Methods Coordination Committee (MCC) according to the written standard operating procedure (SOP). If considered relevant and applicable by the MCC, the modified procedure would then be subject to a technical review, which follows a rigid SOP and checklist set forth by the MCC. Prior to submittal to the MCC, several additional, future studies are recommended.

The ability to achieve consistent, adequate homogenization of the spiked sample matrices and keep the solutions consistently homogenized during the 75-minute count time used to characterize the empirical efficiency curves, proved very difficult. It is therefore recommended that future works involving this bottle have a standard professionally made in the proposed container using radioactive material permanently and homogenously suspended in a static, fixed, density equivalent matrix. The creation of such standard would allow for more reproducible results, allowing for multiple studies into the MDC of the proposed container relative to many different detectors. It is recommended that studies such as this be conducted at several FERN certified laboratories to ensure the MDC of the proposed container is adequate across the applicable range of potential detectors with subtle geometry differences. An evaluation of whether a significant amount of sample settling and return to heterogeneity occurs during the shorter count time used for actual samples should also be conducted. In conjunction with MDC studies, participating laboratories should conduct practice tests using the current procedure and container, and then using the proposed substitute container. This would yield information on estimated time savings across multiple laboratories, as well as allow for data regarding cross contamination to be gathered. Both are recommended future studies.

REFERENCES

Armbruster, D. A., & Pry, T. (2008, August). Limit of Blank, Limit of Detection, Limit of Quantification. *The Clinical Biochemist Reviews*, pp. S49-S52.

Bronson, F. (2003, January). Validation of the Accuracy of the LabSOCS Software for Mathematical Efficiency Calibration of Ge Detectors for Typical Laboratory Samples. *Journal of Radioanalytical and Nuclear Chemistry, 255*(1), pp. 137-141.

Brooks, S. (2016). *Food Emergency Response Network (FERN): Integrating the Nation's Food Testing Laboratories to Improve Food Defense and Food Safety System.* U.S. Food and Drug Administration.

Cap and Neck Finishes. (2018). Retrieved from SKS Bottle & Packaging, Inc.: https://www.sks-bottle.com/CapNeck.html

Cember, H., & Johnson, T. (2009). *Introduction to Health Physics* (Fourth ed.). New Baskerville: The McGraw-Hill Companies, Inc.

Chu, S., Ekstrom, L., & Firestone, R. (1999, February). *WWW Table of Radioactive Isotopes*. Retrieved from The Lund.LBNL Nuclear Data Search Version 2.0: http://nucleardata.nuclear.lu.se/toi/Gamma.asp?sql=&Min=794.8&Max=796.8

Currie, L. A. (1968). Limits for Qualitative Detection and Quantitative Determination: Application to Radiochemistry. *Analytical Chemistry, 40*, pp. 586-593.

Day, E. (2009). *Lessons Learned from TOPOFF 4- 9385.* Manassas: Pell Resources Company.

FERN. (2018). Retrieved from fernlab.org: https://www.fernlab.org/

Gilmore, G. (2008). *Practical Gamma-ray Spectroscopy* (Second ed.). Chichester: John Wiley & Sons Ltd.

Gomez-Diaz, D., Navaza, J., & Quintans-Riveiro, L. (2009). Effect of Temperature on the Viscosity of Honey. *International Journal of Food Properties*, pp. 396-404.

Healey, S. (2015). *Gamma Spectrometry Analysis for Food.* U.S. Food and Drug Administration.

Healey, S. (2016). *FERN Gamma Spectrometric Methods.* U.S. Food and Drug Administration.

ISOCS/LabSOCS Detector Efficiency Characterization. (2017). Retrieved from canberra.com: http://www.canberra.com/products/radiochemistry_lab/isocs-characterization.asp

Knoll, G. F. (2010). *Radiation Detection and Measurement.* Hoboken: John Wiley & Sons, Inc.

Martin, J. E. (2013). *Physics for Radiation Protection* (Third ed.). Weinheim: Wiley-VCH Verlag GmbH & Co.

Office of Plant and Dairy Foods in the Center for Food Safety and Applied Nutrition. (2005). *CPG Sec.560.750 Radionuclides in Imported Foods- Levels of Concern.* U.S. Food and Drug Administration.

Oresegun, M. O., Decker, K., & Sanderson, C. (1993). Determination of Self-Sbsoprtion Corrections by Computation in Routine Gamma-Ray Spectrometry for Typical Environmental Samples. *Radioactivity & Radiochemistry, 4*(1), pp. 38-45.

Peck, R. (2015). *Statistics: Learning from Data.* Stamford: Cengage Learning.

Radiological Response: Assessing Environmental and Clinical Laboratory Capabilities. (2007). *Hearing before the Subcommitte on Investigations and Oversight Committee on Science and Technology House of Representatives One Hundred Tenth Congress* (p. 43). Washington, D.C.: U.S. Government Printing Office.

Rolle, C., Healey, S., & Lin, Z. (2016). *Density Corrections for the Detection of Radioactive Contamination in Food with Gamma Spectroscopy.* Winchester Engineering and Analytical Center, U.S. Food and Drug Administration.

Tsoulfanidis, N., & Landsberger, S. (2011). *Measurement and Detection of Radiation* (Third ed.). Boca Raton: Taylor & Francis Group.

U.S. Food and Drug Administration. (1998). *Accidental Radioactive Contamination of Human Food and Animal Feeds: Recommnedations for State and Local Agencies.*

Winchester Engineering and Analytical Center. (2014). *Determination of Gamma-Ray Emitting Radionuclides in Foods by High-Purity Germanium Spectroscopy.* FDA Office of Regulatory Affairs.

Zi-Ning, T., Xiao-Ping, O., Yang, L., Liang, C., Jin-Liang, L., Xian-Peng, Z., . . . Ming, Z. (2014). Self-attenuation Corrections Calculated by LabSOCS Simulations for Gamma-Spectrometric Measurements with HPGe Detectors. *Chinese Physics C, 38*(7), p. 076002.

APPENDICES

Appendix A: Counting Statistics: L_C, L_D, MDA

Appendix B: Certificate for Liquid Mixed Gamma Source

Appendix C: Modelled and Empirical Efficiency Curves and Percentages by Source Energy Lines

Appendix D: Modelled and Empirical Efficiency Data DILs, MDCs, and DCFs

Appendix A

Counting Statistics: L$_C$, L$_D$, MDA

Radioactive decay is best describe using a Poisson distribution. The standard deviation of a Poisson distribution is:

$$\sigma = \sqrt{\bar{x}} \qquad \text{Equation 1}$$

Where: σ= the standard deviation
$\bar{x}$= the mean. In the case of counting statistics, this taken to be the total number of recorded counts, x.

The fractional standard deviation, which is the conventional method of calculating counting error for radioactivity, is then:

$$\sigma = \frac{\sqrt{x}}{x} = \frac{1}{\sqrt{x}} \qquad \text{Equation 2}$$

The critical limit, L$_c$, is conventionally based off the desire to attain a 95% confidence level that the net count perceived by the detector is not statistically significant. In other words, if a net count greater than background is seen, there is a 95% that it can be attributed to the statistical fluctuation in the counts, and only a 5% chance it is truly above background. The z-score associated with this situation, a one-tailed confidence interval at 95%, is 1.645. Consider the equation for net counts:

$$Net\ Counts\ (Net) = Total\ Counts(Tot) - Background\ Count(Bkg) \quad \text{Equation 3}$$

Standard propagation of error for this equation would give the variance in the net counts as follows:

$$\sigma_{net}^2 = \sigma_{tot}^2 + \sigma_{bkg}^2 \qquad \text{Equation 4}$$

For the situation of L_c, the total counts would be equal to the background counts because the sample being considered is one that that has no activity above background. The variance then becomes:

$$\sigma_{net}^2 = \sigma_{bkg}^2 + \sigma_{bkg}^2 = 2\sigma_{bkg}^2 \quad \text{Equation 5}$$

Stated as error and substituting Equation 1:

$$\sigma_{net} = \sqrt{2}\sigma_{bkg} = 1.4142\sqrt{Bkg} \qquad \text{Equation 6}$$

Taken at the 95% confidence level:

$$\sigma_{net} = 1.645 \times 1.4142\sqrt{Bkg} = 2.33\sqrt{Bkg} \quad \text{Equation 7}$$

This is L_c, the level at which a 5% error is accommodated in the observation that a sample is not above background.

The detection limit, L_D, is conventionally based off the desire to attain a 95% confidence level that net counts which are truly above background will be detected, and only a 5% chance the positive counts would be attributed to statistical fluctuations in the background counts. Let σ_D be equal to the standard deviation of a sample with net counts equal to the exact level of L_D and k_β be the z-score associated with the desired confidence level for L_D, decided here to be 95%. Let σ_0 and k_α be the standard deviation of the net counts when the net counts is equal to 0 (the situation described by L_C) and the z-score associated with the desired confidence level associated with L_C, decided here to be 95%.

$$L_D = L_C + k_\beta \sigma_D = k_\alpha \sigma_0 + k_\beta \sigma_D \qquad \text{Equation 8}$$

Remember that α and β are both 95%, therefore $k_\alpha = k_\beta = 1.645$, and the net counts is equal to L_D. A quick substitution of Equation 1 into Equation 4, using the σ_D notation established above, yields:

$$\sigma_{net}^2 = \sigma_D^2 = \sqrt{Tot}^2 + \sqrt{Bkg}^2 = Tot + Bkg \quad \text{Equation 9}$$

For the situation of L_D, the total counts must be equal to L_D plus the background counts for the

net counts to be equal to L_D, as follows:

$$Net = Tot - Bkg = L_D + Bkg - Bkg = L_D \qquad \text{Equation 10}$$

Restating Equation 6 using the σ_0 notation established above yields:

$$\sigma_0^2 = 2Bkg \quad \text{Equation 11}$$

Combining Equation 9, 10, and 11 yields:

$$\sigma_D^2 = L_D + Bkg + Bkg = L_D + 2Bkg = L_D + \sigma_0^2 \quad \text{Equation 12}$$

Substituting Equation 12 into Equation 8, and remembering $k_\alpha = k_\beta = 1.645$, yields:

$$L_D = k_\alpha \sigma_0 + k_\alpha \sqrt{L_D + \sigma_0^2} \quad \text{Equation 13}$$

Several algebraic manipulations of this equation rearranges it to:

$$L_D = k_\alpha^2 + 2k_\alpha \sigma_0 \quad \text{Equation 14}$$

Substitution of $k_\alpha = 1.645$ and Equation 11 gives:

$$L_D = 2.71 + 4.65 \sqrt{Bkg} \qquad \text{Equation 15}$$

This is L_D, the level at which a 5% error is accommodated in the observation that a sample is

above background.

The minimum detectable activity, MDA, is the activity equivalent of L_D and is derived by

changing L_D, a level associated with counts, to an activity using:

$$A = \frac{C}{E \times Y \times t} \qquad \text{Equation 16}$$

Where: A=activity
C=counts
E= efficiency of the detector
Y= yield
t= count time

In the case of MDA, the counts are equal to L_D, therefore:

$$MDA = \frac{L_D}{E \times Y \times t} \qquad \text{Equation 17}$$

The minimum detectable concentration, MDC, is found by simply dividing MDA by mass to yield an activity per mass value. The equations for MDA or MDC are occasionally broken down into the elemental components of L_D and may be decay corrected for a source using the decay equation:

$$A = A_0 e^{-\lambda t} \quad \text{Equation 18}$$

Where: A= the activity at the desired time
A_0= the initial activity, in this case, the uncorrected MDA
λ= the decay coefficient
t= time

This appendix was prepared using statements from *Practical Gamma Ray Spectroscopy* by Gordon Gilmore and *Radiation Detection and Measurement* by Glenn F. Knoll, as well as notes and discussions from Dr. Richard Brey, Professor of Health Physics at Idaho State University during the years 2017-2018.

Appendix B

Certificate for Liquid Mixed Gamma

Eckert & Ziegler
Analytics

1380 Seaboard Industrial Blvd.
Atlanta, Georgia 30318
Tel 404·352·8677
Fax 404·352·2837
www.ezag.com

CERTIFICATE OF CALIBRATION
Standard Reference Source

SRS Number: 109376   ES# 5 77 22
Source Description: 5 mL Liquid in NIST Flamed Sealed Ampoule
Product Code: 8400
Customer: Idaho State University
P.O. Number: P0027125, Item 1

This standard radionuclide source was prepared from an aliquot measured gravimetrically from a master radionuclide solution calibrated with a germanium gamma-ray spectrometer system. Calibration and purity were checked using germanium gamma-ray spectrometry. At the time of calibration no interfering gamma-ray emitting impurities were detected. The gamma-ray emission rates for the most intense gamma-ray lines are given. Eckert & Ziegler Analytics (EZA) maintains traceability to the National Institute of Standards and Technology (NIST) through a Measurements Assurance Program as described in USNRC Regulatory Guide 4.15, Revision 2, July 2007, and compliance with ANSI N42.22-1995, "Traceability of Radioactive Sources to NIST."

Reference Date: 01-January-2018   12:00 PM EST

MGS Mixture

Isotope	Gamma-Ray Energy, keV	Half-Life, d	Activity, Bq	Flux, s⁻¹	u_A, %	u_B, %	U, %*	Calibration Method**
Cd-109	88.0	4.614E+02	2.461E+05	9.104E+03	0.5	1.3	2.8	HPGe
Co-57	122.1	2.717E+02	5.586E+03	4.781E+03	0.4	0.7	1.6	HPGe
Ce-139	165.9	1.376E+02	8.406E+03	6.725E+03	0.4	0.9	2.0	HPGe
Hg-203	279.2	4.659E+01	1.812E+04	1.478E+04	0.3	0.8	1.7	HPGe
Sn-113	391.7	1.151E+02	1.438E+04	9.343E+03	0.4	1.2	2.5	HPGe
Cs-137	661.7	1.099E+04	7.050E+03	6.000E+03	0.7	1.2	2.8	HPGe
Y-88	898.0	1.066E+02	2.411E+04	2.259E+04	0.7	0.8	2.1	HPGe
Y-88	1836.1	———	———	2.392E+04	0.7	0.8	2.1	———
Co-60	1173.2	1.925E+03	1.104E+04	1.102E+04	0.7	1.0	2.4	HPGe
Co-60	1332.5	———	———	1.103E+04	0.7	1.0	2.4	———

Mixed Gamma (MGS) master solution is EZA's eight isotope mixture which is calibrated quarterly and consists of Cd-109, Co-57, Ce-139, Hg-203, Sn-113, Cs-137, Y-88, and Co-60. **Uncertainty:** U - Relative expanded uncertainty, k = 2. See NIST Technical Note 1297, "Guidelines for Evaluating and Expressing the Uncertainty of NIST Measurement Results." **Calibration Methods:** 4π LS - 4π Liquid Scintillation Counting, HPGe - High Purity Germanium Gamma-Ray Spectrometer, IC - Ionization Chamber.

(Certificate continued on reverse side)

F-CR-32 Rev. 0, 01 Nov 14

EZA Certificate Program Rev. 0, 07-DEC-2015

Page 1 of 2

Corporate Office
24937 Avenue Tibbitts   Valencia, California 91355

Laboratory
1380 Seaboard Industrial Blvd. Atlanta, Georgia, 30318

SRS Number: 109376

Comments:
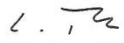
5.30982 g of 4 M HCl solution with approximately 30 µg/g each of Cd, Co, Ce, Hg, Sn, Sr, Cs, and Y carriers.

Expiration Date: 01-January-2019.

Source Prepared by: _____

K. Eardley, Radiochemist

QC Approved by: _____ Date: 13 Apr 18

L. Tkavadze, Nuclear Metrologist

Appendix C

Modelled and Empirical Efficiency Curves and Percentages by Source Energy Lines

Table 20. The efficiencies and associated error by energy line contained within the liquid mixed-gamma source, for the honey 300-mL fill volume in the 500-mL bottle on the ORTEC detector. The density correction factors and an analysis of whether the LabSOCS model would have given a conservative estimate of activity is also included.

ORTEC Honey 300-mL in 500-mL Bottle				
R^2 Predicted:	0.9205	Regression SD	0.0008	
Energy (keV)	Efficiency (%)	Error (%)	DCF	Model Conservative
88	0.0082	0.0002	1.5834	N
122.1	0.0108	0.0002	1.6759	N
165.9	0.0113	0.0002	1.6460	N
279.2	0.0080	0.0002	1.6459	N
391.7	0.0067	0.0002	1.5648	N
661.7	0.0048	0.0001	1.4160	N
898	0.0037	0.0001	1.4658	N
1173.2	0.0030	0.0001	1.4329	N
1332.5	0.0027	0.0001	1.3895	N
1836.1	0.0021	0.0000	1.3961	N
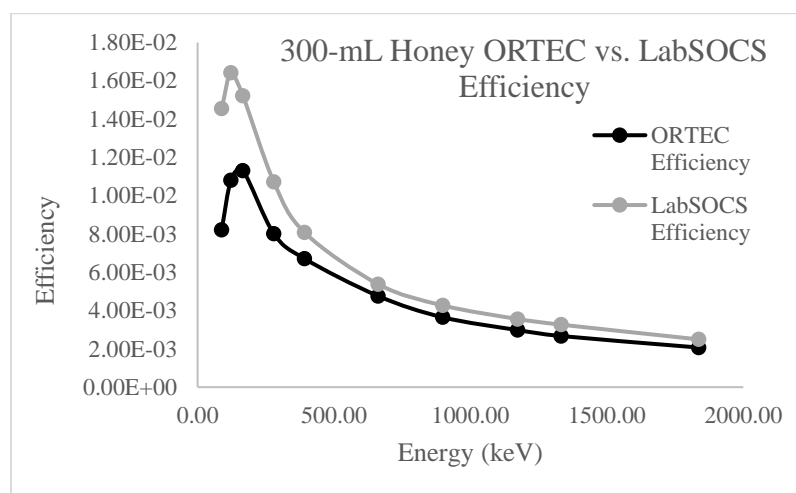
Figure 17. A graph of the ORTEC empirical efficiency points versus the LabSOCS modelled efficiency point for the honey 300-mL fill volume in the 500-mL bottle on the ORTEC detector.

Table 21. The efficiencies and associated error by energy line contained within the liquid mixed-gamma source, for the honey 400-mL fill volume in the 500-mL bottle on the ORTEC detector. The density correction factors and an analysis of whether the LabSOCS model would have given a conservative estimate of activity is also included.

ORTEC Honey 400-mL in 500-mL Bottle				
R^2 Predicted:	0.9084	Regression SD	0.0008	
Energy (keV)	Efficiency (%)	Error (%)	DCF	Model Conservative
88	0.0070	0.0002	1.4530	N
122.1	0.0097	0.0002	1.4508	N
165.9	0.0100	0.0002	1.4300	N
279.2	0.0073	0.0001	1.4050	N
391.7	0.0059	0.0002	1.3946	N
661.7	0.0041	0.0001	1.3245	Y
898	0.0032	0.0001	1.3333	N
1173.2	0.0027	0.0001	1.2830	N
1332.5	0.0024	0.0001	1.2638	N
1836.1	0.0018	0.0000	1.2787	N

Figure 18. A graph of the ORTEC empirical efficiency points versus the LabSOCS modelled efficiency point for the honey 400-mL fill volume in the 500-mL bottle on the ORTEC detector.

Table 22. The efficiencies and associated error by energy line contained within the liquid mixed-gamma source, for the honey 500-mL fill volume in the 500-mL bottle on the ORTEC detector. The density correction factors and an analysis of whether the LabSOCS model would have given a conservative estimate of activity is also included.

ORTEC Honey 500-mL in 500-mL Bottle				
R^2 Predicted:	0.9293	Regression SD	0.0006	
Energy (keV)	Efficiency (%)	Error (%)	DCF	Model Conservative
88	0.0063	0.0002	1.3079	N
122.1	0.0088	0.0002	1.2642	N
165.9	0.0086	0.0002	1.3589	N
279.2	0.0062	0.0001	1.3011	N
391.7	0.0051	0.0001	1.3294	Y
661.7	0.0037	0.0001	1.2425	Y
898	0.0028	0.0001	1.2077	Y
1173.2	0.0024	0.0001	1.1957	Y
1332.5	0.0021	0.0001	1.1787	Y
1836.1	0.0016	0.0000	1.2000	Y

Figure 19. A graph of the ORTEC empirical efficiency points versus the LabSOCS modelled efficiency point for the honey 500-mL fill volume in the 500-mL bottle on the ORTEC detector.

Table 23. The efficiencies and associated error by energy line contained within the liquid mixed-gamma source, for the honey 500-mL fill volume in the 1-L bottle on the ORTEC detector. The density correction factors and an analysis of whether the LabSOCS model would have given a conservative estimate of activity is also included.

ORTEC Honey 500-mL in 1-L Bottle				
R^2 Predicted:	0.9004	Regression SD	0.0011	
Energy (keV)	Efficiency (%)	Error (%)	DCF	Model Conservative
88	0.0094	0.0003	1.1444	N
122.1	0.0135	0.0002	1.1481	N
165.9	0.0144	0.0003	1.1319	Y
279.2	0.0101	0.0002	1.1485	Y
391.7	0.0084	0.0002	1.1176	Y
661.7	0.0059	0.0002	1.0793	Y
898	0.0045	0.0001	1.0776	Y
1173.2	0.0037	0.0001	1.0740	Y
1332.5	0.0033	0.0001	1.0399	Y
1836.1	0.0026	0.0001	1.0431	Y

Figure 20. A graph of the ORTEC empirical efficiency points versus the LabSOCS modelled efficiency point for the honey 500-mL fill volume in the 1-L bottle on the ORTEC detector.

Table 24. The efficiencies and associated error by energy line contained within the liquid mixed-gamma source, for the honey 750-mL fill volume in the 1-L bottle on the ORTEC detector. The density correction factors and an analysis of whether the LabSOCS model would have given a conservative estimate of activity is also included.

ORTEC Honey 750-mL in 1-L Bottle				
R^2 Predicted:	0.8837	Regression SD	0.0008	
Energy (keV)	Efficiency (%)	Error (%)	DCF	Model Conservative
88	0.0059	0.0002	1.2432	N
122.1	0.0083	0.0002	1.2485	N
165.9	0.0091	0.0002	1.2184	Y
279.2	0.0066	0.0001	1.2530	Y
391.7	0.0055	0.0001	1.2220	Y
661.7	0.0040	0.0001	1.1519	Y
898	0.0030	0.0001	1.1755	Y
1173.2	0.0025	0.0001	1.1480	Y
1332.5	0.0022	0.0001	1.1455	Y
1836.1	0.0017	0.0000	1.1503	Y

Figure 21. A graph of the ORTEC empirical efficiency points versus the LabSOCS modelled efficiency point for the honey 750-mL fill volume in the 1-L bottle on the ORTEC detector.

Table 25. The efficiencies and associated error by energy line contained within the liquid mixed-gamma source, for the honey 1-L fill volume in the 1-L bottle on the ORTEC detector. The density correction factors and an analysis of whether the LabSOCS model would have given a conservative estimate of activity is also included.

| ORTEC Honey 1-L in 1-L Bottle				
R^2 Predicted:	0.8629	Regression SD	0.0005	
Energy (keV)	Efficiency (%)	Error (%)	DCF	Model Conservative
88	0.0039	0.0001	1.4742	N
122.1	0.0056	0.0001	1.4640	N
165.9	0.0061	0.0001	1.4029	N
279.2	0.0044	0.0001	1.4379	N
391.7	0.0038	0.0001	1.3596	Y
661.7	0.0027	0.0001	1.2930	Y
898	0.0021	0.0000	1.2676	Y
1173.2	0.0018	0.0000	1.2614	Y
1332.5	0.0016	0.0000	1.2581	N
1836.1	0.0012	0.0000	1.2520	N

Figure 22. A graph of the ORTEC empirical efficiency points versus the LabSOCS modelled efficiency point for the honey 1-L fill volume in the 1-L bottle on the ORTEC detector.

Table 26. The efficiencies and associated error by energy line contained within the liquid mixed-gamma source, for the honey 300-mL fill volume in the 500-mL bottle on the Canberra detector. The density correction factors and an analysis of whether the LabSOCS model would have given a conservative estimate of activity is also included.

Canberra Honey 300-mL in 500-mL Bottle				
R^2 Predicted:	0.9964	Regression SD	0.0002	
Energy (keV)	Efficiency (%)	Error (%)	DCF	Model Conservative
88	0.0115	0.0003	1.6522	N
122.1	0.0124	0.0002	1.6613	N
165.9	0.0116	0.0002	1.6379	N
279.2	0.0079	0.0002	1.5929	N
391.7	0.0065	0.0002	1.5464	N
661.7	0.0044	0.0001	1.4908	N
898	0.0034	0.0001	1.4604	N
1173.2	0.0028	0.0001	1.4357	N
1332.5	0.0025	0.0001	1.4409	N
1836.1	0.0020	0.0000	1.3930	N

Figure 23. A graph of the Canberra empirical efficiency points versus the LabSOCS modelled efficiency point for the honey 300-mL fill volume in the 5m00-L bottle on the Canberra detector.
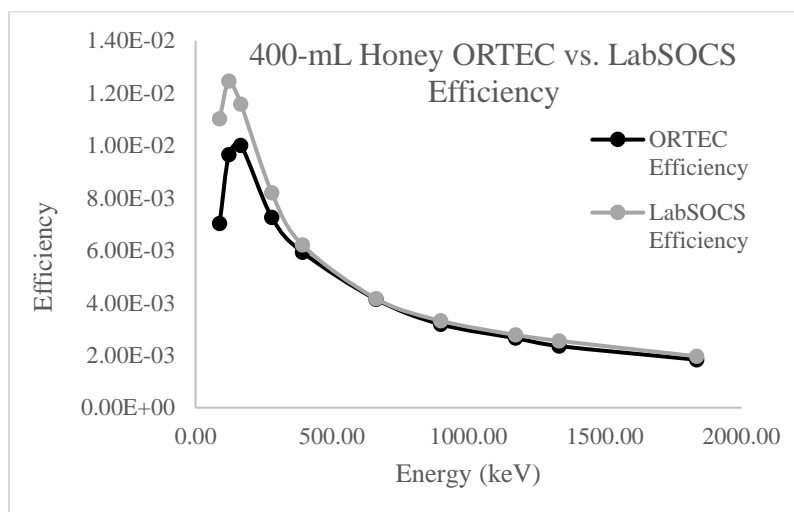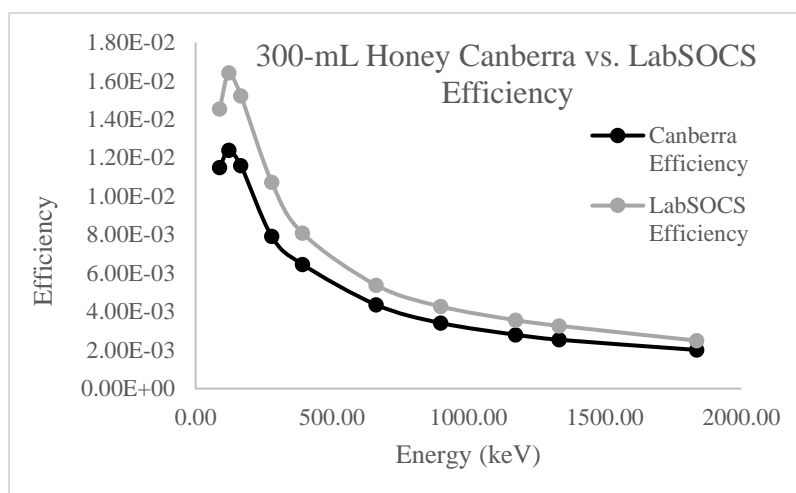
Table 27. The efficiencies and associated error by energy line contained within the liquid mixed-gamma source, for the honey 400-mL fill volume in the 500-mL bottle on the Canberra detector. The density correction factors and an analysis of whether the LabSOCS model would have given a conservative estimate of activity is also included.

Canberra Honey 400-mL in 500-mL Bottle				
R^2 Predicted:	0.9960	Regression SD	0.0002	
Energy (keV)	Efficiency (%)	Error (%)	DCF	Model Conservative
88	0.0099	0.0003	1.5010	N
122.1	0.0106	0.0002	1.5000	N
165.9	0.0100	0.0002	1.4815	N
279.2	0.0068	0.0001	1.4381	N
391.7	0.0054	0.0001	1.4301	N
661.7	0.0038	0.0001	1.3264	N
898	0.0029	0.0001	1.3459	N
1173.2	0.0024	0.0001	1.3182	N
1332.5	0.0022	0.0001	1.2902	N
1836.1	0.0017	0.0000	1.3006	N

Figure 24. A graph of the Canberra empirical efficiency points versus the LabSOCS modelled efficiency point for the honey 400-mL fill volume in the 500-mL bottle on the Canberra detector.
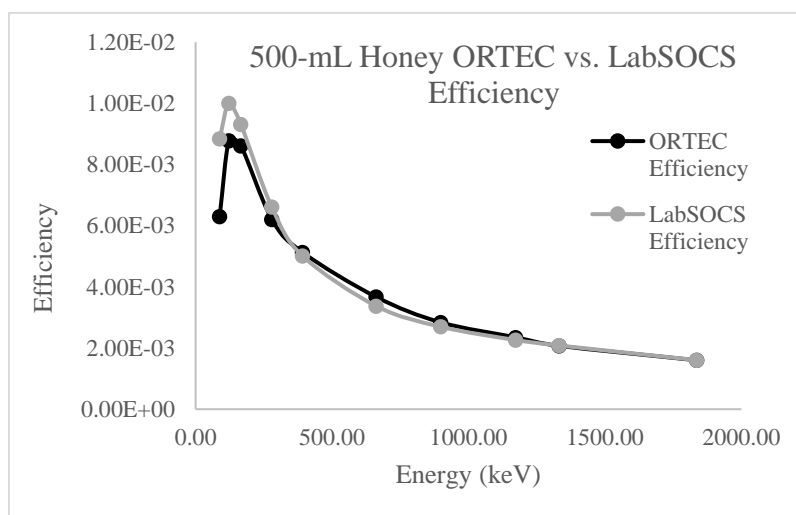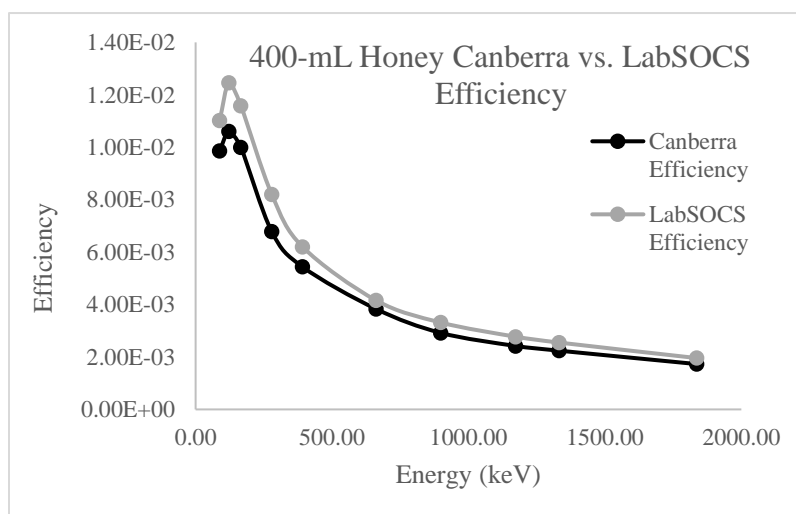
Table 28. The efficiencies and associated error by energy line contained within the liquid mixed-gamma source, for the honey 500-mL fill volume in the 1-L bottle on the Canberra detector. The density correction factors and an analysis of whether the LabSOCS model would have given a conservative estimate of activity is also included.

Canberra Honey 500-mL in 1-L Bottle				
R^2 Predicted:	0.9956	Regression SD	0.0003	
Energy (keV)	Efficiency (%)	Error (%)	DCF	Model Conservative
88	0.0140	0.0004	1.1357	Y
122.1	0.0157	0.0003	1.1338	Y
165.9	0.0148	0.0003	1.1419	Y
279.2	0.0100	0.0002	1.1423	Y
391.7	0.0081	0.0002	1.1084	Y
661.7	0.0055	0.0002	1.0745	Y
898	0.0043	0.0001	1.0751	Y
1173.2	0.0035	0.0001	1.0747	Y
1332.5	0.0032	0.0001	1.0694	Y
1836.1	0.0025	0.0001	1.0607	Y

Figure 25. A graph of the Canberra empirical efficiency points versus the LabSOCS modelled efficiency point for the honey 500-mL fill volume in the 1-L bottle on the Canberra detector.
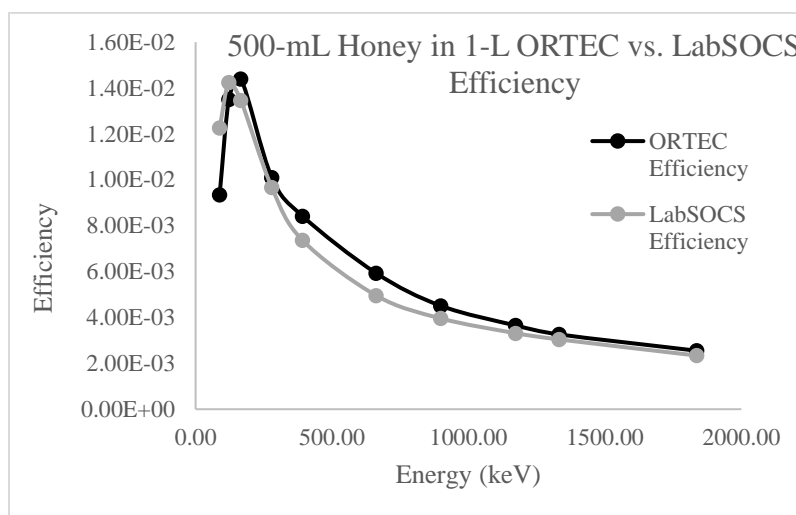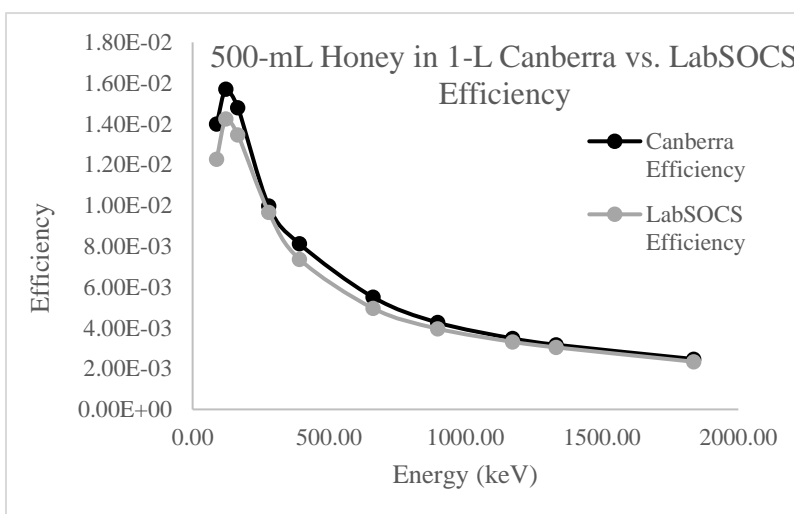
Table 29. The efficiencies and associated error by energy line contained within the liquid mixed-gamma source, for the honey 750-mL fill volume in the 1-L bottle on the Canberra detector. The density correction factors and an analysis of whether the LabSOCS model would have given a conservative estimate of activity is also included.

Canberra Honey 750-mL in 1-L Bottle				
R^2 Predicted:	0.9957	Regression SD	0.0002	
Energy (keV)	Efficiency (%)	Error (%)	DCF	Model Conservative
88	0.0089	0.0003	1.3805	Y
122.1	0.0100	0.0002	1.3869	Y
165.9	0.0096	0.0002	1.3674	Y
279.2	0.0065	0.0001	1.3760	Y
391.7	0.0054	0.0001	1.3506	Y
661.7	0.0037	0.0001	1.3123	Y
898	0.0029	0.0001	1.2962	Y
1173.2	0.0024	0.0001	1.2966	Y
1332.5	0.0021	0.0001	1.2757	Y
1836.1	0.0017	0.0000	1.2722	Y

Figure 26. A graph of the Canberra empirical efficiency points versus the LabSOCS modelled efficiency point for the honey 750-mL fill volume in the 1-L bottle on the Canberra detector.
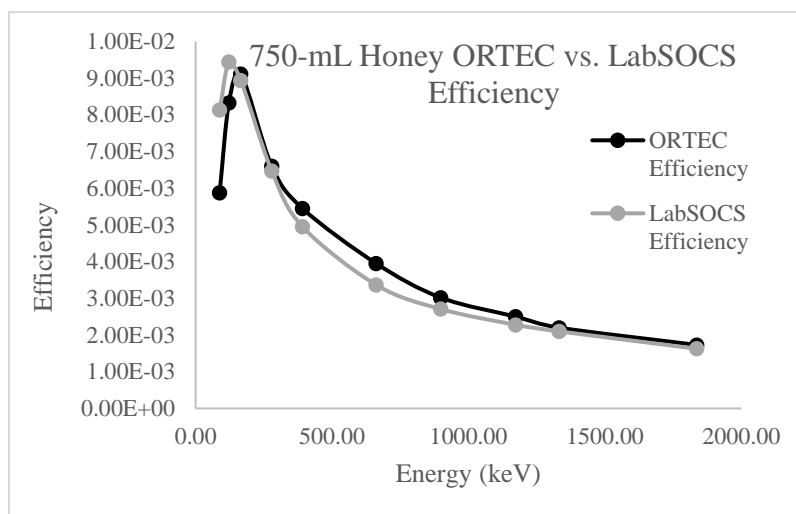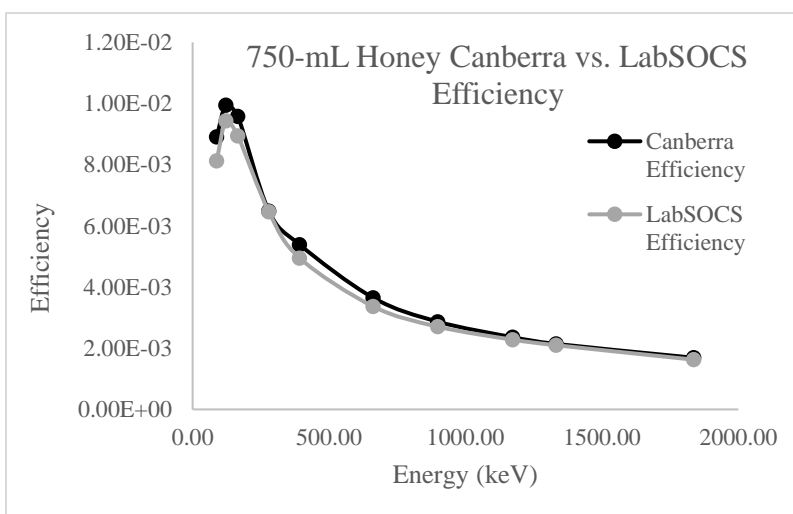
Table 30. The efficiencies and associated error by energy line contained within the liquid mixed-gamma source, for the honey 1-L fill volume in the 1-L bottle on the Canberra detector. The density correction factors and an analysis of whether the LabSOCS model would have given a conservative estimate of activity is also included.

Canberra Honey 1-L in 1-L Bottle				
R^2 Predicted:	0.9965	Regression SD	0.0001	
Energy (keV)	Efficiency (%)	Error (%)	DCF	Model Conservative
88	0.0061	0.0002	1.3668	Y
122.1	0.0069	0.0001	1.3533	N
165.9	0.0064	0.0001	1.3813	N
279.2	0.0045	0.0001	1.3407	N
391.7	0.0037	0.0001	1.3118	N
661.7	0.0026	0.0001	1.3020	Y
898	0.0020	0.0000	1.2814	N
1173.2	0.0017	0.0000	1.2471	N
1332.5	0.0015	0.0000	1.2418	N
1836.1	0.0012	0.0000	1.2314	N

Figure 27. A graph of the Canberra empirical efficiency points versus the LabSOCS modelled efficiency point for the honey 1-L fill volume in the 1-L bottle on the Canberra detector.
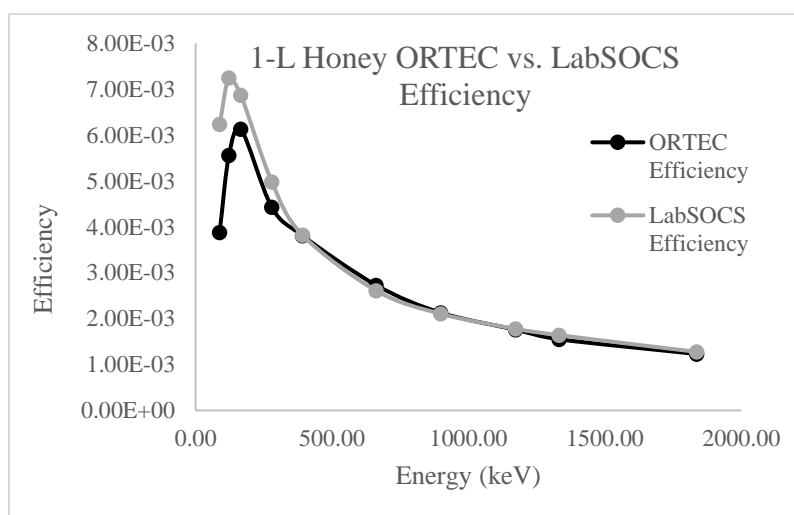
Table 31. The efficiencies and associated error by energy line contained within the liquid mixed-gamma source, for the honey 300-mL fill volume in the 500-mL bottle modelled by LabSOCS. The density correction factors are also included.

LabSOCS Honey 300-mL in 500-mL Bottle			
Energy (keV)	Efficiency (%)	Error (%)	DCF
88	0.0145	0.0015	1.1416
122.1	0.0164	0.0016	1.1329
165.9	0.0152	0.0012	1.1251
279.2	0.0107	0.0009	1.1106
391.7	0.0081	0.0006	1.1004
661.7	0.0054	0.0003	1.0839
898	0.0043	0.0003	1.0745
1173.2	0.0036	0.0001	1.0664
1332.5	0.0033	0.0001	1.0630
1836.1	0.0025	0.0001	1.0543

Table 32. The efficiencies and associated error by energy line contained within the liquid mixed-gamma source, for the honey 400-mL fill volume in the 500-mL bottle modelled by LabSOCS. The density correction factors are also included.

| LabSOCS Honey 400-mL in 500-mL Bottle			
Energy (keV)	Efficiency (%)	Error (%)	DCF
88	0.0110	0.0011	1.1500
122.1	0.0125	0.0012	1.1417
165.9	0.0116	0.0009	1.1345
279.2	0.0082	0.0007	1.1206
391.7	0.0062	0.0005	1.1106
661.7	0.0042	0.0002	1.0938
898	0.0033	0.0002	1.0839
1173.2	0.0028	0.0001	1.0753
1332.5	0.0025	0.0001	1.0717
1836.1	0.0020	0.0001	1.0623

Table 33. The efficiencies and associated error by energy line contained within the liquid mixed-gamma source, for the honey 500-mL fill volume in the 500-mL bottle modelled by LabSOCS. The density correction factors are also included.

| LabSOCS Honey 500-mL in 500-mL Bottle			
Energy (keV)	Efficiency (%)	Error (%)	DCF
88	0.0088	0.0009	1.1539
122.1	0.0100	0.0010	1.1461
165.9	0.0093	0.0007	1.1394
279.2	0.0066	0.0005	1.1263
391.7	0.0050	0.0004	1.1167
661.7	0.0034	0.0002	1.1002
898	0.0027	0.0002	1.0903
1173.2	0.0023	0.0001	1.0816
1332.5	0.0021	0.0001	1.0778
1836.1	0.0016	0.0001	1.0680

Table 34. The efficiencies and associated error by energy line contained within the liquid mixed-gamma source, for the honey 500-mL fill volume in the 1-L bottle modelled by LabSOCS. The density correction factors are also included.

LabSOCS Honey 500-mL in 1-L Bottle			
Energy (keV)	Efficiency (%)	Error (%)	DCF
88	0.0123	0.0012	1.1571
122.1	0.0142	0.0014	1.1436
165.9	0.0135	0.0011	1.1329
279.2	0.0097	0.0008	1.1149
391.7	0.0074	0.0006	1.1031
661.7	0.0050	0.0003	1.0847
898	0.0040	0.0002	1.0741
1173.2	0.0033	0.0001	1.0654
1332.5	0.0030	0.0001	1.0618
1836.1	0.0023	0.0001	1.0525

Table 35. The efficiencies and associated error by energy line contained within the liquid mixed-gamma source, for the honey 750-mL fill volume in the 1-L bottle modelled by LabSOCS. The density correction factors are also included.

| LabSOCS Honey 750-mL in 1-L Bottle			
Energy (keV)	Efficiency (%)	Error (%)	DCF
88	0.0081	0.0008	1.2097
122.1	0.0094	0.0009	1.1992
165.9	0.0089	0.0007	1.1902
279.2	0.0065	0.0005	1.1733
391.7	0.0050	0.0004	1.1611
661.7	0.0034	0.0002	1.1409
898	0.0027	0.0002	1.1290
1173.2	0.0023	0.0001	1.1186
1332.5	0.0021	0.0001	1.1142
1836.1	0.0016	0.0001	1.1028

Table 36. The efficiencies and associated error by energy line contained within the liquid mixed-gamma source, for the honey 1-L fill volume in the 1-L bottle modelled by LabSOCS. The density correction factors are also included.

| LabSOCS Honey 1-L in 1-L Bottle			
Energy (keV)	Efficiency (%)	Error (%)	DCF
88	0.0062	0.0006	1.2009
122.1	0.0072	0.0007	1.1911
165.9	0.0069	0.0005	1.1830
279.2	0.0050	0.0004	1.1678
391.7	0.0038	0.0003	1.1566
661.7	0.0026	0.0002	1.1377
898	0.0021	0.0001	1.1263
1173.2	0.0018	0.0001	1.1162
1332.5	0.0016	0.0001	1.1119
1836.1	0.0013	0.0001	1.1005

Table 37. The efficiencies and associated error by energy line contained within the liquid mixed-gamma source, for the water 300-mL fill volume in the 500-mL bottle on the ORTEC detector. An analysis of whether the LabSOCS model would have given a conservative estimate of activity is also included.

ORTEC Water 300-mL in 500-mL Bottle			
R^2 Predicted:	0.9096	Regression SD	0.0015
Energy (keV)	Efficiency (%)	Error (%)	Model Conservative
88	0.0130	0.0004	N
122.1	0.0181	0.0003	N
165.9	0.0186	0.0004	Y
279.2	0.0132	0.0002	Y
391.7	0.0105	0.0003	Y
661.7	0.0067	0.0002	Y
898	0.0054	0.0001	Y
1173.2	0.0043	0.0001	Y
1332.5	0.0037	0.0001	Y
1836.1	0.0029	0.0001	Y

Figure 28. A graph of the ORTEC empirical efficiency points versus the LabSOCS modelled efficiency point for the water 300-mL fill volume in the 500-mL bottle on the ORTEC detector.
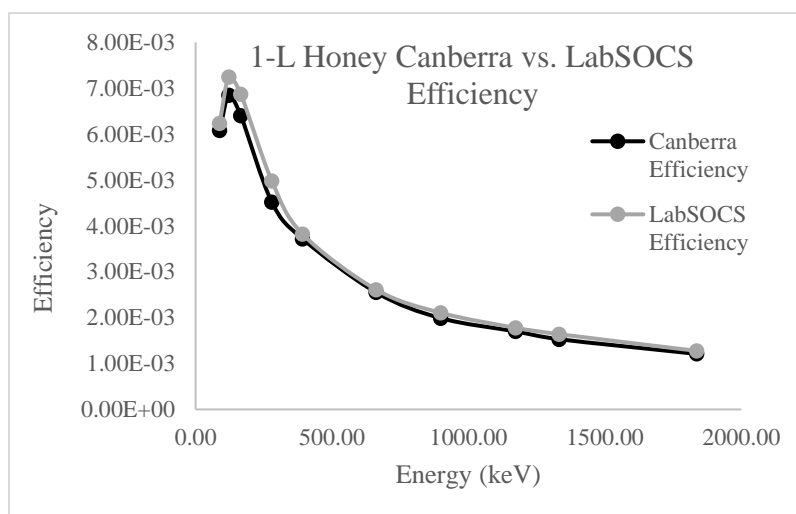
Table 38. The efficiencies and associated error by energy line contained within the liquid mixed-gamma source, for the water 400-mL fill volume in the 500-mL bottle on the ORTEC detector. An analysis of whether the LabSOCS model would have given a conservative estimate of activity is also included.

ORTEC Water 400-mL in 500-mL Bottle			
R^2 Predicted:	0.9170	Regression SD	0.0011
Energy (keV)	Efficiency (%)	Error (%)	Model Conservative
88	0.0102	0.0003	N
122.1	0.0140	0.0002	Y
165.9	0.0143	0.0003	Y
279.2	0.0102	0.0002	Y
391.7	0.0083	0.0002	Y
661.7	0.0055	0.0002	Y
898	0.0042	0.0001	Y
1173.2	0.0034	0.0001	Y
1332.5	0.0030	0.0001	Y
1836.1	0.0023	0.0001	Y

Figure 29. A graph of the ORTEC empirical efficiency points versus the LabSOCS modelled efficiency point for the water 400-mL fill volume in the 500-mL bottle on the ORTEC detector.

Table 39. The efficiencies and associated error by energy line contained within the liquid mixed-gamma source, for the water 500-mL fill volume in the 500-mL bottle on the ORTEC detector. An analysis of whether the LabSOCS model would have given a conservative estimate of activity is also included.

ORTEC Water 500-mL in 500-mL Bottle			
R^2 Predicted:	0.9110	Regression SD	0.0009
Energy (keV)	Efficiency (%)	Error (%)	Model Conservative
88	0.0082	0.0002	N
122.1	0.0111	0.0002	N
165.9	0.0117	0.0002	Y
279.2	0.0081	0.0001	Y
391.7	0.0068	0.0002	Y
661.7	0.0046	0.0001	Y
898	0.0034	0.0001	Y
1173.2	0.0028	0.0001	Y
1332.5	0.0024	0.0001	Y
1836.1	0.0019	0.0000	Y

Figure 30. A graph of the ORTEC empirical efficiency points versus the LabSOCS modelled efficiency point for the water 500-mL fill volume in the 500-mL bottle on the ORTEC detector.

Table 40. The efficiencies and associated error by energy line contained within the liquid mixed-gamma source, for the water 500-mL fill volume in the 1-L bottle on the ORTEC detector. An analysis of whether the LabSOCS model would have given a conservative estimate of activity is also included.

ORTEC Water 500-mL in 1-L Bottle			
R^2 Predicted:	0.8960	Regression SD	0.0014
Energy (keV)	Efficiency (%)	Error (%)	Model Conservative
88	0.0107	0.0003	N
122.1	0.0155	0.0003	N
165.9	0.0163	0.0003	Y
279.2	0.0116	0.0002	Y
391.7	0.0094	0.0002	Y
661.7	0.0064	0.0002	Y
898	0.0049	0.0001	Y
1173.2	0.0039	0.0001	Y
1332.5	0.0034	0.0001	Y
1836.1	0.0027	0.0001	Y

Figure 31. A graph of the ORTEC empirical efficiency points versus the LabSOCS modelled efficiency point for the water 500-mL fill volume in the 1-L bottle on the ORTEC detector.

Table 41. The efficiencies and associated error by energy line contained within the liquid mixed-gamma source, for the water 750-mL fill volume in the 1-L bottle on the ORTEC detector. An analysis of whether the LabSOCS model would have given a conservative estimate of activity is also included.

ORTEC Water 750-mL in 1-L Bottle			
R^2 Predicted:	0.8852	Regression SD	0.0010
Energy (keV)	Efficiency (%)	Error (%)	Model Conservative
88	0.0073	0.0002	N
122.1	0.0104	0.0002	N
165.9	0.0111	0.0002	Y
279.2	0.0083	0.0002	Y
391.7	0.0067	0.0002	Y
661.7	0.0046	0.0001	Y
898	0.0036	0.0001	Y
1173.2	0.0029	0.0001	Y
1332.5	0.0025	0.0001	Y
1836.1	0.0020	0.0000	Y

Figure 32. A graph of the ORTEC empirical efficiency points versus the LabSOCS modelled efficiency point for the water 750-mL fill volume in the 1-L bottle on the ORTEC detector.

Table 42. The efficiencies and associated error by energy line contained within the liquid mixed-gamma source, for the water 1-L fill volume in the 1-L bottle on the ORTEC detector. An analysis of whether the LabSOCS model would have given a conservative estimate of activity is also included.

ORTEC Water 1-L in 1-L Bottle			
R^2 Predicted:	0.8950	Regression SD	0.0007
Energy (keV)	Efficiency (%)	Error (%)	Model Conservative
88	0.0057	0.0002	N
122.1	0.0081	0.0001	N
165.9	0.0086	0.0002	Y
279.2	0.0064	0.0001	Y
391.7	0.0052	0.0001	Y
661.7	0.0035	0.0001	Y
898	0.0027	0.0001	Y
1173.2	0.0022	0.0001	Y
1332.5	0.0020	0.0000	Y
1836.1	0.0015	0.0000	Y

Figure 33. A graph of the ORTEC empirical efficiency points versus the LabSOCS modelled efficiency point for the water 1-L fill volume in the 1-L bottle on the ORTEC detector.
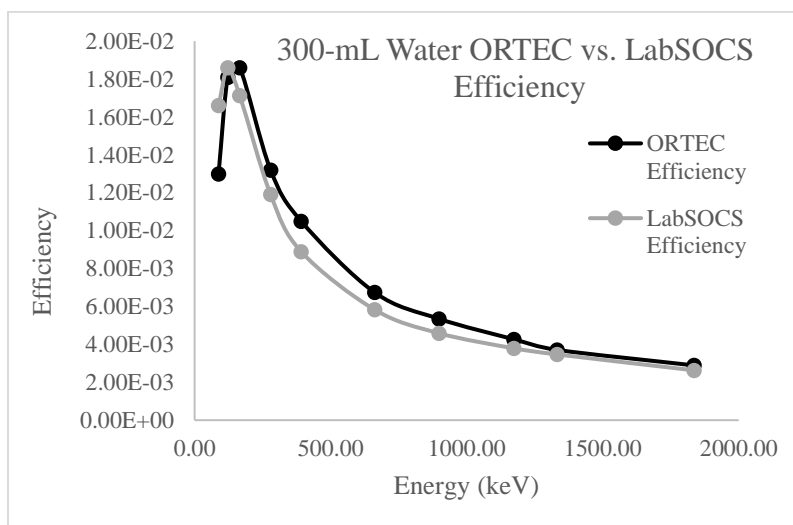
Table 43. The efficiencies and associated error by energy line contained within the liquid mixed-gamma source, for the water 300-mL fill volume in the 500-mL bottle on the Canberra detector. An analysis of whether the LabSOCS model would have given a conservative estimate of activity is also included.

Canberra Water 300-mL in 500-mL Bottle			
R^2 Predicted:	0.9975	Regression SD	0.0003
Energy (keV)	Efficiency (%)	Error (%)	Model Conservative
88	0.0190	0.0005	Y
122.1	0.0206	0.0003	Y
165.9	0.0190	0.0004	Y
279.2	0.0126	0.0002	Y
391.7	0.0100	0.0003	Y
661.7	0.0065	0.0002	Y
898	0.0050	0.0001	Y
1173.2	0.0040	0.0001	Y
1332.5	0.0037	0.0001	Y
1836.1	0.0028	0.0001	Y

Figure 34. A graph of the Canberra empirical efficiency points versus the LabSOCS modelled efficiency point for the water 300-mL fill volume in the 500-mL bottle on the Canberra detector.
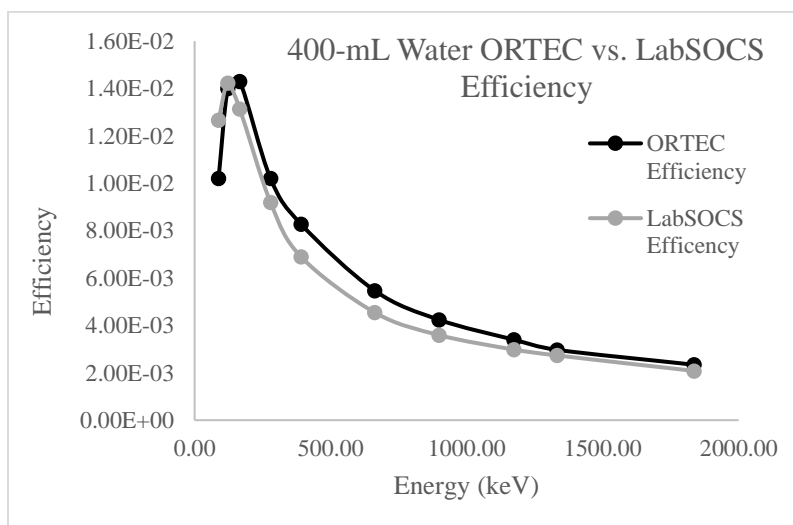
Table 44. The efficiencies and associated error by energy line contained within the liquid mixed-gamma source, for the water 400-mL fill volume in the 500-mL bottle on the Canberra detector. An analysis of whether the LabSOCS model would have given a conservative estimate of activity is also included.

Canberra Water 400-mL in 500-mL Bottle			
R^2 Predicted:	0.9963	Regression SD	0.0003
Energy (keV)	Efficiency (%)	Error (%)	Model Conservative
88	0.0148	0.0004	Y
122.1	0.0159	0.0003	Y
165.9	0.0148	0.0003	Y
279.2	0.0098	0.0002	Y
391.7	0.0078	0.0002	Y
661.7	0.0051	0.0001	Y
898	0.0039	0.0001	Y
1173.2	0.0032	0.0001	Y
1332.5	0.0029	0.0001	Y
1836.1	0.0023	0.0000	Y

Figure 35. A graph of the Canberra empirical efficiency points versus the LabSOCS modelled efficiency point for the water 400-mL fill volume in the 500-mL bottle on the Canberra detector.
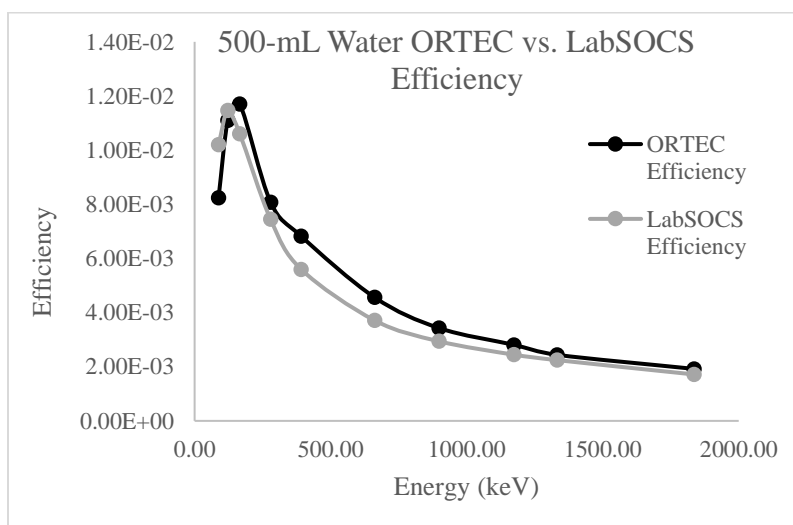
Table 45. The efficiencies and associated error by energy line contained within the liquid mixed-gamma source, for the water 500-mL fill volume in the 1-L bottle on the Canberra detector. An analysis of whether the LabSOCS model would have given a conservative estimate of activity is also included.

Canberra Water 500-mL in 1-L Bottle			
R^2 Predicted:	0.9984	Regression SD	0.0002
Energy (keV)	Efficiency (%)	Error (%)	Model Conservative
88	0.0159	0.0004	Y
122.1	0.0178	0.0003	Y
165.9	0.0169	0.0003	Y
279.2	0.0114	0.0002	Y
391.7	0.0090	0.0002	Y
661.7	0.0059	0.0002	Y
898	0.0046	0.0001	Y
1173.2	0.0037	0.0001	Y
1332.5	0.0034	0.0001	Y
1836.1	0.0026	0.0001	Y

Figure 36. A graph of the Canberra empirical efficiency points versus the LabSOCS modelled efficiency point for the water 500-mL fill volume in the 1-L bottle on the Canberra detector.
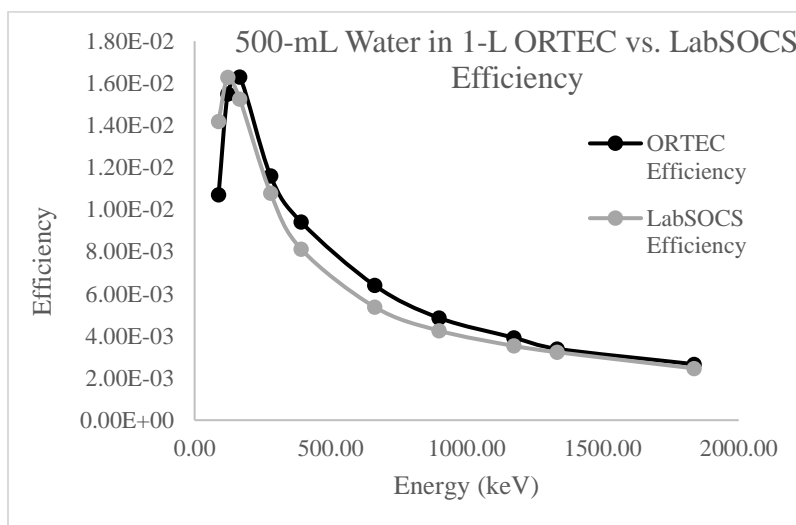
Table 46. The efficiencies and associated error by energy line contained within the liquid mixed-gamma source, for the water 750-mL fill volume in the 1-L bottle on the Canberra detector. An analysis of whether the LabSOCS model would have given a conservative estimate of activity is also included.

Canberra Water 750-mL in 1-L Bottle			
R^2 Predicted:	0.9977	Regression SD	0.0002
Energy (keV)	Efficiency (%)	Error (%)	Model Conservative
88	0.0123	0.0003	Y
122.1	0.0138	0.0002	Y
165.9	0.0131	0.0003	Y
279.2	0.0089	0.0002	Y
391.7	0.0073	0.0002	Y
661.7	0.0048	0.0001	Y
898	0.0037	0.0001	Y
1173.2	0.0031	0.0001	Y
1332.5	0.0027	0.0001	Y
1836.1	0.0022	0.0000	Y

Figure 37. A graph of the Canberra empirical efficiency points versus the LabSOCS modelled efficiency point for the water 750-mL fill volume in the 1-L bottle on the Canberra detector.
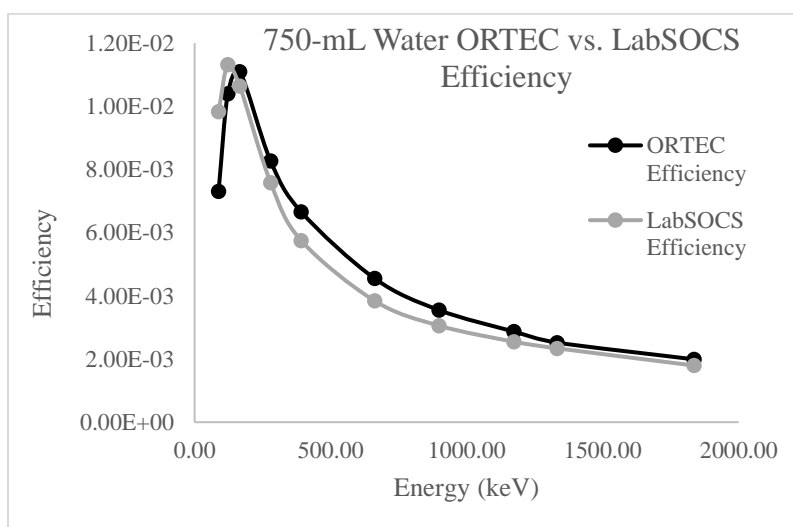
Table 47. The efficiencies and associated error by energy line contained within the liquid mixed-gamma source, for the water 1-L fill volume in the 1-L bottle on the Canberra detector. An analysis of whether the LabSOCS model would have given a conservative estimate of activity is also included.

Canberra Water 1-L in 1-L Bottle			
R^2 Predicted:	0.9976	Regression SD	0.0001
Energy (keV)	Efficiency (%)	Error (%)	Model Conservative
88	0.0083	0.0002	Y
122.1	0.0093	0.0002	Y
165.9	0.0088	0.0002	Y
279.2	0.0061	0.0001	Y
391.7	0.0049	0.0001	Y
661.7	0.0033	0.0001	Y
898	0.0026	0.0001	Y
1173.2	0.0021	0.0001	Y
1332.5	0.0019	0.0000	Y
1836.1	0.0015	0.0000	Y

Figure 38. A graph of the Canberra empirical efficiency points versus the LabSOCS modelled efficiency point for the water 1-L fill volume in the 1-L bottle on the Canberra detector.
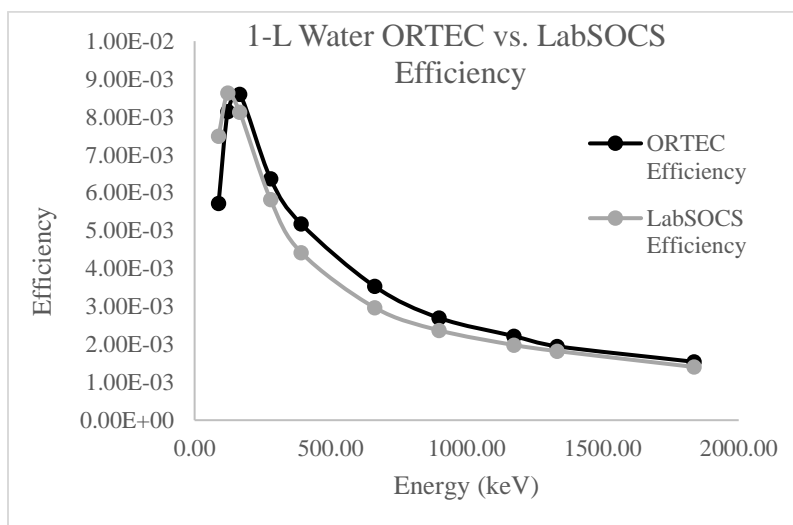
Table 48. The efficiencies and associated error by energy line contained within the liquid mixed-gamma source, for the water 300-mL fill volume in the 500-mL bottle modelled by LabSOCS.

LabSOCS Water 300-mL in 500-mL Bottle		
Energy (keV)	Efficiency (%)	Error (%)
88	0.0166	0.0017
122.1	0.0186	0.0019
165.9	0.0171	0.0014
279.2	0.0119	0.0010
391.7	0.0089	0.0007
661.7	0.0058	0.0003
898	0.0046	0.0003
1173.2	0.0038	0.0002
1332.5	0.0035	0.0001
1836.1	0.0026	0.0001

Table 49. The efficiencies and associated error by energy line contained within the liquid mixed-gamma source, for the water 400-mL fill volume in the 500-mL bottle modelled by LabSOCS.

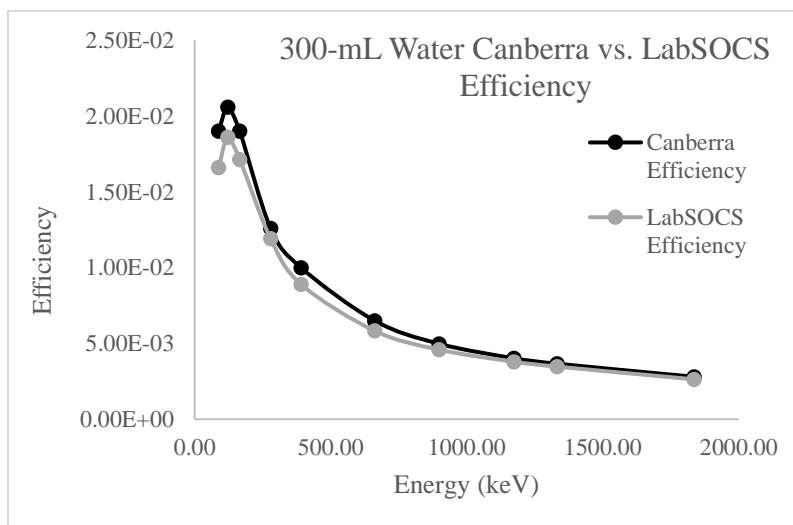| LabSOCS Water 400-mL in 500-mL Bottle		
Energy (keV)	Efficiency (%)	Error (%)
88	0.0127	0.0013
122.1	0.0142	0.0014
165.9	0.0131	0.0011
279.2	0.0092	0.0007
391.7	0.0069	0.0006
661.7	0.0045	0.0003
898	0.0036	0.0002
1173.2	0.0030	0.0001
1332.5	0.0027	0.0001
1836.1	0.0021	0.0001

Table 50. The efficiencies and associated error by energy line contained within the liquid mixed-gamma source, for the water 500-mL fill volume in the 500-mL bottle modelled by LabSOCS.

LabSOCS Water 500-mL in 500-mL Bottle		
Energy (keV)	Efficiency (%)	Error (%)
88	0.0142	0.0014
122.1	0.0163	0.0016
165.9	0.0152	0.0012
279.2	0.0108	0.0009
391.7	0.0081	0.0006
661.7	0.0054	0.0003
898	0.0043	0.0003
1173.2	0.0035	0.0001
1332.5	0.0032	0.0001
1836.1	0.0025	0.0001

Table 51. The efficiencies and associated error by energy line contained within the liquid mixed-gamma source, for the water 500-mL fill volume in the 1-L bottle modelled by LabSOCS.

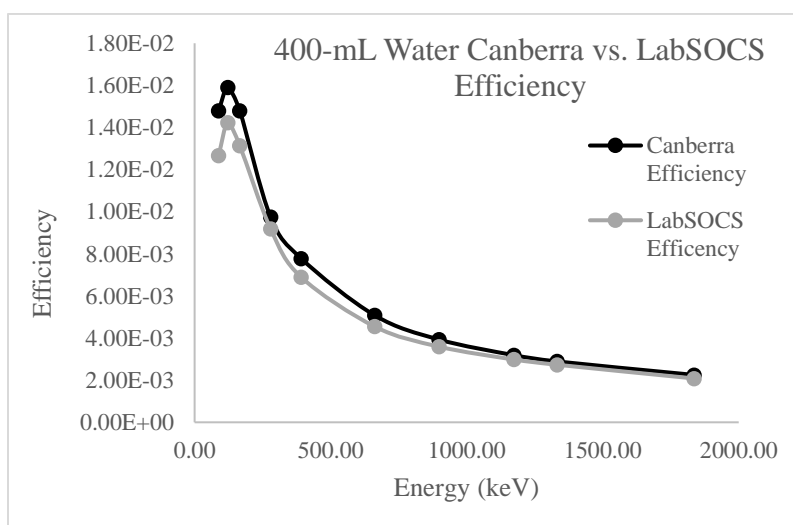| LabSOCS Water 500-mL in 1-L Bottle		
Energy (keV)	Efficiency (%)	Error (%)
88	0.0142	0.0014
122.1	0.0163	0.0016
165.9	0.0152	0.0012
279.2	0.0108	0.0009
391.7	0.0081	0.0006
661.7	0.0054	0.0003
898	0.0043	0.0003
1173.2	0.0035	0.0001
1332.5	0.0032	0.0001
1836.1	0.0025	0.0001

Table 52. The efficiencies and associated error by energy line contained within the liquid mixed-gamma source, for the water 750-mL fill volume in the 1-L bottle modelled by LabSOCS.

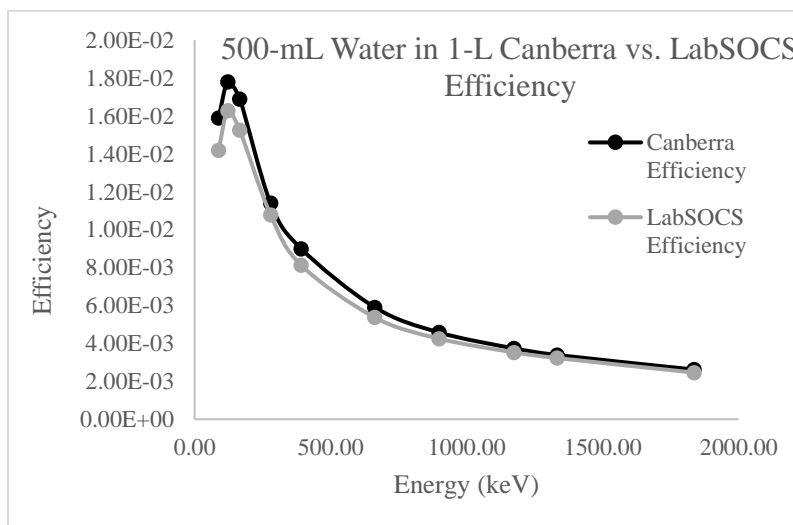| LabSOCS Water 750-mL in 1-L Bottle		
Energy (keV)	Efficiency (%)	Error (%)
88	0.0098	0.0010
122.1	0.0113	0.0011
165.9	0.0106	0.0009
279.2	0.0076	0.0006
391.7	0.0058	0.0005
661.7	0.0038	0.0002
898	0.0031	0.0002
1173.2	0.0025	0.0001
1332.5	0.0023	0.0001
1836.1	0.0018	0.0001

Table 53. The efficiencies and associated error by energy line contained within the liquid mixed-gamma source, for the water 1-L fill volume in the 1-L bottle modelled by LabSOCS.

LabSOCS Water 1-L in 1-L Bottle		
Energy (keV)	Efficiency (%)	Error (%)
88	0.0075	0.0007
122.1	0.0086	0.0009
165.9	0.0081	0.0007
279.2	0.0058	0.0005
391.7	0.0044	0.0004
661.7	0.0030	0.0002
898	0.0024	0.0001
1173.2	0.0020	0.0001
1332.5	0.0018	0.0001
1836.1	0.0014	0.0001

Table 54. The efficiencies and associated error by energy line contained within the liquid mixed-gamma source, for the tea 300-mL fill volume in the 500-mL bottle on the ORTEC detector. The density correction factors and an analysis of whether the LabSOCS model would have given a conservative estimate of activity is also included.

ORTEC Tea 300-mL in 500-mL Bottle				
R^2 Predicted:	0.9394	Regression SD	0.0015	
Energy (keV)	Efficiency (%)	Error (%)	DCF	Model Conservative
88	0.0162	0.0005	0.8025	N
122.1	0.0210	0.0003	0.8619	N
165.9	0.0212	0.0004	0.8774	Y
279.2	0.0141	0.0003	0.9362	N
391.7	0.0115	0.0003	0.9130	Y
661.7	0.0074	0.0002	0.9170	Y
898	0.0057	0.0001	0.9386	Y
1173.2	0.0045	0.0001	0.9596	Y
1332.5	0.0039	0.0001	0.9587	Y
1836.1	0.0030	0.0001	0.9633	Y

Figure 39. A graph of the ORTEC empirical efficiency points versus the LabSOCS modelled efficiency point for the tea 300-mL fill volume in the 500-mL bottle on the ORTEC detector.
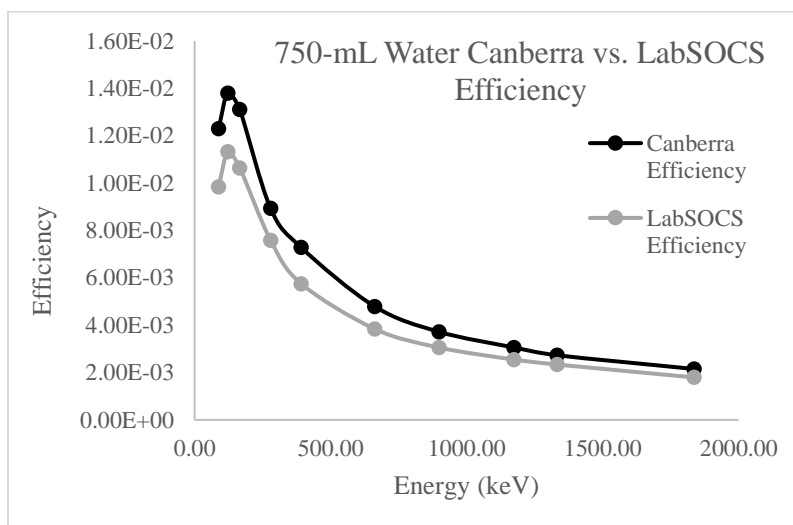
Table 55. The efficiencies and associated error by energy line contained within the liquid mixed-gamma source, for the tea 400-mL fill volume in the 500-mL bottle on the ORTEC detector. The density correction factors and an analysis of whether the LabSOCS model would have given a conservative estimate of activity is also included.

ORTEC Tea 400-mL in 500-mL Bottle				
R^2 Predicted:	0.9071	Regression SD	0.0013	
Energy (keV)	Efficiency (%)	Error (%)	DCF	Model Conservative
88	0.0111	0.0003	0.9189	N
122.1	0.0143	0.0002	0.9790	N
165.9	0.0145	0.0003	0.9862	N
279.2	0.0113	0.0002	0.9027	Y
391.7	0.0084	0.0002	0.9799	Y
661.7	0.0053	0.0002	1.0321	Y
898	0.0040	0.0001	1.0680	N
1173.2	0.0032	0.0001	1.0794	N
1332.5	0.0028	0.0001	1.0722	N
1836.1	0.0021	0.0000	1.1090	N

Figure 40. A graph of the ORTEC empirical efficiency points versus the LabSOCS modelled efficiency point for the tea 400-mL fill volume in the 500-mL bottle on the ORTEC detector.
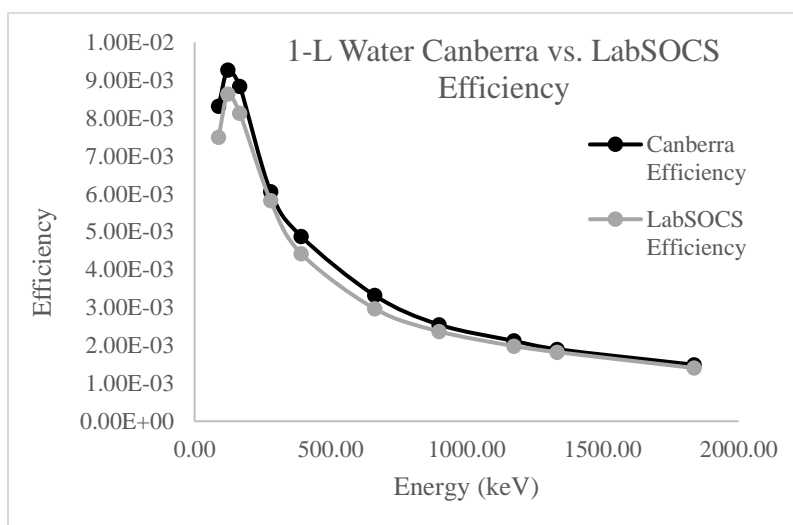
Table 56. The efficiencies and associated error by energy line contained within the liquid mixed-gamma source, for the tea 500-mL fill volume in the 500-mL bottle on the ORTEC detector. The density correction factors and an analysis of whether the LabSOCS model would have given a conservative estimate of activity is also included.

ORTEC Tea 500-mL in 500-mL Bottle				
R^2 Predicted:	0.8974	Regression SD	0.0011	
Energy (keV)	Efficiency (%)	Error (%)	DCF	Model Conservative
88	0.0093	0.0003	0.8908	N
122.1	0.0121	0.0002	0.9174	N
165.9	0.0124	0.0003	0.9435	N
279.2	0.0097	0.0002	0.8338	Y
391.7	0.0072	0.0002	0.9512	Y
661.7	0.0046	0.0001	0.9913	Y
898	0.0035	0.0001	0.9828	Y
1173.2	0.0028	0.0001	1.0144	Y
1332.5	0.0025	0.0001	0.9799	Y
1836.1	0.0019	0.0000	1.0159	Y

Figure 41. A graph of the ORTEC empirical efficiency points versus the LabSOCS modelled efficiency point for the tea 500-mL fill volume in the 500-mL bottle on the ORTEC detector.

Table 57. The efficiencies and associated error by energy line contained within the liquid mixed-gamma source, for the tea 500-mL fill volume in the 1-L bottle on the ORTEC detector. The density correction factors and an analysis of whether the LabSOCS model would have given a conservative estimate of activity is also included.

ORTEC Tea 500-mL in 1-L Bottle				
R^2 Predicted:	0.8999	Regression SD	0.0016	
Energy (keV)	Efficiency (%)	Error (%)	DCF	Model Conservative
88	0.0132	0.0004	0.8106	N
122.1	0.0183	0.0003	0.8470	N
165.9	0.0193	0.0004	0.8446	Y
279.2	0.0134	0.0002	0.8657	Y
391.7	0.0107	0.0003	0.8794	Y
661.7	0.0069	0.0002	0.9222	Y
898	0.0053	0.0001	0.9153	Y
1173.2	0.0042	0.0001	0.9356	Y
1332.5	0.0037	0.0001	0.9237	Y
1836.1	0.0029	0.0001	0.9204	Y

Figure 42. A graph of the ORTEC empirical efficiency points versus the LabSOCS modelled efficiency point for the tea 500-mL fill volume in the 1-L bottle on the ORTEC detector.

Table 58. The efficiencies and associated error by energy line contained within the liquid mixed-gamma source, for the tea 750-mL fill volume in the 1-L bottle on the ORTEC detector. The density correction factors and an analysis of whether the LabSOCS model would have given a conservative estimate of activity is also included.

ORTEC Tea 750-mL in 1-L Bottle				
R^2 Predicted:	0.7766	Regression SD	0.0017	
Energy (keV)	Efficiency (%)	Error (%)	DCF	Model Conservative
88	0.0076	0.0002	0.9644	N
122.1	0.0136	0.0002	0.7647	N
165.9	0.0140	0.0003	0.7929	Y
279.2	0.0097	0.0002	0.8535	Y
391.7	0.0080	0.0002	0.8356	Y
661.7	0.0052	0.0001	0.8784	Y
898	0.0040	0.0001	0.8965	Y
1173.2	0.0032	0.0001	0.9111	Y
1332.5	0.0028	0.0001	0.9097	Y
1836.1	0.0022	0.0000	0.9256	Y

Figure 43. A graph of the ORTEC empirical efficiency points versus the LabSOCS modelled efficiency point for the tea 750-mL fill volume in the 1-L bottle on the ORTEC detector.
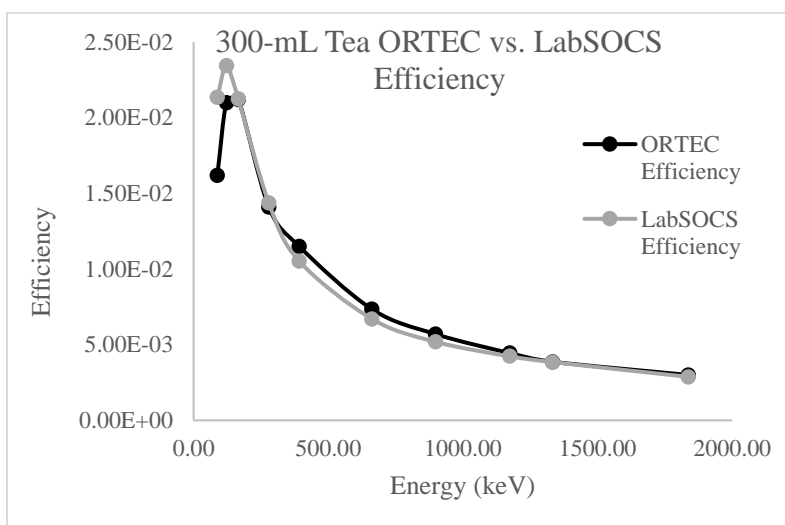
Table 59. The efficiencies and associated error by energy line contained within the liquid mixed-gamma source, for the tea 1-L fill volume in the 1-L bottle on the ORTEC detector. The density correction factors and an analysis of whether the LabSOCS model would have given a conservative estimate of activity is also included.

ORTEC Tea 1-L in 1-L Bottle				
R^2 Predicted:	0.9154	Regression SD	0.0010	
Energy (keV)	Efficiency (%)	Error (%)	DCF	Model Conservative
88	0.0092	0.0003	0.6231	N
122.1	0.0127	0.0002	0.6409	Y
165.9	0.0132	0.0003	0.6515	Y
279.2	0.0089	0.0002	0.7125	Y
391.7	0.0074	0.0002	0.7000	Y
661.7	0.0049	0.0001	0.7219	Y
898	0.0037	0.0001	0.7239	Y
1173.2	0.0030	0.0001	0.7400	Y
1332.5	0.0026	0.0001	0.7500	Y
1836.1	0.0020	0.0000	0.7586	Y

Figure 44. A graph of the ORTEC empirical efficiency points versus the LabSOCS modelled efficiency point for the tea 1-L fill volume in the 1-L bottle on the ORTEC detector.
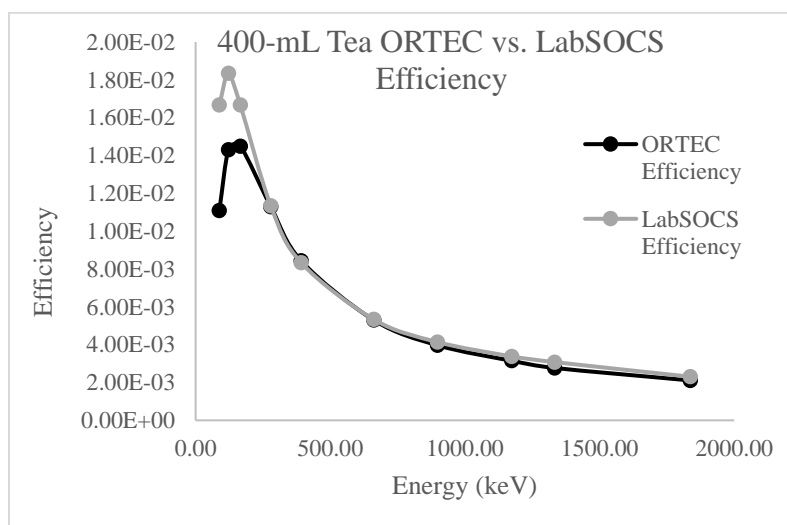
Table 60. The efficiencies and associated error by energy line contained within the liquid mixed-gamma source, for the tea 300-mL fill volume in the 500-mL bottle on the Canberra detector. The density correction factors and an analysis of whether the LabSOCS model would have given a conservative estimate of activity is also included.

Canberra Tea 300-mL in 500-mL Bottle				
R^2 Predicted:	0.9965	Regression SD	0.0004	
Energy (keV)	Efficiency (%)	Error (%)	DCF	Model Conservative
88	0.0222	0.0006	0.8559	Y
122.1	0.0235	0.0004	0.8766	Y
165.9	0.0217	0.0004	0.8756	Y
279.2	0.0136	0.0002	0.9265	N
391.7	0.0109	0.0003	0.9165	Y
661.7	0.0069	0.0002	0.9475	Y
898	0.0053	0.0001	0.9486	Y
1173.2	0.0042	0.0001	0.9640	Y
1332.5	0.0037	0.0001	0.9786	N
1836.1	0.0029	0.0001	0.9756	Y

Figure 45. A graph of the Canberra empirical efficiency points versus the LabSOCS modelled efficiency point for the tea 300-mL fill volume in the 500-mL bottle on the Canberra detector.
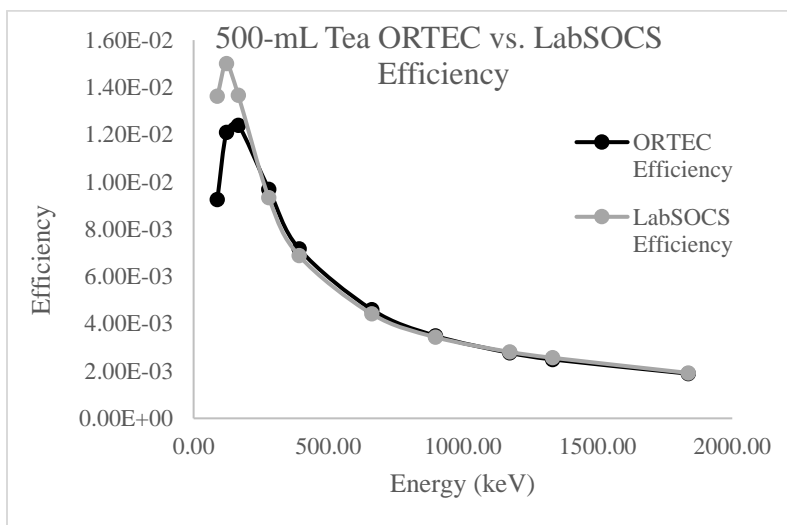
Table 61. The efficiencies and associated error by energy line contained within the liquid mixed-gamma source, for the tea 400-mL fill volume in the 500-mL bottle on the Canberra detector. The density correction factors and an analysis of whether the LabSOCS model would have given a conservative estimate of activity is also included.

Canberra Tea 400-mL in 500-mL Bottle				
R^2 Predicted:	0.9922	Regression SD	0.0004	
Energy (keV)	Efficiency (%)	Error (%)	DCF	Model Conservative
88	0.0157	0.0004	0.9427	N
122.1	0.0162	0.0003	0.9815	N
165.9	0.0148	0.0003	1.0000	N
279.2	0.0111	0.0002	0.8784	N
391.7	0.0081	0.0002	0.9629	N
661.7	0.0050	0.0001	1.0201	N
898	0.0038	0.0001	1.0452	N
1173.2	0.0030	0.0001	1.0669	N
1332.5	0.0027	0.0001	1.0743	N
1836.1	0.0021	0.0000	1.0976	N

Figure 46. A graph of the Canberra empirical efficiency points versus the LabSOCS modelled efficiency point for the tea 400-mL fill volume in the 500-mL bottle on the Canberra detector.
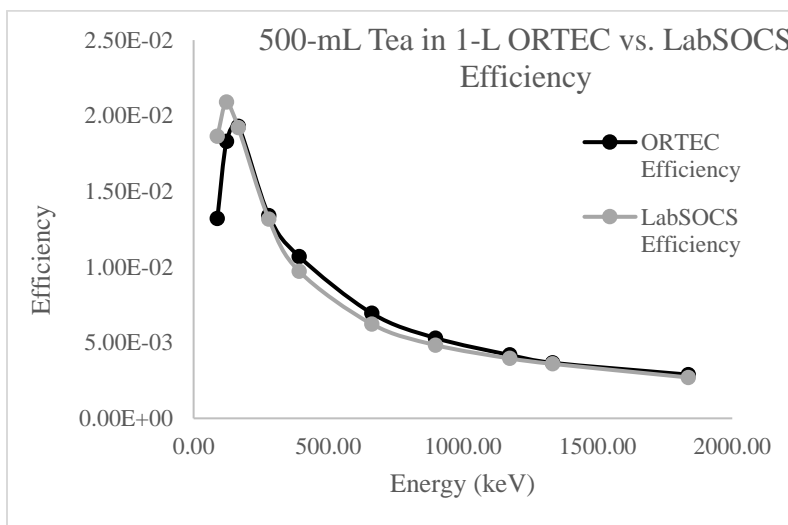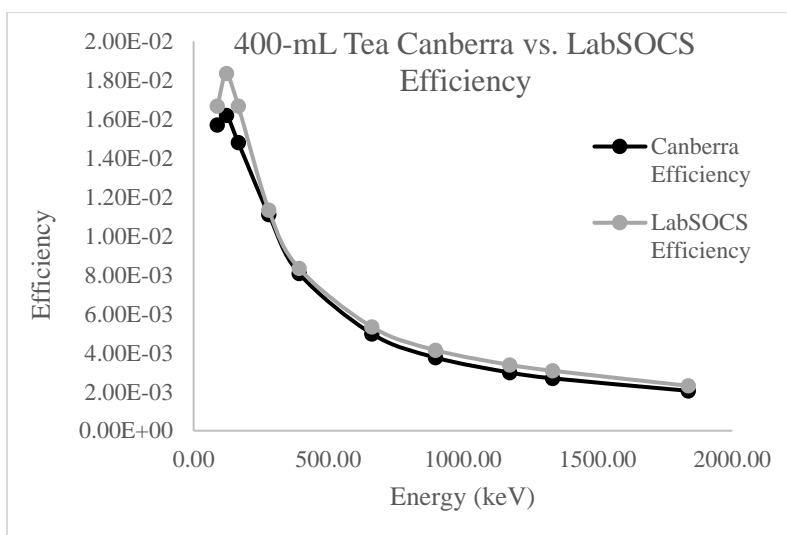
Table 62. The efficiencies and associated error by energy line contained within the liquid mixed-gamma source, for the tea 500-mL fill volume in the 1-L bottle on the Canberra detector. The density correction factors and an analysis of whether the LabSOCS model would have given a conservative estimate of activity is also included.

Canberra Tea 500-mL in 1-L Bottle				
R^2 Predicted:	0.9972	Regression SD	0.0003	
Energy (keV)	Efficiency (%)	Error (%)	DCF	Model Conservative
88	0.0198	0.0006	0.8030	Y
122.1	0.0215	0.0004	0.8279	Y
165.9	0.0199	0.0004	0.8492	Y
279.2	0.0129	0.0002	0.8837	N
391.7	0.0103	0.0003	0.8738	Y
661.7	0.0066	0.0002	0.8995	Y
898	0.0050	0.0001	0.9160	Y
1173.2	0.0040	0.0001	0.9257	Y
1332.5	0.0036	0.0001	0.9522	Y
1836.1	0.0028	0.0001	0.9424	Y

Figure 47. A graph of the Canberra empirical efficiency points versus the LabSOCS modelled efficiency point for the tea 500-mL fill volume in the 1-L bottle on the Canberra detector.
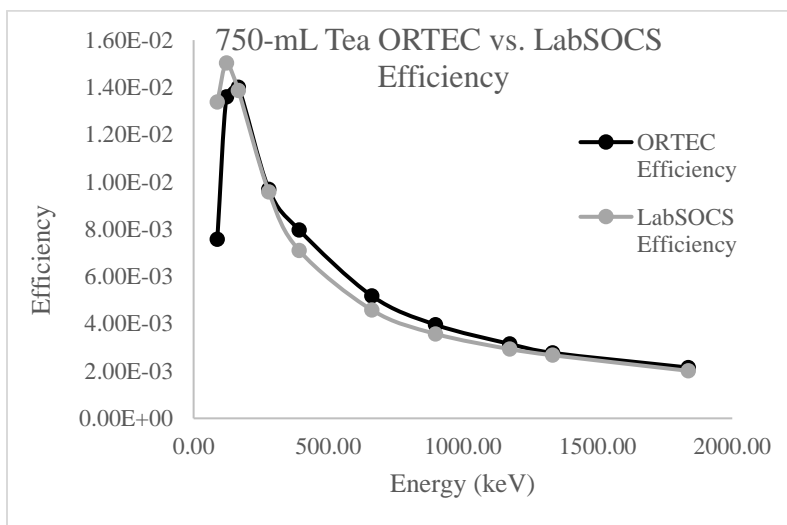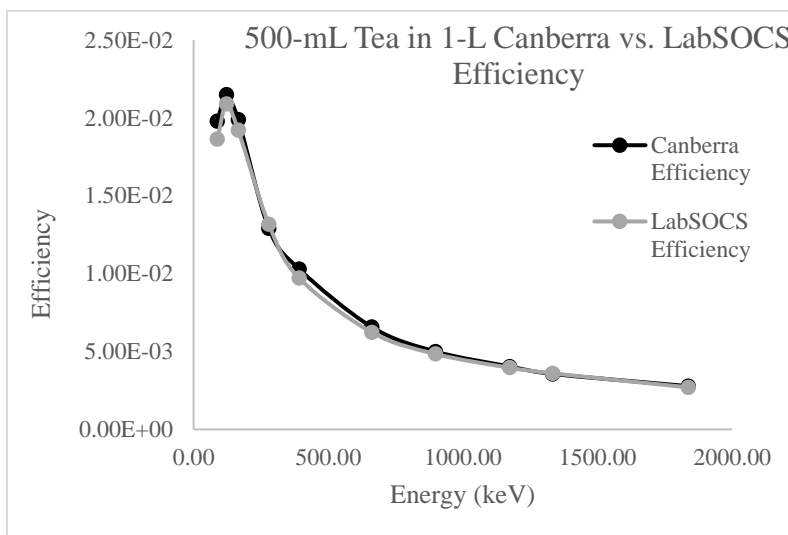
Table 63. The efficiencies and associated error by energy line contained within the liquid mixed-gamma source, for the tea 750-mL fill volume in the 1-L bottle on the Canberra detector. The density correction factors and an analysis of whether the LabSOCS model would have given a conservative estimate of activity is also included.

Canberra Tea 750-mL in 1-L Bottle				
R^2 Predicted:	0.9871	Regression SD	0.0005	
Energy (keV)	Efficiency (%)	Error (%)	DCF	Model Conservative
88	0.0154	0.0004	0.7987	Y
122.1	0.0155	0.0003	0.8903	Y
165.9	0.0146	0.0003	0.8973	Y
279.2	0.0094	0.0002	0.9551	N
391.7	0.0075	0.0002	0.9759	Y
661.7	0.0047	0.0001	1.0105	Y
898	0.0037	0.0001	1.0109	Y
1173.2	0.0030	0.0001	1.0373	Y
1332.5	0.0026	0.0001	1.0341	Y
1836.1	0.0021	0.0000	1.0337	Y

Figure 48. A graph of the Canberra empirical efficiency points versus the LabSOCS modelled efficiency point for the tea 750-mL fill volume in the 1-L bottle on the Canberra detector.
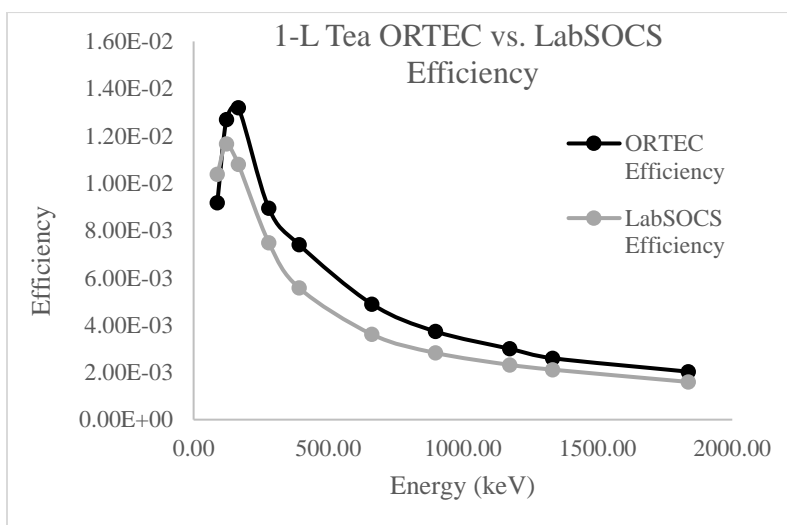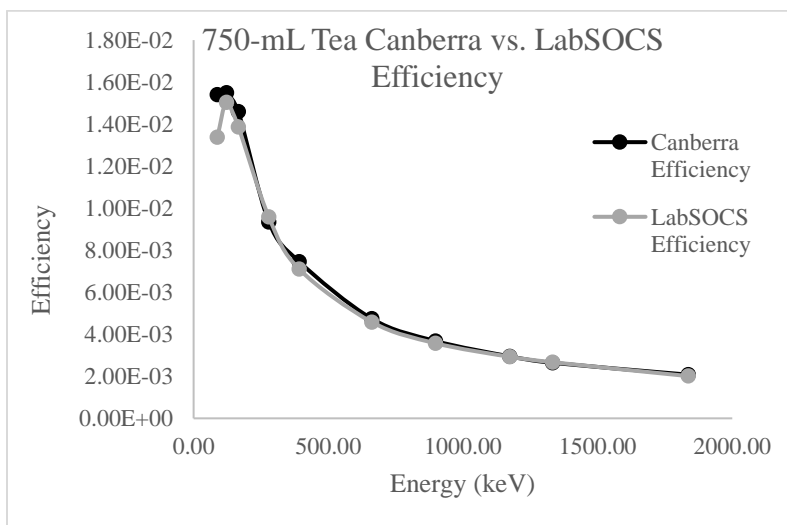
Table 64. The efficiencies and associated error by energy line contained within the liquid mixed-gamma source, for the tea 1-L fill volume in the 1-L bottle on the Canberra detector. The density correction factors and an analysis of whether the LabSOCS model would have given a conservative estimate of activity is also included.

Canberra Tea 1-L in 1-L Bottle				
R^2 Predicted:	0.9927	Regression SD	0.0004	
Energy (keV)	Efficiency (%)	Error (%)	DCF	Model Conservative
88	0.0134	0.0004	0.6201	Y
122.1	0.0144	0.0002	0.6438	Y
165.9	0.0135	0.0003	0.6548	Y
279.2	0.0084	0.0002	0.7189	Y
391.7	0.0069	0.0002	0.7114	Y
661.7	0.0046	0.0001	0.7249	Y
898	0.0035	0.0001	0.7349	Y
1173.2	0.0028	0.0001	0.7599	Y
1332.5	0.0025	0.0001	0.7540	Y
1836.1	0.0020	0.0000	0.7563	Y

Figure 49. A graph of the Canberra empirical efficiency points versus the LabSOCS modelled efficiency point for the tea 1-L fill volume in the 1-L bottle on the Canberra detector.
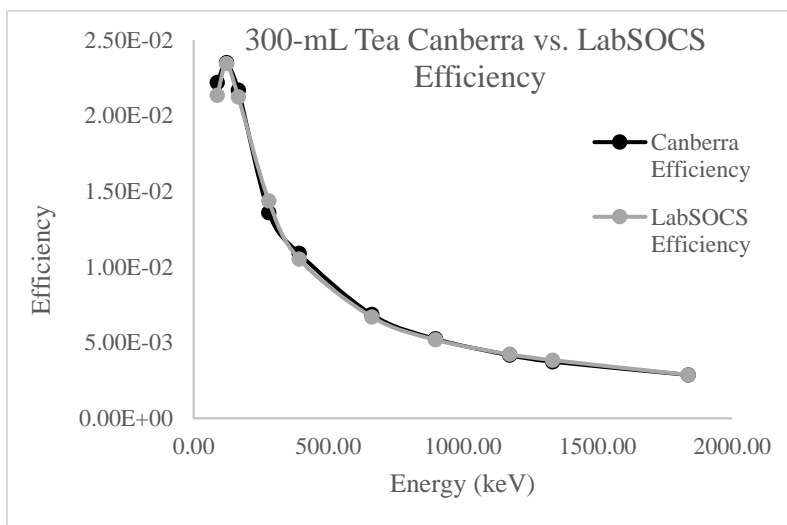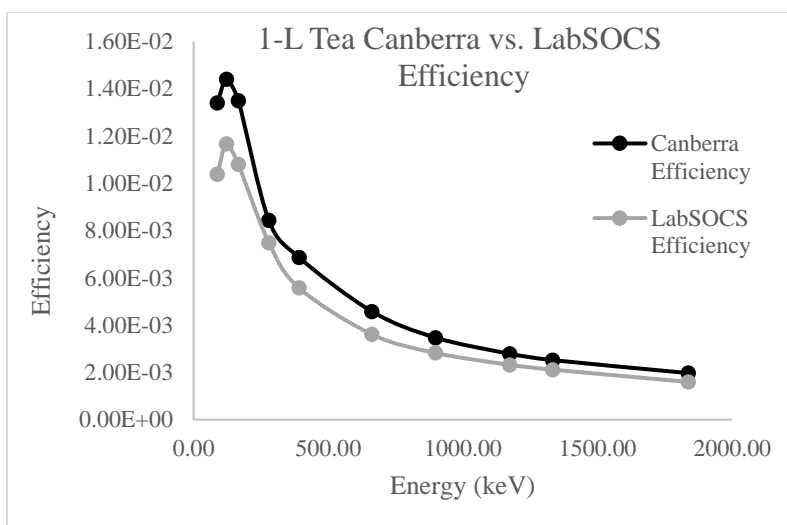
Table 65. The efficiencies and associated error by energy line contained within the liquid mixed-gamma source, for the tea 300-mL fill volume in the 500-mL bottle modelled by LabSOCS. The density correction factors are also included.

| LabSOCS Tea 300-mL in 500-mL Bottle			
Energy (keV)	Efficiency (%)	Error (%)	DCF
88	0.0214	0.0021	0.7776
122.1	0.0234	0.0023	0.7933
165.9	0.0212	0.0017	0.8061
279.2	0.0144	0.0011	0.8287
391.7	0.0105	0.0008	0.8444
661.7	0.0067	0.0004	0.8695
898	0.0052	0.0003	0.8840
1173.2	0.0042	0.0002	0.8964
1332.5	0.0038	0.0002	0.9016
1836.1	0.0029	0.0001	0.9149

Table 66. The efficiencies and associated error by energy line contained within the liquid mixed-gamma source, for the tea 400-mL fill volume in the 500-mL bottle modelled by LabSOCS. The density correction factors are also included.

LabSOCS Tea 400-mL in 500-mL Bottle			
Energy (keV)	Efficiency (%)	Error (%)	DCF
88	0.0167	0.0017	0.7597
122.1	0.0183	0.0018	0.7753
165.9	0.0167	0.0013	0.7878
279.2	0.0113	0.0009	0.8102
391.7	0.0083	0.0007	0.8263
661.7	0.0053	0.0003	0.8526
898	0.0041	0.0002	0.8681
1173.2	0.0034	0.0001	0.8815
1332.5	0.0031	0.0001	0.8872
1836.1	0.0023	0.0001	0.9019

Table 67. The efficiencies and associated error by energy line contained within the liquid mixed-gamma source, for the tea 500-mL fill volume in the 500-mL bottle modelled by LabSOCS. The density correction factors are also included.

| LabSOCS Tea 500-mL in 500-mL Bottle			
Energy (keV)	Efficiency (%)	Error (%)	DCF
88	0.0136	0.0014	0.7490
122.1	0.0150	0.0015	0.7642
165.9	0.0137	0.0011	0.7761
279.2	0.0093	0.0007	0.7978
391.7	0.0069	0.0006	0.8138
661.7	0.0044	0.0003	0.8404
898	0.0034	0.0002	0.8563
1173.2	0.0028	0.0001	0.8703
1332.5	0.0026	0.0001	0.8763
1836.1	0.0019	0.0001	0.8918

Table 68. The efficiencies and associated error by energy line contained within the liquid mixed-gamma source, for the tea 500-mL fill volume in the 1-L bottle modelled by LabSOCS. The density correction factors are also included.

LabSOCS Tea 500-mL in 1-L Bottle			
Energy (keV)	Efficiency (%)	Error (%)	DCF
88	0.0186	0.0019	0.7616
122.1	0.0209	0.0021	0.7792
165.9	0.0192	0.0015	0.7936
279.2	0.0132	0.0011	0.8186
391.7	0.0097	0.0008	0.8357
661.7	0.0062	0.0004	0.8626
898	0.0048	0.0003	0.8780
1173.2	0.0040	0.0002	0.8912
1332.5	0.0036	0.0001	0.8968
1836.1	0.0027	0.0001	0.9109

Table 69. The efficiencies and associated error by energy line contained within the liquid mixed-gamma source, for the tea 750-mL fill volume in the 1-L bottle modelled by LabSOCS. The density correction factors are also included.

| LabSOCS Tea 750-mL in 1-L Bottle			
Energy (keV)	Efficiency (%)	Error (%)	DCF
88	0.0134	0.0013	0.7350
122.1	0.0150	0.0015	0.7529
165.9	0.0139	0.0011	0.7670
279.2	0.0096	0.0008	0.7918
391.7	0.0071	0.0006	0.8095
661.7	0.0046	0.0003	0.8382
898	0.0036	0.0002	0.8552
1173.2	0.0029	0.0001	0.8698
1332.5	0.0027	0.0001	0.8761
1836.1	0.0020	0.0001	0.8921

Table 70. The efficiencies and associated error by energy line contained within the liquid mixed-gamma source, for the tea 1-L fill volume in the 1-L bottle modelled by LabSOCS. The density correction factors are also included.

LabSOCS Tea 1-L in 1-L Bottle			
Energy (keV)	Efficiency (%)	Error (%)	DCF
88	0.0104	0.0010	0.7219
122.1	0.0117	0.0012	0.7394
165.9	0.0108	0.0009	0.7528
279.2	0.0075	0.0006	0.7767
391.7	0.0056	0.0004	0.7940
661.7	0.0036	0.0002	0.8229
898	0.0028	0.0002	0.8403
1173.2	0.0023	0.0001	0.8556
1332.5	0.0021	0.0001	0.8622
1836.1	0.0016	0.0001	0.8792

Appendix D

Modelled and Empirical Efficiency Data DILs, MDCs, and DCFs

Table 7120. The FDA DQO for MDC by radionuclide of concern, the corresponding calculated MDC, and the density correction factors for the honey 300-mL fill volume in the 500-mL bottle on the ORTEC detector.

ORTEC Honey 300-mL in 500-mL Bottle			
Radionuclide	1/3 DIL (Bq/kg)	Calculated MDC (Bq/kg)	DCF
I-131	57	1.6197	1.5751
Cs-134+Cs-137	400	3.4080	1.4878, 1.4741
Ru-103	2267	1.8830	1.5213
Ru-106	150	7.4810	1.4635

Table 7221. The FDA DQO for MDC by radionuclide of concern, the corresponding calculated MDC, and the density correction factors for the honey 400-mL fill volume in the 500-mL bottle on the ORTEC detector.

ORTEC Honey 400-mL in 500-mL Bottle			
Radionuclide	1/3 DIL (Bq/kg)	Calculated MDC (Bq/kg)	DCF
I-131	57	1.56	1.3919
Cs-134+Cs-137	400	3.98	1.3587, 1.3506
Ru-103	2267	1.51	1.3778
Ru-106	150	7.29	1.3429

Table 7322. The FDA DQO for MDC by radionuclide of concern, the corresponding calculated MDC, and the density correction factors for the honey 500-mL fill volume in the 500-mL bottle on the ORTEC detector.

ORTEC Honey 500-mL in 500-mL Bottle			
Radionuclide	1/3 DIL (Bq/kg)	Calculated MDC (Bq/kg)	DCF
I-131	57	1.76	1.3119
Cs-134+Cs-137	400	2.82	1.2493, 1.2375
Ru-103	2267	1.56	1.2752
Ru-106	150	6.73	1.2012

Table 7423. The FDA DQO for MDC by radionuclide of concern, the corresponding calculated MDC, and the density correction factors for the honey 500-mL fill volume in the 1-L bottle on the ORTEC detector.

ORTEC Honey 500-mL in 1-L Bottle			
Radionuclide	1/3 DIL (Bq/kg)	Calculated MDC (Bq/kg)	DCF
I-131	57	1.08	1.1303
Cs-134+Cs-137	400	2.17	1.0988, 1.0915
Ru-103	2267	0.86	1.1105
Ru-106	150	3.94	1.0861

Table 7524. The FDA DQO for MDC by radionuclide of concern, the corresponding calculated MDC, and the density correction factors for the honey 750-mL fill volume in the 1-L bottle on the ORTEC detector.

ORTEC Honey 750-mL in 1-L Bottle			
Radionuclide	1/3 DIL (Bq/kg)	Calculated MDC (Bq/kg)	DCF
I-131	57	1.07	1.2246
Cs-134+Cs-137	400	1.98	0.9869, 1.1775
Ru-103	2267	1.01	1.2022
Ru-106	150	3.83	1.1713

Table 7625. The FDA DQO for MDC by radionuclide of concern, the corresponding calculated MDC, and the density correction factors for the honey 1-L fill volume in the 1-L bottle on the ORTEC detector.

ORTEC Honey 1-L in 1-L Bottle			
Radionuclide	1/3 DIL (Bq/kg)	Calculated MDC (Bq/kg)	DCF
I-131	57	0.92	1.3785
Cs-134+Cs-137	400	2.01	1.3087, 1.2936
Ru-103	2267	0.82	1.3344
Ru-106	150	3.48	1.2874

Table 7726. The FDA DQO for MDC by radionuclide of concern, the corresponding calculated MDC, and the density correction factors for the honey 300-mL fill volume in the 500-mL bottle on the Canberra detector.

Canberra Honey 300-mL in 500-mL Bottle			
Radionuclide	1/3 DIL (Bq/kg)	Calculated MDC (Bq/kg)	DCF
I-131	57	4.50	1.5616
Cs-134+Cs-137	400	9.94	1.4956, 1.4849
Ru-103	2267	4.32	1.5141
Ru-106	150	18.33	1.4779

Table 7827. The FDA DQO for MDC by radionuclide of concern, the corresponding calculated MDC, and the density correction factors for the honey 400-mL fill volume in the 500-mL bottle on the Canberra detector.

Canberra Honey 400-mL in 500-mL Bottle			
Radionuclide	1/3 DIL (Bq/kg)	Calculated MDC (Bq/kg)	DCF
I-131	57	6.65	1.4140
Cs-134+Cs-137	400	10.26	1.3661, 1.3584
Ru-103	2267	4.33	1.3846
Ru-106	150	17.98	1.3543

Table 7928. The FDA DQO for MDC by radionuclide of concern, the corresponding calculated MDC, and the density correction factors for the honey 500-mL fill volume in the 1-L bottle on the Canberra detector.

Canberra Honey 500-mL in 1-L Bottle			
Radionuclide	1/3 DIL (Bq/kg)	Calculated MDC (Bq/kg)	DCF
I-131	57	2.49	1.1192
Cs-134+Cs-137	400	4.84	1.0866, 1.0773
Ru-103	2267	2.34	1.0942
Ru-106	150	9.39	1.0723

Table 8029. The FDA DQO for MDC by radionuclide of concern, the corresponding calculated MDC, and the density correction factors for the honey 750-mL fill volume in the 1-L bottle on the Canberra detector.

Canberra Honey 750-mL in 1-L Bottle			
Radionuclide	1/3 DIL (Bq/kg)	Calculated MDC (Bq/kg)	DCF
I-131	57	2.08	1.3544
Cs-134+Cs-137	400	4.23	1.3238, 1.3140
Ru-103	2267	2.08	1.3356
Ru-106	150	9.72	1.3099

Table 8130. The FDA DQO for MDC by radionuclide of concern, the corresponding calculated MDC, and the density correction factors for the honey 1-L fill volume in the 1-L bottle on the Canberra detector.

Canberra Honey 1-L in 1-L Bottle			
Radionuclide	1/3 DIL (Bq/kg)	Calculated MDC (Bq/kg)	DCF
I-131	57	2.76	1.3298
Cs-134+Cs-137	400	5.42	1.2947, 1.2936
Ru-103	2267	2.39	1.3127
Ru-106	150	9.29	1.2899

Table 8231. The FDA DQO for MDC by radionuclide of concern, the corresponding calculated MDC, and the density correction factors for the honey 300-mL fill volume in the 500-mL bottle modelled using LabSOCS.

LabSOCS Honey 300-mL in 500-mL Bottle			
Radionuclide	1/3 DIL (Bq/kg)	Calculated MDC (Bq/kg)	DCF
I-131	57	3.67	1.1031
Cs-134+Cs-137	400	7.55	1.0817, 1.0848
Ru-103	2267	2.12	1.0949
Ru-106	150	7.10	1.0817

Table 8332. The FDA DQO for MDC by radionuclide of concern, the corresponding calculated MDC, and the density correction factors for the honey 400-mL fill volume in the 500-mL bottle modelled using LabSOCS.

LabSOCS Honey 400-mL in 500-mL Bottle			
Radionuclide	1/3 DIL (Bq/kg)	Calculated MDC (Bq/kg)	DCF
I-131	57	4.69	1.1116
Cs-134+Cs-137	400	5.85	1.0957, 1.0942
Ru-103	2267	2.61	1.1053
Ru-106	150	10.48	1.0932

Table 8433. The FDA DQO for MDC by radionuclide of concern, the corresponding calculated MDC, and the density correction factors for the honey 500-mL fill volume in the 500-mL bottle modelled using LabSOCS.

LabSOCS Honey 500-mL in 500-mL Bottle			
Radionuclide	1/3 DIL (Bq/kg)	Calculated MDC (Bq/kg)	DCF
I-131	57	4.66	0.9763
Cs-134+Cs-137	400	7.13	0.9782, 0.9768
Ru-103	2267	3.50	0.9765
Ru-106	150	13.94	0.9775

Table 8534. The FDA DQO for MDC by radionuclide of concern, the corresponding calculated MDC, and the density correction factors for the honey 500-mL fill volume in the 1-L bottle modelled using LabSOCS.

LabSOCS Honey 500-mL in 1-L Bottle			
Radionuclide	1/3 DIL (Bq/kg)	Calculated MDC (Bq/kg)	DCF
I-131	57	2.83	1.1049
Cs-134+Cs-137	400	4.45	1.0903, 1.0861
Ru-103	2267	2.29	1.0961
Ru-106	150	8.81	1.0835

Table 8635. The FDA DQO for MDC by radionuclide of concern, the corresponding calculated MDC, and the density correction factors for the honey 750-mL fill volume in the 1-L bottle modelled using LabSOCS.

LabSOCS Honey 750-mL in 1-L Bottle			
Radionuclide	1/3 DIL (Bq/kg)	Calculated MDC (Bq/kg)	DCF
I-131	57	2.32	1.1638
Cs-134+Cs-137	400	3.83	1.1458, 1.1436
Ru-103	2267	2.00	1.1523
Ru-106	150	8.92	1.1380

Table 8736. The FDA DQO for MDC by radionuclide of concern, the corresponding calculated MDC, and the density correction factors for the honey 1-L fill volume in the 1-L bottle modelled using LabSOCS.

LabSOCS Honey 1-L in 1-L Bottle			
Radionuclide	1/3 DIL (Bq/kg)	Calculated MDC (Bq/kg)	DCF
I-131	57	2.75	1.1605
Cs-134+Cs-137	400	4.41	1.1441, 1.1379
Ru-103	2267	2.05	1.1489
Ru-106	150	7.63	1.1342

Table 8837. The FDA DQO for MDC by radionuclide of concern and the corresponding calculated MDC for the water 300-mL fill volume in the 500-mL bottle on the ORTEC detector.

ORTEC Water 300-mL in 500-mL Bottle		
Radionuclide	1/3 DIL (Bq/kg)	Calculated MDC (Bq/kg)
I-131	57	1.37
Cs-134+Cs-137	400	3.07
Ru-103	2267	1.64
Ru-106	150	6.78

Table 8938. The FDA DQO for MDC by radionuclide of concern and the corresponding calculated MDC for the water 400-mL fill volume in the 500-mL bottle on the ORTEC detector.

ORTEC Water 400-mL in 500-mL Bottle		
Radionuclide	1/3 DIL (Bq/kg)	Calculated MDC (Bq/kg)
I-131	57	1.42
Cs-134+Cs-137	400	3.72
Ru-103	2267	1.38
Ru-106	150	6.83

Table 9039. The FDA DQO for MDC by radionuclide of concern and the corresponding calculated MDC for the water 500-mL fill volume in the 500-mL bottle on the ORTEC detector.

ORTEC Water 500-mL in 500-mL Bottle		
Radionuclide	1/3 DIL (Bq/kg)	Calculated MDC (Bq/kg)
I-131	57	1.72
Cs-134+Cs-137	400	2.91
Ru-103	2267	1.56
Ru-106	150	7.13

Table 9140. The FDA DQO for MDC by radionuclide of concern and the corresponding calculated MDC for the water 500-mL fill volume in the 1-L bottle on the ORTEC detector.

ORTEC Water 500-mL in 1-L Bottle		
Radionuclide	1/3 DIL (Bq/kg)	Calculated MDC (Bq/kg)
I-131	57	1.16
Cs-134+Cs-137	400	2.42
Ru-103	2267	0.93
Ru-106	150	4.40

Table 9241. The FDA DQO for MDC by radionuclide of concern and the corresponding calculated MDC for the water 750-mL fill volume in the 1-L bottle on the ORTEC detector.

ORTEC Water 750-mL in 1-L Bottle		
Radionuclide	1/3 DIL (Bq/kg)	Calculated MDC (Bq/kg)
I-131	57	1.11
Cs-134+Cs-137	400	2.26
Ru-103	2267	1.06
Ru-106	150	4.11

Table 9342. The FDA DQO for MDC by radionuclide of concern and the corresponding calculated MDC for the water   1-L fill volume in the 1-L bottle on the ORTEC detector.

ORTEC Water 1-L in 1-L Bottle		
Radionuclide	1/3 DIL (Bq/kg)	Calculated MDC (Bq/kg)
I-131	57	0.86
Cs-134+Cs-137	400	1.99
Ru-103	2267	0.79
Ru-106	150	3.46

Table 9443. The FDA DQO for MDC by radionuclide of concern and the corresponding calculated MDC for the water   300-mL fill volume in the 500-mL bottle on the Canberra detector.

Canberra Water 300-mL in 500-mL Bottle		
Radionuclide	1/3 DIL (Bq/kg)	Calculated MDC (Bq/kg)
I-131	57	3.83
Cs-134+Cs-137	400	8.90
Ru-103	2267	3.78
Ru-106	150	16.44

Table 9544. The FDA DQO for MDC by radionuclide of concern and the corresponding calculated MDC for the water   400-mL fill volume in the 500-mL bottle on the Canberra detector.

Canberra Water 400-mL in 500-mL Bottle		
Radionuclide	1/3 DIL (Bq/kg)	Calculated MDC (Bq/kg)
I-131	57	5.94
Cs-134+Cs-137	400	9.53
Ru-103	2267	3.94
Ru-106	150	16.71

Table 9645. The FDA DQO for MDC by radionuclide of concern and the corresponding calculated MDC for the water   500-mL fill volume in the 1-L bottle on the Canberra detector.

Canberra Water 500-mL in 1-L Bottle		
Radionuclide	1/3 DIL (Bq/kg)	Calculated MDC (Bq/kg)
I-131	57	2.70
Cs-134+Cs-137	400	5.45
Ru-103	2267	2.60
Ru-106	150	10.61

Table 9746. The FDA DQO for MDC by radionuclide of concern and the corresponding calculated MDC for the water   750-mL fill volume in the 1-L bottle on the Canberra detector.

Canberra Water 750-mL in 1-L Bottle		
Radionuclide	1/3 DIL (Bq/kg)	Calculated MDC (Bq/kg)
I-131	57	1.94
Cs-134+Cs-137	400	4.06
Ru-103	2267	1.96
Ru-106	150	9.33

Table 9847. The FDA DQO for MDC by radionuclide of concern and the corresponding calculated MDC for the water   1-L fill volume in the 1-L bottle on the Canberra detector.

Canberra Water 1-L in 1-L Bottle		
Radionuclide	1/3 DIL (Bq/kg)	Calculated MDC (Bq/kg)
I-131	57	2.66
Cs-134+Cs-137	400	5.40
Ru-103	2267	2.33
Ru-106	150	9.22

Table 9948. The FDA DQO for MDC by radionuclide of concern and the corresponding calculated MDC for the water   300-mL fill volume in the 500-mL bottle modelled using LabSOCS.

LabSOCS Water 300-mL in 500-mL Bottle		
Radionuclide	1/3 DIL (Bq/kg)	Calculated MDC (Bq/kg)
I-131	57	4.25
Cs-134+Cs-137	400	9.14
Ru-103	2267	2.48
Ru-106	150	8.52

Table 10049. The FDA DQO for MDC by radionuclide of concern and the corresponding calculated MDC for the water   400-mL fill volume in the 500-mL bottle modelled using LabSOCS.

LabSOCS Water 400-mL in 500-mL Bottle		
Radionuclide	1/3 DIL (Bq/kg)	Calculated MDC (Bq/kg)
I-131	57	5.11
Cs-134+Cs-137	400	6.64
Ru-103	2267	2.87
Ru-106	150	11.80

Table 10150. The FDA DQO for MDC by radionuclide of concern and the corresponding calculated MDC for the water   500-mL fill volume in the 500-mL bottle modelled using LabSOCS.

LabSOCS Water 500-mL in 500-mL Bottle		
Radionuclide	1/3 DIL (Bq/kg)	Calculated MDC (Bq/kg)
I-131	57	5.34
Cs-134+Cs-137	400	8.72
Ru-103	2267	4.07
Ru-106	150	16.55

Table 10251. The FDA DQO for MDC by radionuclide of concern and the corresponding calculated MDC for the water 500-mL fill volume in the 1-L bottle modelled using LabSOCS.

LabSOCS Water 500-mL in 1-L Bottle		
Radionuclide	1/3 DIL (Bq/kg)	Calculated MDC (Bq/kg)
I-131	57	2.99
Cs-134+Cs-137	400	4.90
Ru-103	2267	2.45
Ru-106	150	9.64

Table 10352. The FDA DQO for MDC by radionuclide of concern and the corresponding calculated MDC for the water 750-mL fill volume in the 1-L bottle modelled using LabSOCS.

LabSOCS Water 750-mL in 1-L Bottle		
Radionuclide	1/3 DIL (Bq/kg)	Calculated MDC (Bq/kg)
I-131	57	2.42
Cs-134+Cs-137	400	4.17
Ru-103	2267	2.10
Ru-106	150	9.65

Table 10453. The FDA DQO for MDC by radionuclide of concern and the corresponding calculated MDC for the water 1-L fill volume in the 1-L bottle modelled using LabSOCS.

LabSOCS Water 1-L in 1-L Bottle		
Radionuclide	1/3 DIL (Bq/kg)	Calculated MDC (Bq/kg)
I-131	57	2.93
Cs-134+Cs-137	400	4.90
Ru-103	2267	2.21
Ru-106	150	8.44

Table 10554. The FDA DQO for MDC by radionuclide of concern, the corresponding calculated MDC, and the density correction factors for the tea 300-mL fill volume in the 500-mL bottle on the ORTEC detector.

ORTEC Tea 300-mL in 500-mL Bottle			
Radionuclide	1/3 DIL (Bq/kg)	Calculated MDC (Bq/kg)	DCF
I-131	57	2.6281	0.9316
Cs-134+Cs-137	400	5.8143	0.9199, 0.9231
Ru-103	2267	3.1267	0.9206
Ru-106	150	12.9740	0.9250

Table 10655. The FDA DQO for MDC by radionuclide of concern, the corresponding calculated MDC, and the density correction factors for the tea 400-mL fill volume in the 500-mL bottle on the ORTEC detector.

ORTEC Tea 400-mL in 500-mL Bottle			
Radionuclide	1/3 DIL (Bq/kg)	Calculated MDC (Bq/kg)	DCF
I-131	57	2.81	0.9417
Cs-134+Cs-137	400	8.06	1.0244, 1.0380
Ru-103	2267	2.90	0.9913
Ru-106	150	15.16	1.0491

Table 10756. The FDA DQO for MDC by radionuclide of concern, the corresponding calculated MDC, and the density correction factors for the tea 500-mL fill volume in the 500-mL bottle on the ORTEC detector.

ORTEC Tea 500-mL in 500-mL Bottle			
Radionuclide	1/3 DIL (Bq/kg)	Calculated MDC (Bq/kg)	DCF
I-131	57	3.28	0.8943
Cs-134+Cs-137	400	6.06	0.9736, 0.9824
Ru-103	2267	3.15	0.9424
Ru-106	150	14.85	0.9717

Table 10857. The FDA DQO for MDC by radionuclide of concern, the corresponding calculated MDC, and the density correction factors for the tea 500-mL fill volume in the 1-L bottle on the ORTEC detector.

ORTEC Tea 500-mL in 1-L Bottle			
Radionuclide	1/3 DIL (Bq/kg)	Calculated MDC (Bq/kg)	DCF
I-131	57	2.17	0.8750
Cs-134+Cs-137	400	4.70	0.9088, 0.9133
Ru-103	2267	1.80	0.8970
Ru-106	150	8.65	0.9165

Table 10958. The FDA DQO for MDC by radionuclide of concern, the corresponding calculated MDC, and the density correction factors for the tea 750-mL fill volume in the 1-L bottle on the ORTEC detector.

ORTEC Tea 750-mL in 1-L Bottle			
Radionuclide	1/3 DIL (Bq/kg)	Calculated MDC (Bq/kg)	DCF
I-131	57	2.08	0.8649
Cs-134+Cs-137	400	3.97	0.7190, 0.8640
Ru-103	2267	2.00	0.8653
Ru-106	150	7.76	0.8653

Table 11059. The FDA DQO for MDC by radionuclide of concern, the corresponding calculated MDC, and the density correction factors for the tea 1-L fill volume in the 1-L bottle on the ORTEC detector.

ORTEC Tea 1-L in 1-L Bottle			
Radionuclide	1/3 DIL (Bq/kg)	Calculated MDC (Bq/kg)	DCF
I-131	57	1.37	0.7111
Cs-134+Cs-137	400	3.20	0.7159, 0.7175
Ru-103	2267	1.27	0.7148
Ru-106	150	5.62	0.7187

Table 11160. The FDA DQO for MDC by radionuclide of concern, the corresponding calculated MDC, and the density correction factors for the tea 300-mL fill volume in the 500-mL bottle on the Canberra detector.

Canberra Tea 300-mL in 500-mL Bottle			
Radionuclide	1/3 DIL (Bq/kg)	Calculated MDC (Bq/kg)	DCF
I-131	57	7.3377	0.9286
Cs-134+Cs-137	400	17.2072	0.9389, 0.9401
Ru-103	2267	7.3095	0.9329
Ru-106	150	32.1129	0.9437

Table 11261. The FDA DQO for MDC by radionuclide of concern, the corresponding calculated MDC, and the density correction factors for the tea 400-mL fill volume in the 500-mL bottle on the Canberra detector.

Canberra Tea 400-mL in 500-mL Bottle			
Radionuclide	1/3 DIL (Bq/kg)	Calculated MDC (Bq/kg)	DCF
I-131	57	11.50	0.9190
Cs-134+Cs-137	400	20.18	1.0018, 1.0141
Ru-103	2267	8.03	0.9633
Ru-106	150	36.35	1.0282

Table 11362. The FDA DQO for MDC by radionuclide of concern, the corresponding calculated MDC, and the density correction factors for the tea 500-mL fill volume in the 1-L bottle on the Canberra detector.

Canberra Tea 500-mL in 1-L Bottle			
Radionuclide	1/3 DIL (Bq/kg)	Calculated MDC (Bq/kg)	DCF
I-131	57	5.15	0.8858
Cs-134+Cs-137	400	10.41	0.8944, 0.8986
Ru-103	2267	4.95	0.8894
Ru-106	150	20.50	0.9015

Table 11463. The FDA DQO for MDC by radionuclide of concern, the corresponding calculated MDC, and the density correction factors for the tea 750-mL fill volume in the 1-L bottle on the Canberra detector.

Canberra Tea 750-mL in 1-L Bottle			
Radionuclide	1/3 DIL (Bq/kg)	Calculated MDC (Bq/kg)	DCF
I-131	57	4.09	0.9702
Cs-134+Cs-137	400	8.85	1.0020, 1.0063
Ru-103	2267	4.25	0.9916
Ru-106	150	20.56	1.0090

Table 11564. The FDA DQO for MDC by radionuclide of concern, the corresponding calculated MDC, and the density correction factors for the tea 1-L fill volume in the 1-L bottle on the Canberra detector.

Canberra Tea 1-L in 1-L Bottle			
Radionuclide	1/3 DIL (Bq/kg)	Calculated MDC (Bq/kg)	DCF
I-131	57	4.30	0.7185
Cs-134+Cs-137	400	8.78	0.7229, 0.7277
Ru-103	2267	3.79	0.7209
Ru-106	150	15.17	0.7292

Table 11665. The FDA DQO for MDC by radionuclide of concern, the corresponding calculated MDC, and the density correction factors for the tea 300-mL fill volume in the 500-mL bottle modelled using LabSOCS.

LabSOCS Tea 300-mL in 500-mL Bottle			
Radionuclide	1/3 DIL (Bq/kg)	Calculated MDC (Bq/kg)	DCF
I-131	57	7.6332	0.8351
Cs-134+Cs-137	400	16.4963	0.8636, 0.8668
Ru-103	2267	4.5278	0.8515
Ru-106	150	15.6952	0.8710

Table 11766. The FDA DQO for MDC by radionuclide of concern, the corresponding calculated MDC, and the density correction factors for the tea 400-mL fill volume in the 500-mL bottle modelled using LabSOCS.

LabSOCS Tea 400-mL in 500-mL Bottle			
Radionuclide	1/3 DIL (Bq/kg)	Calculated MDC (Bq/kg)	DCF
I-131	57	9.22	0.8207
Cs-134+Cs-137	400	12.04	0.8442, 0.8505
Ru-103	2267	5.24	0.8348
Ru-106	150	21.84	0.8558

Table 11867. The FDA DQO for MDC by radionuclide of concern, the corresponding calculated MDC, and the density correction factors for the tea 500-mL fill volume in the 500-mL bottle modelled using LabSOCS.

LabSOCS Tea 500-mL in 500-mL Bottle			
Radionuclide	1/3 DIL (Bq/kg)	Calculated MDC (Bq/kg)	DCF
I-131	57	9.40	0.7220
Cs-134+Cs-137	400	15.07	0.7537, 0.7599
Ru-103	2267	7.24	0.7393
Ru-106	150	29.71	0.7637

Table 11968. The FDA DQO for MDC by radionuclide of concern, the corresponding calculated MDC, and the density correction factors for the tea 500-mL fill volume in the 1-L bottle modelled using LabSOCS.

LabSOCS Tea 500-mL in 1-L Bottle			
Radionuclide	1/3 DIL (Bq/kg)	Calculated MDC (Bq/kg)	DCF
I-131	57	5.53	0.8308
Cs-134+Cs-137	400	9.07	0.8505, 0.8553
Ru-103	2267	4.56	0.8399
Ru-106	150	18.17	0.8604

Table 12069. The FDA DQO for MDC by radionuclide of concern, the corresponding calculated MDC, and the density correction factors for the tea 750-mL fill volume in the 1-L bottle modelled using LabSOCS.

LabSOCS Tea 750-mL in 1-L Bottle			
Radionuclide	1/3 DIL (Bq/kg)	Calculated MDC (Bq/kg)	DCF
I-131	57	4.40	0.8029
Cs-134+Cs-137	400	7.62	0.8259, 0.8304
Ru-103	2267	3.87	0.8140
Ru-106	150	17.99	0.8356

Table 12170. The FDA DQO for MDC by radionuclide of concern, the corresponding calculated MDC, and the density correction factors for the tea 1-L fill volume in the 1-L bottle modelled using LabSOCS.

LabSOCS Tea 1-L in 1-L Bottle			
Radionuclide	1/3 DIL (Bq/kg)	Calculated MDC (Bq/kg)	DCF
I-131	57	5.40	0.7873
Cs-134+Cs-137	400	9.09	0.8104, 0.8139
Ru-103	2267	4.11	0.7985
Ru-106	150	15.92	0.8184